学位論文

Upward and Downward Wave-Activity Propagation across the Tropopause Associated with Submonthly Fluctuations

季節内変動に伴う波活動度の成層圏対流圏間の上方下方伝播に関する研究

平成17年12月博士 (理学) 申請

東京大学大学院理学系研究科
地球惑星科学専攻

西井和晃

Abstract

A new aspect of dynamical linkage between the stratosphere and troposphere in the wintertime extra-tropics is proposed. Upward and downward propagation of Rossby wave activity across the tropopause associated with a zonally-confined Rossby wave train that consists of submonthly fluctuations is found to play an important role in that linkage, by using a phase-independent wave-activity flux and refractive index, both of which are suited for diagnosing stationary Rossby wave propagation on a zonally-asymmetric time-mean flow.

As a typical example of this linkage, a particular event of large-scale, quasi-stationary cyclogenesis observed in the troposphere of the Southern Hemisphere (SH) in August 1997 is discussed, to which downward wave-activity injection from anticyclonic anomalies upstream that had developed in the exit region of the lower-stratospheric polar-night jet (PNJ) contributed substantially. Consistent with that downward injection, phase lines of observed streamfunction anomalies exhibited a distinct eastward tilt with height. The development of the anticyclonic anomalies occurred at the leading edge of a quasi-stationary Rossby wave train propagating along the PNJ that had originated from a tropospheric blocking ridge farther upstream.

Though less often than upward wave-activity injection across the tropopause, similar events of downward wave-activity injection occurred several times during late winter of 1997, primarily in the regions south of Australia and over the central South Pacific, over each of which the PNJ exit overlapped with a tropospheric subpolar jet (SPJ) to form a vertical waveguide locally. It is argued that the downward wave-activity propagation is essentially due to refraction in the vertically sheared westerlies, and the zonal asymmetries

in the time-mean flow are a likely factor for the observed geographical preference of the downward wave-activity injection.

The climatology and interannual variability of the upward and downward wave-activity propagation across the tropopause are also studied in the SH late winter based on reanalysis data from 1979 to 2003. The upward and downward wave-activity propagation is prominent over the Southeastern Pacific and South Atlantic, where the axes of the climatological-mean PNJ and SPJ are meridionally close to one another and submonthly circulation fluctuations are active both in the lower stratosphere and troposphere.

Interannual enhancement in local downward wave-activity injection into the troposphere to the south of Australia and over the South Pacific tends to be associated with a poleward shift of the stratospheric PNJ axis upstream and the strengthened SPJ in the troposphere underneath. These wind structure changes influence the formation of local waveguides across the tropopause through the meridional and vertical curvature changes in the time-mean flow. Downstream of enhanced regions of prominent downward wave-activity injection, tropospheric submonthly fluctuations also tends to be enhanced.

Influence of interannual variability associated with the SH annular mode (SAM) and El Niño/Southern Oscillation (ENSO) on downward wave-activity injection is also examined. In association with the above-mentioned wind structure changes, downward wave-activity injection does enhance significantly, but only slightly over certain regions in most cases. Their influence on the tropospheric submonthly fluctuations is also limited.

These results are obtained on the basis of a particular framework in which a planetary-scale wave in the lower stratosphere is considered as a zonally-confined "wave packet" propagating zonally as well as vertically on a zonally-asymmetric time-mean flow. Such a framework is rarely used in the previous studies on the stratospheric planetary-scale waves, most of which do not take propagation in the zonal direction and dependence on a zonally-asymmetric basic state of wave propagation into consideration.

Abstract (in Japanese)

従来の冬季成層圏の大規模波動伝播の研究においては、循環の東西非対称成分全体を波動と捉え、その各東西波数成分の子午面伝播に対する東西平均場の影響や、東西平均場と各波数成分間との相互作用が議論されてきた。この枠組は数学的により厳密な取り扱いを可能とするが、東西方向への伝播の表現や局所的な波源の特定ができず、また伝播特性の経度依存性が議論できない。一方、対流圏循環の研究においては、着目する変動よりも長い時間スケールの平均場を基本場と定義し、それからの偏差を波動と捉えることが多い。この枠組では WKB 的な近似が用いられるため数学的な厳密性がやや低下するものの、この方法を成層圏波動擾乱に適用すれば、東西方向にも限定された擾乱の波束的な振舞が解析でき、その 3 次元伝播特性の東西非一様な基本場への依存性の議論や、東西方向にも局所的な対流圏における波源の特定も可能になる。更に上方伝播するプラネタリー波の変調部分を取り扱うため、局所的に成層圏から対流圏へ下方伝播する波束を取り扱うことができる。

極夜ジェットの卓越する冬季の成層圏上部では、東西波数 1 程度の波が卓越する一方、風速が比較的弱い成層圏下部では東西波数 3 程度までの成分も存在し得る。これらの東西波数成分を持つ擾乱はそのスケールの大きさのため、厳密には東西方向に限定された波束として振舞うとは限らない。しかし、成層圏で観測された大規模波動の波束的な振舞いを統計的に示した先行研究は僅かながら存在する (Randell 1988)。また、成層圏を模した簡単な数値実験によって循環変動の波束的な振舞を示すことができる。特に、高度と共に線型に増加する西風基本場を含むモデル下端に局所的な地形を与えた場合の循環偏差場の時間発展は、波動が一度上向きに伝播した後、転向高度にて屈折されて下方へ伝播する波束的な振舞を見せる。この循環場偏差はほぼ東西波数 1 か

ら３の成分で構成されている。

本研究では、１９７９－２００３年の大気再解析データに基づき、冬季下部成層圏循環に見られる季節内変動の波束的な振舞に着目し、西風ジェットの立体構造や、波束の鉛直伝播を通じた局所的な対流圏循環変動との関連性などを広く調査した。波束伝播に対する基本場は、緩やかな季節進行を反映する３１日移動平均循環場とし、それに重畳する準停滞性の季節内変動は切離周期8日の低周波フィルタを施した場から基本場を差し引くことにより定義した。南半球晩冬において、成層圏極夜ジェットの存在する緯度帯における上部対流圏の一地点を基準点にした、季節内変動に伴う高度偏差の相互相関係数の東西高度分布を求めると、基準点付近の対流圏から東方の成層圏へと、上向きの群速度伝播を伴う波束構造が認められる経度帯がある。一方季節内変動の周期帯以外の変動ではそのようなシグナルは認められないため、対流圏成層圏間の波束伝播の解析において、上記で定義した時間フィルタを用いることは妥当と判断される。解析においては、波束伝播に伴って保存される波活動度 (Takaya and Nakamura 2001) の群速度伝播を力学的に診断し、それを基本場に基づいて評価される停滞性ロスビー波の屈折率が表す導波管構造との関係に特に着目した。

まず、成層圏の波動擾乱が対流圏の局所的な循環偏差の形成に影響した典型例として、１９９７年8月上旬にオーストラリアのはるか南方海上で発達した準停滞性の地上低気圧について詳細に解析を行った。この低気圧は対流圏上層に及ぶ順圧的な構造を有していた。この低気圧性偏差の上流側では成層圏からの下向き波活動度の流入が顕著であり、これがこの準停滞性の低気圧性偏差の発達に寄与していた。実際、波活動度フラックスの鉛直収束は水平収束と同等の大きさであり、かつ、低気圧性偏差の増幅と空間的に良く一致していた。この下向き伝播が存在した経度帯の上流側では、下部成層圏の極夜ジェットに沿って、大西洋からインド洋上空にかけて東向きに群速度伝播する波束構造が見られた。そのさらに上流側のドレーク海峡上空では対流圏のブロッキング高気圧から上向き波活動度の流入が顕著であった。これらの波活動度の上向き伝播が顕著であった領域では高度偏差の位相が高さと共に西に、下向き活動度の流入が顕著な領域では逆に東にそれぞれ傾き、鉛直伝播する定常ロスビー波について

理論的に予想される構造と整合的であった。また、波活動度の鉛直伝播は波が重畳する東西非一様な西風構造に伴って局所的に形成される鉛直方向に伸びた導波管構造によく対応していた。このことは波活動度フラックス導出の際に用いた、基本場が波動擾乱より十分ゆっくり変化すると仮定するWKB近似が定性的には有効であったことを示唆している。

同様なロスビー波束に伴う波活動度の成層圏からの流入は９月中旬に南大西洋で発達したブロッキング高気圧でも顕著であった。実際、１９９７年晩冬（８－９月）においては、これら２つの事例の他にも、成層圏下部の高度偏差場において南緯５０度から６０度付近を東向きに伝播する波束的な構造がしばしば確認された。これらの波束構造の上流側では対流圏からの波活動度の上方流入、また波束の先端付近では対流圏への下方射出を伴う事例が多く観測された。そして、対流圏ではこの波活動度の流入を受け、さらに下流側へと波束伝播がみられた。このように、成層圏からの下向き波活動度の流入が、対流圏の準停滞性季節内変動の形成の一要因であることが初めて明確に示された。

次に、近年の２５年間の大気再解析データを用いて南半球晩冬の中高緯度下部成層圏にて観測される季節内変動とその波束的な3次元伝播についての気候学的分布を明らかにした。周期8日以上の準停滞性変動は、一般に極夜ジェットの軸に沿って活発で、特に著しいのは南東太平洋から南米上空にかけてである。これらの地域は、ブロッキング高気圧など対流圏の季節内変動が活発な領域のやや下流側に位置し、圏界面を越えての波活動度の上向き流入が顕著なことから、対流圏の局所的循環偏差が波源となっていたことが示唆される。一方、これらの領域のさらに下流側では、逆に成層圏から対流圏への波活動度の流入が顕著である。いずれの領域においても、成層圏の極夜ジェットと対流圏の亜寒帯ジェットの軸がほぼ上下に重なり、波動が鉛直伝播しやすい導波管構造が存在していることが示唆された。

更に、晩冬において成層圏から対流圏への下向き波活動度の流入にみられる経年変動が特に大きなオーストラリアの南方域において、流入が特に顕著だった月と不明瞭であった月の合成図を作成し、成層圏対流圏の季節内変動の活動や導波管構造の違い

を調査した。下向き波活動度の流入が顕著であった月においては、その地域で対流圏で亜寒帯ジェットが強化され、そのやや上流で成層圏極夜ジェットの軸が極側にやや変位する傾向がみられた。また、当該領域のやや下流側で対流圏季節内変動が活発化する傾向も見られた。また、気候平均場で下向き波活動度流入の顕著な中緯度南太平洋域でも同様な傾向が認められた。こられの下向き伝播の顕著な月では、そうでない月に比べて対流圏界面付近の西風の南北・鉛直方向の負の曲率が増大し、これが極夜ジェットと亜寒帯ジェットを結ぶ鉛直の導波管構造の形成に寄与したものと理解できる。

一方、南半球中高緯度の対流圏では、極域と中緯度の気圧シーソーを表す環状モード（SAM）に伴う経年変動と、エルニーニョ南方振動 (ENSO) の遠隔影響としての経年変動とが卓越する。しかしながら、これらの変動が季節内変動に伴う波活動度の鉛直伝播に与える影響はあまり顕著ではないことが判明した。これは半球的な規模で西風を変化させるこれらの変動よりも、局所的な西風導波管構造の変化の方が、季節内変動に伴う鉛直伝播には大きな影響を与え得ることを示唆している。例外として、ラニーニャ現象に伴って、オーストラリアの南方で成層圏からの波活動度の流入が増大し、その下流側で対流圏季節内変動が顕著になる傾向が確認された。

本研究においては対流圏界面を上向き・下向きに越えて伝播する経度方向に限定された準停滞性のロスビー波束という新しい概念を導入し、そうした波束を介した対流圏・成層圏の結合変動を提唱した。つまり、成層圏へ波束が伝播しやすい西風構造 (導波管構造) をもつ経度帯で、対流圏で季節内変動に伴う循環偏差が増幅すると、そこから上方に波活動度が射出されて下部成層圏に達し極夜ジェットに沿って東方に伝播する波束を形成する。冬季成層圏中では西風は高さと共に風速が増大するために、波束を形成する東西波数成分のうち、東西波数１の成分はさらに上方へ伝播するが、東西波数２～３の成分は上向きから下向きへ向きを変えようとする。この波束が下流側で鉛直に伸びた導波管構造をもつ経度帯に達すると、波活動度を下向きに射出し、対流圏で別の循環偏差を形成するように働く。成層圏循環から対流圏循環への力学的な影響については、「環状モードシグナルの下方伝播」 (Baldwind and Dunkerton 1999) や「上方伝播する惑星波を構成する東西波数 1 成分の成層圏中での反射」 (Perlwitz and Harnik

2003) など近年活発に議論され始めた。しかし、成層圏の季節内波動擾乱が下向きの波活動度伝播を通じて局所的な対流圏循環に及ぼす影響は、本研究で初めて明らかにされたものである。これは、従来の成層圏循環の研究とは異なり、成層圏波動擾乱の波束的な振舞に着目することで初めて可能になったもので、対流圏の季節内変動の形成に新たな要因を付加するものである。

Contents

Chapter 1

General Introduction

1.1 Upward propagating planetary waves into the stratosphere from the troposphere

The vertical propagation of planetary Rossby waves has been recognized as one of the most fundamental processes involved in the linkage between the tropospheric and stratospheric circulation. It is now widely accepted that the intensity and meridional-vertical structure of the zonal-mean westerlies significantly influence the vertical propagation of planetary waves from the troposphere to the stratosphere (e.g., Charney and Drazin 1961; Dickinson 1968). Zonal asymmetries in the stratospheric stationary circulation over the wintertime Northern Hemisphere (NH), as observed by Muench (1965) and others (Fig. 1.1a), are generated by upward-propagating planetary waves forced by large-scale topography and/or land-sea contrasts (e.g., Matsuno 1970). Figures 1.1a and d show the climatology of 10-hPa geopotential height of the NH winter (January) and the Southern Hemisphere (SH) winter (July). The former has larger deviations from zonal mean than the latter, which suggests that the amplitude of the NH planetary waves is larger than the SH counterpart due to stronger forcing in the NH.

Temporal variations in the upward propagation are considered to be one of the major

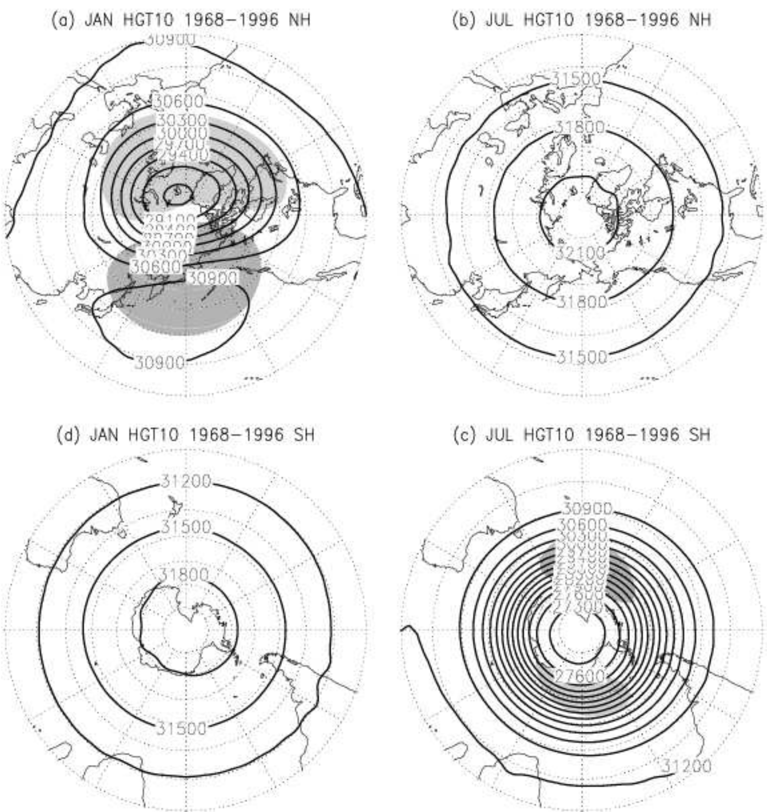

Figure 1.1: Climatology of 10-hPa geopotential height on (a) NH January, (b) NH July, (c) SH January and (d) SH July. Contour interval is 300 [m]. Heavy and lightly shading denotes deviations from its zonal mean exceeds 200 [m] positively and negatively. The NCEP/NCAR data set is used and the period is from 1968 to 1996.

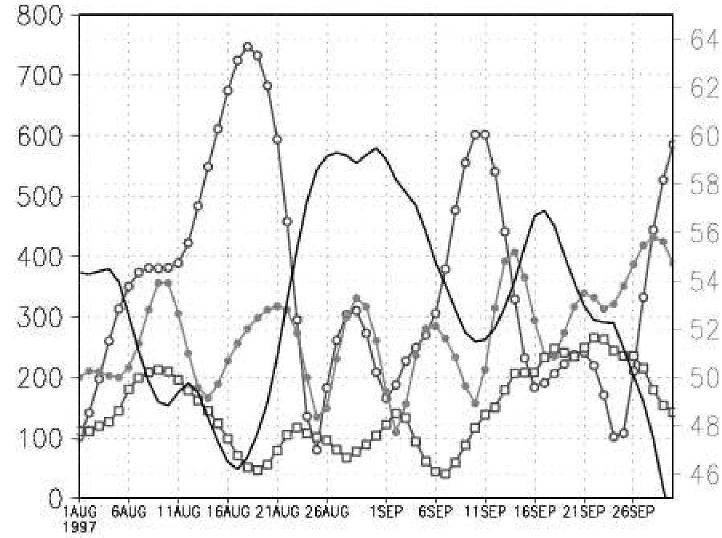

Figure 1.2: Time series of zonal-mean zonal wind (a line without a mark) and amplitudes of *k*=1 (a line with open circles), *k*=2 (a line with closed circles) and *k*=3 (a line with open squares) at 50-hPa level along 60°S from 1 August to 30 September, 1997. The unit of zonal wind is [m/s] (right hand side) and amplitude, [m] (left hand side). All quantities are moving averaged for 5 days.

causes of the fluctuations observed in the stratospheric circulation. For example, Hirota and Sato (1969) focused the negative correlation between day-to-day variations in the zonal mean westerly wind speed and the amplitude of the zonal wavenumber one (*k*=1) component of stratospheric planetary waves (Fig. 1.2). Matsuno (1971) demonstrated that the breakdown of a stratospheric westerly jet during a stratospheric sudden warming (SSW) event is caused by planetary waves propagating from the troposphere. (Fig. 1.3) Temporal variations in the upward propagating planetary waves have been considered to be caused by various tropospheric processes, including the development of blocking ridges (Julian and Labitzke 1965; Quiroz 1986), amplification of intraannual variation associated with Pacific North American Pattern (Baldwin and O'Sullivan 1995; Itoh and Harada 2004), the "valving" effect of the tropopause (Chen and Robinson 1992) and the nonlinear effect of ensemble of synoptic-scale eddies (Scinocca and Haynes 1998; Hio and Hirota 2002).

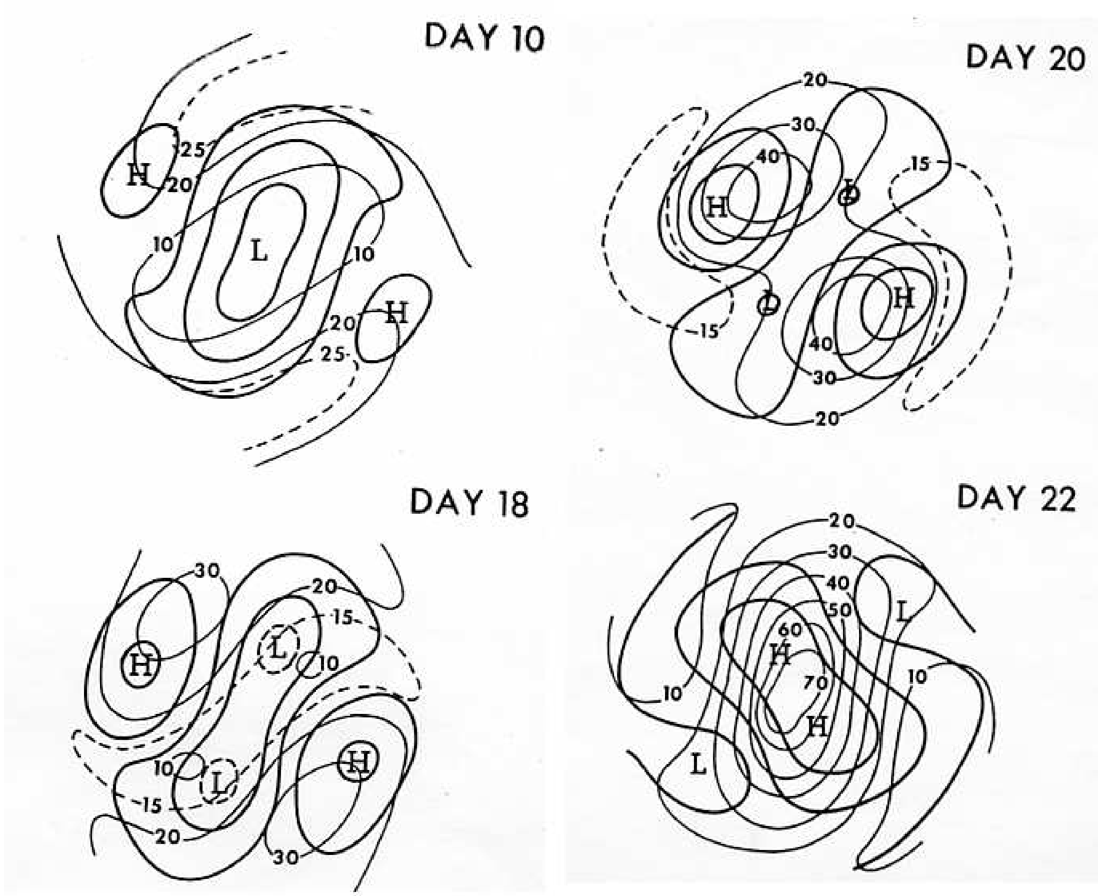

Figure 1.3: Time evolution of isobaric height (500 m contours) and temperature deviations from initial state (°C, thin line) at about 13 hPa from output of a numerical experiment of a SSW forced at the virtual tropopause. Adapted from Fig. 15 of Matsuno (1971).

1.2 Theoretical foundations of vertical propagating Rossby waves

In this section, fundamental properties of extratropical planetary waves propagating in a meridional plane are reviewed, which have been the basis of studies related to the dynamical linkage between the stratosphere and troposphere including above-mentioned ones. First, the condition for vertical propagation of planetary waves is discussed. On a β plane, quasi-geostrophic potential vorticity q defined in the logarithm pressure coordinate ($z = -H \log p$), as

$$q = f_0 + \beta y + \frac{\partial^2 \psi}{\partial x^2} + \frac{\partial^2 \psi}{\partial y^2} + \frac{f_0^2}{\rho_0} \frac{\partial}{\partial z} \left(\frac{\rho_0}{N^2} \frac{\partial \psi}{\partial z} \right), \tag{1.1}$$

satisfies a following equation under the condition of no viscosity and diabatic heating,

$$\frac{\partial q}{\partial t} + u \frac{\partial q}{\partial x} + v \frac{\partial q}{\partial y} = 0, \tag{1.2}$$

where H is the scale height. ψ the geostrophic streamfunction, $(u, v)^T = \vec{u} = (-\psi_y, \psi_x)^T$ the geostrophic velocity, f_0 the Coriolis parameter at specified latitude, β meridional gradient of Coriolis parameter, ρ_0 air density (depends only on height) and N the Brunt-Väisälä frequency. For simplicity, N is taken as a constant. Linearizing (1.2), we obtain

$$(\frac{\partial}{\partial t} + [u] \frac{\partial}{\partial x}) q^* + [q]_y \frac{\partial \psi^*}{\partial x} = 0, \tag{1.3}$$

where $[()]$ and $()^*$ denotes zonal mean and eddies (deviations from zonal mean), respectively. q^* may be written as

$$q^* = \frac{\partial^2 \psi^*}{\partial x^2} + \frac{\partial^2 \psi^*}{\partial y^2} + \frac{f_0^2}{\rho_0} \frac{\partial}{\partial z} \left(\frac{\rho_0}{N^2} \frac{\partial \psi^*}{\partial z} \right), \tag{1.4}$$

and $[q]$ may be written as

$$[q] = f_0 + \beta y + \frac{\partial^2 [\psi]}{\partial y^2} + \frac{f_0^2}{\rho_0} \frac{\partial}{\partial z} \left(\frac{\rho_0}{N^2} \frac{\partial [\psi]}{\partial z} \right). \tag{1.5}$$

If the solution of the equation (1.3) is taken as harmonic waves with zonal and meridional wavenumbers (k and l), respectively, and angular frequency ω;

$$\psi^*(x,y,z,t) = \Psi(z)\exp(i(kx+ly-\omega t)+\frac{z}{2H}), \tag{1.6}$$

where Ψ is a function only of z. Substituting to the equation (1.3), we obtain

$$\frac{d^2\Psi}{dz^2}+m^2\Psi = 0, \tag{1.7}$$

where

$$m^2 = \frac{N^2}{f_0^2}(\frac{[q]_y}{[u]-C_{px}}-(k^2+l^2))-\frac{1}{4H^2}. \tag{1.8}$$

and zonal phase speed $C_{px} = \omega/k$. For vertical propagation, m^2 must be positive, thus the condition of $[u]$ for vertical propagation is

$$C_{px} < [u] < C_{px}+\frac{[q]_y}{(k^2+l^2+\frac{f_0{}^2}{4N^2H^2})} \equiv U_{ck}. \tag{1.9}$$

This condition suggests that stationary ($C_{px} = 0$) Rossby waves cannot propagate vertically in the easterlies (Charney and Drazin 1961). This theory can be confirmed in the difference between the wintertime and summertime stratospheric circulations (Fig. 1.1). In winter, the zonal-mean zonal wind is westerly ($[u] > 0$) and the circulation is characterized by the presence of the stationary planetary-scale disturbances associated with upward-propagating Rossby waves forced in the troposphere. Contrastingly in summer, the circulation is highly zonally symmetric because the zonal-mean zonal easterlies ($[u] < 0$) prevent tropospheric Rossby waves from propagating upward. In the westerlies, only the Rossby waves with planetary scales can propagate vertically in the strong wind speed. If the westerly speed increases with height under condition of constant $[q]_y$, upward propagating waves reaching at some level where $[u] = U_{ck}$ for each k cannot propagate farther above that level. Since

U_{ck} is larger for smaller k, waves with larger scales (smaller k) can propagate farther upward than smaller scale waves can.

If $[u]$ satisfies the above condition (1.9), Ψ may be written as

$$\Psi(z) = \psi_0 \exp(imz), \tag{1.10}$$

where ψ_0 is a constant and i represents imaginary part. The equation (1.6) becomes

$$\psi^*(x,y,z,t) = \psi_0 \exp(i(kx + ly + mz - \omega t) + z/(2H)), \tag{1.11}$$

for which we obtain a dispersion relation;

$$\omega = [u]k - \frac{k[q]_y}{K^2 + \frac{f_0{}^2}{4HN^2}}, \tag{1.12}$$

where

$$K^2 = k^2 + l^2 + \frac{f_0^2}{N^2}m^2 \tag{1.13}$$

$$= \frac{[q]_y}{[u] - C_{px}} - \frac{f^2}{4N^2H^2}. \tag{1.14}$$

The group velocity, $\vec{C}_g = (C_{gx}, C_{gy}, C_{gz})^T$, may be written as,

$$C_{gx} = C_{px} + \frac{2[q]_y k^2}{(K^2 + \frac{f_0{}^2}{4HN^2})^2}, \tag{1.15}$$

$$C_{gy} = \frac{2[q]_y kl}{(K^2 + \frac{f_0{}^2}{4HN^2})^2}, \tag{1.16}$$

$$C_{gz} = \frac{2\frac{f_0{}^2}{N^2}[q]_y km}{(K^2 + \frac{f_0{}^2}{4HN^2})^2}. \tag{1.17}$$

For stationary waves ($C_{px} = 0$),

$$\vec{C}_g = \frac{2[u]k}{K^2 + \frac{f_0{}^2}{4HN^2}} \times (k, l, \frac{f_0{}^2}{N^2} m), \tag{1.18}$$

holds. Thus, the group velocity of a stationary Rossby wave is tangent to phase lines in a horizontal plane, phase lines associated with the upward- (downward-) propagating Rossby wave group velocity are tilted westward (eastward) with height [1]. It is also shown that the magnitude of the group velocity is almost twice as large as $[u]$.

In diagnosing Rossby wave propagation in a meridional plane, Eliassen-Palm (E-P) flux (Eliassen and Palm 1961; Andrews and McIntyre 1976) is a useful tool. By zonally averaging the equation (1.3), we obtain

$$\frac{\partial [q]}{\partial t} = -\frac{\partial [q^* v^*]}{\partial y}. \tag{1.19}$$

Potential vorticity flux $[q^* v^*]$ satisfies following equation

$$\begin{aligned} [q^* v^*] &= -\frac{\partial [u^* v^*]}{\partial y} + \frac{f_0^2}{\rho_0} \frac{\partial}{\partial z} (\frac{\rho_0}{N^2} [v^* \frac{\partial \psi}{\partial z}]) \\ &= \rho_0{}^{-1} \vec{\nabla} \cdot \vec{F}, \end{aligned} \tag{1.20}$$

where the E-P flux $\vec{F}$ is defined as

$$\vec{F} = (0, -\rho_0 [u^* v^*], \frac{\rho_0 f^2}{N^2} [v^* \frac{\partial \psi^*}{\partial z}]). \tag{1.21}$$

The y- and z- components of the E-P flux are proportional to meridional westerly momentum and heat flux, respectively. Note that

$$\frac{\partial \psi^*}{\partial z} = \frac{R_a}{f_0 H} T^*, \tag{1.22}$$

[1]In a vertically elongated coordinate where $z' = \frac{N}{f} z$, the group velocity is also tangent to phase lines in meridional and zonal cross sections. Note that the group velocity of stationary Rossby waves is always eastward.

where T denotes air temperature and R_a the gas constant of dry air. From (1.19) and (1.20), we obtain

$$\frac{\partial [q]}{\partial t} = -\frac{\partial}{\partial y}(\rho_0{}^{-1}\vec{\nabla}\cdot\vec{F}), \tag{1.23}$$

which means that it is not the heat flux or westerly momentum flux alone but the E-P flux whose divergence contributes to changes in the zonal-mean state. With adequate boundary conditions, we can obtain the following relationship; the zonal-mean zonal wind is accelerated (decelerated) with divergence (convergence) of the E-P flux. This explains the results of Hirota and Sato (1969) and Matsuno (1971) that show zonal-mean zonal wind deceleration in association with amplification of planetary Rossby waves.

Another important relation can be obtained from (1.3) by multiplying $\rho_0 q^*/[q]_y$ and neglecting differential of $[q]_t$ as taken into differential operator (because it is second order term as known by (1.19)),

$$\frac{\partial A}{\partial t} + \vec{\nabla}\cdot\vec{F} = 0, \tag{1.24}$$

where

$$A = \frac{\rho_0 [q^{*2}]}{2[q]_y}, \tag{1.25}$$

is called wave-activity density that is proportional to the squared amplitude of waves. Taking (1.11) into consideration, we obtain

$$A = \frac{(K^2 + \frac{f_0{}^2}{4HN^2})^2 \psi_0^2}{4[q]_y}, \tag{1.26}$$

and

$$\vec{F} = (0, -\frac{1}{2}\rho_0 kl\psi_0^2, \frac{1}{2}\rho_0 \frac{f^2}{N^2} lm\psi_0^2). \tag{1.27}$$

Thus the following relation on a meridional plane can be obtained,

$$\vec{F} = \vec{C}_g A, \tag{1.28}$$

which shows that the E-P flux is proportional to group velocity and its proportionality constant is wave-activity density A. Thus the E-P flux is also called as a wave-activity flux. (1.24) and (1.28) express conservation relation of wave-active density under the condition without friction and diabatic heating and thus wave activity is conserved along wave group propagation. In addition, (1.23) and (1.24) suggest that the zonal-mean state would not be changed by wave forcing if the divergence of the E-P flux is zero. Under this condition, divergence of meridional heat and momentum fluxes is canceled out mutually, which is called "nonaccelaration condition" (Charney and Drazin 1961).

The direction of wave propagation in a meridional plane is controlled by the zonal mean westerly structures (Karoly and Hoskins 1982). If k is constant along a ray path, ω is a function only of y, z and K^2;

$$\omega = F(y, z, K^2). \tag{1.29}$$

Thus, the group velocity in a meridional plane may be written as

$$C_{gy} = \frac{\partial \omega}{\partial l} = 2l \frac{\partial F}{\partial (K^2)}, \tag{1.30}$$

$$C_{gz} = \frac{\partial \omega}{\partial m} = 2m \frac{\partial F}{\partial (K^2)}. \tag{1.31}$$

Thus the ratio of the vertical and meridional components of the group velocity is

$$\frac{C_{gz}}{C_{gy}} = \frac{m}{l} \equiv \tan\theta_{ml}. \tag{1.32}$$

For a prescribed wave frequency ω, the corresponding K_ω is defined. Then

$$\frac{\partial F}{\partial y} + \frac{\partial F}{\partial (K^2)} \frac{\partial K_\omega^2}{\partial y} = 0, \tag{1.33}$$

$$\frac{\partial F}{\partial z} + \frac{\partial F}{\partial (K^2)} \frac{\partial K_\omega^2}{\partial z} = 0. \tag{1.34}$$

Using (1.31), (1.32) and

$$\frac{d_g l}{dt} = -\frac{\partial F}{\partial y}, \tag{1.35}$$
$$\frac{d_g m}{dt} = -\frac{\partial F}{\partial z}, \tag{1.36}$$

where $\frac{d_g}{dt}$ denotes the derivative along the group velocity vector, we obtain,

$$\frac{d_g \theta_{ml}}{dt} = \frac{K_\omega}{K_\omega^2 - k^2} \vec{i} \cdot \vec{C}_g \times \vec{\nabla} K_\omega, \tag{1.37}$$

where $\vec{i}$ is a unit vector in the zonal (x) direction. Thus the ray is refracted toward the direction of larger K_ω. If the westerly wind speed increases with height under the condition of constant $[q]_y$, K^2 decreases. Upward propagating waves ($m > 0$) cannot propagate beyond the level $[u] = U_{ck}$ ($m = 0$) defined in (1.9), where the waves are refracted downward ($m < 0$). The level is called a turning level[2].

1.3 Dynamical influences of the stratosphere on the troposphere

Recently, the dynamical influence of the stratosphere *downward* on the troposphere has been discussed intensively due to its implications for extended-range weather forecasting and the climate variability. As a pioneer work on such an influence, Geller and Alpert (1980) argued on the basis of their numerical experiment that variations in the stratospheric polar-night jet (PNJ) induced by the anomalous solar ultraviolet radiation could influence the tropospheric circulation by modifying vertically propagating planetary waves. Likewise, Boville (1984) showed through his model experiments that changes in the stratospheric PNJ could alter the tropospheric circulation characteristics by modulating planetary wave propagation.

[2]There is a term "critical level" in relation to vertical propagation. The critical level corresponds to the level at which $[u] = C_{px}$. Near the level, K^2 increases toward infi nity and hence waves are directed toward and trapped around the critical level with being their group velocity decreased.

Kodera *et al.* (1990) found that the enhanced upper-stratospheric PNJ in December tends to be followed by the stronger tropospheric westerlies in February over the Arctic region (Fig. 1.4). In that process, weak anomalies in the zonal-mean zonal wind first appear in the stratosphere and then propagate downward into the troposphere within a month, accompanied by anomalous meridional propagation of planetary waves (Kodera *et al.* 1991).

Kodera and Chiba (1995) argued that during and after an SSW event, the modification in the zonal wavenumber 2 (k=2) component of tropospheric planetary waves tends to give rise to a surface cold surge, which leads to the enhancement of stormtrack activity in the North Atlantic and the subsequent blocking formation downstream. Yoden *et al.* (1999) showed through a numerical experiment that zonally-symmetric warm anomalies in the stratospheric polar region and the associated weak westerlies in midlatitudes both tend to propagate downward into the troposphere only during an SSW event in which the k=2 planetary-wave component plays a primary role. In winters of El Niño years, the tendency of wetter and colder weather in the southeastern United States and Mexico is intensified after SSWs (Taguchi and Hartmann 2004).

Essentially the same downward influence of the anomalous stratospheric polar vortex in the NH on the troposphere as mentioned above has recently been discussed in the context of the NH annular mode (NAM). The NAM is characterized by a zonally-symmetric, barotropic seesaw pattern between the polar region and mid-latitude in the troposphere and, in winter, also in the stratosphere (Fig. 1.5). In the cold season, NAM anomalies that emerge rather irregularly in the stratosphere tend to propagate slowly downward into the troposphere within a few weeks (Fig. 1.6) (Baldwin and Dunkerton 1999; Kodera and Kuroda 2000ab; Kodera *et al.* 2000; Kuroda and Kodera 1999, 2001; Christiansen 2001; Thompson and Wallace 2001; Polvani and Kushner 2002; Zhou *et al.* 2002), which is considered to be associated with the interaction between the anomalous polar vortex and the anomalous propagation of planetary waves. Similar mode is also observed in the SH and called SH annular mode (SAM) (Thompson and Wallace 2000). Through the potential-vorticity (PV) inversion tech-

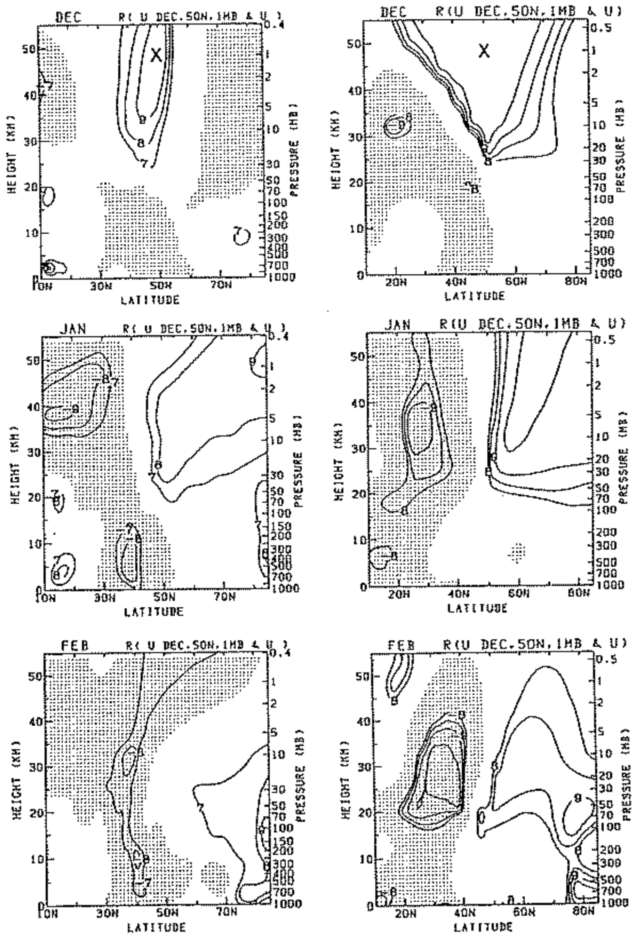

Figure 1.4: Meridional cross sections of the correlation coefficients between the averaged December mean zonal wind at 1 hPa, 50°N (noted by x in the figure) and the averaged monthly-mean zonal wind at each grid point; December (top panel), January (middle panel), and February (bottom panel). The left hand column is the correlation based on observed data and the right hand side column is based on numerical experiments. Values in the figure have been multiplied by 10 and region of negative values are stippled. Adapted from Fig. 2 of Kodera *et al.*(1990).

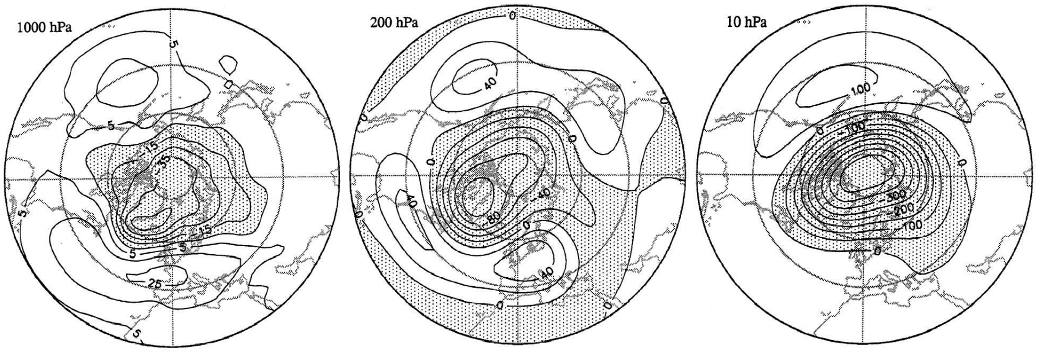

Figure 1.5: Signature of Arctic Oscillation (AO) at 10-, 200-, 1000-hPa levels. Adapted from Fig. 1 of Baldwin and Dunkerton (1999).

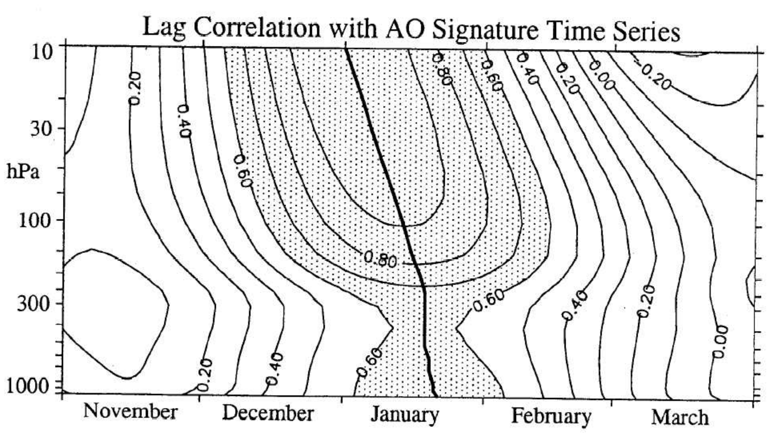

Figure 1.6: Correlations of 90-day low-pass-filtered AO signature at 10-hPa level on January 1 with AO signature at all levels. Adapted from Fig. 5 of Baldwin and Dunkerton (1999).

nique, Hartley *et al.* (1996) showed that the anomalous polar vortex in the lower stratosphere can exert a significant influence upon the tropospheric circulation particularly over the North Atlantic.

Perlwitz and Harnik (2003, hereafter referred to as PH03; 2004) discussed the influence on the tropospheric circulation of the downward propagating planetary waves from the stratosphere that have originated in the troposphere and then been reflected surface back at a “reflecting surface” in the stratosphere that is formed in association with negative vertical

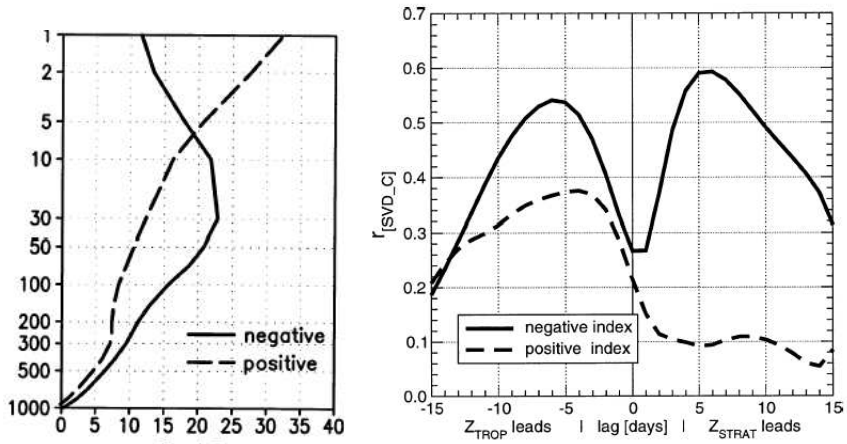

Figure 1.7: (a) Composites of vertical profiles of monthly-mean, zonal-mean zonal wind averaged between 58°N and 74°N for positively sheared (positive months; dashed line) and negatively sheared (negative months; solid line) months between 2- and 10-hPa levels. Adapted from Fig. 11c of Perlwitz and Harnik (2003). (b) The temporal expansion coefficients determined from the time-lagged SVD analyses between 500-hPa k=1 and 10-hPa k=1 components for JFM. The subset is chosen for negative or positive months. A positive time lag indicates that the stratospheric field is leading. Note that in negative months (solid line), signal of amplification of tropospheric k=1 component 5 days before stratospheric k=1 component. Adapted from Fig. 13 of Perlwitz and Harnik (2003).

westerly shear (Fig. 1.7). Meridional PV gradient may be approximately written as;

$$[q]_y = \beta - [u]_{yy} - \frac{f^2}{N^2}[u]_{zz} + \frac{f^2}{N^2 H}[u]_z. \tag{1.38}$$

The third term of the right hand side can be negative associated with a decreasing zonal-mean zonal wind speed with height, which contributes to decreasing K (1.14) to yield m=0. Although the downward propagation of planetary waves has been suggested by several authors (Sato 1974; Bates 1977; Hayashi 1981), PH03 is the first to clearly show the amplification of k =1 component in the troposphere associated with the reflection.

1.4 Zonally-propagating wave packets in the stratosphere

1.4.1 Wave-packet propagation in zonally homogeneous flow

Most of the previous studies as mentioned above focused on the entire field of stratospheric planetary waves or their zonal harmonics in relation to the variability of a zonally-symmetric polar vortex and/or PNJ. However, not much attention has been paid to localized circulation anomalies associated, for example, with a zonally-confined Rossby wave-packet-like structure that propagates zonally as well as vertically. Specifically, not many attempts have been made to identify which particular localized circulation anomalies in the troposphere are the origin of given anomalous behavior of stratospheric planetary waves.

Hayashi (1981) was perhaps the first to introduce such a wave-packet framework into the study of the stratospheric planetary waves. He argued that the dominance of the Aleutian high in the NH wintertime stratosphere in the climatological mean state could be explained if the planetary waves are considered to behave as a wave packet that consists of the k=1-3 components propagating from the tropospheric wave source over the Eurasian continent into the stratosphere over the Aleutians (Fig. 1.8). He noted that application of such a wave-packet framework to stratospheric planetary waves that consist of k=1-3 components might be not adequate mathematically because *the amplitude modulation of midlatitude planetary waves consisting wavenumbers 1 $\sim$ 3 cannot be easily distinguished from their phase variation.* In other words, wave packets may not be confined locally enough to distinguish them from their basic state, i.e. zonally-averaged state. This is the reason why most of the previous works on planetary-scale waves in the stratosphere did not discussed zonally propagating wave packets, but focused on the propagation of zonal harmonics of planetary waves in a meridional plane, which can be discussed under less assumptions without loosing mathematical strictness. However, Hayashi (1981) also note that *their envelope can be visually traced by use of a complex Fourier analysis* [3] , even if at the cost of mathematical strictness.

[3] The complex Fourier analysis is a method to obtain envelope of a wave packet that consists of arbitrary zonal wavenumber components. The envelope is presented in Fig. 1.8.

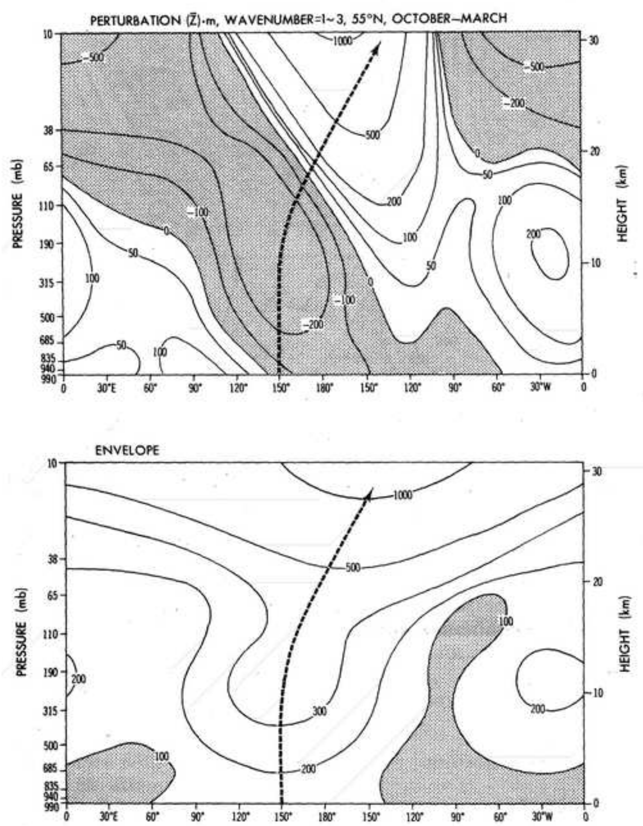

Figure 1.8: Upper panel; Zonal cross sections of October-March averaged geopotential height deviations from zonal mean along 50°E simulated by 11-year GFDL GCM. Lower panel; their envelope consisting of k=1-3. Dashed line indicate the position of the zonal maximum of the envelope. Envelop is obtained by a complex Fourier analysis. Adapted from Fig. 3 of Hayashi (1981)

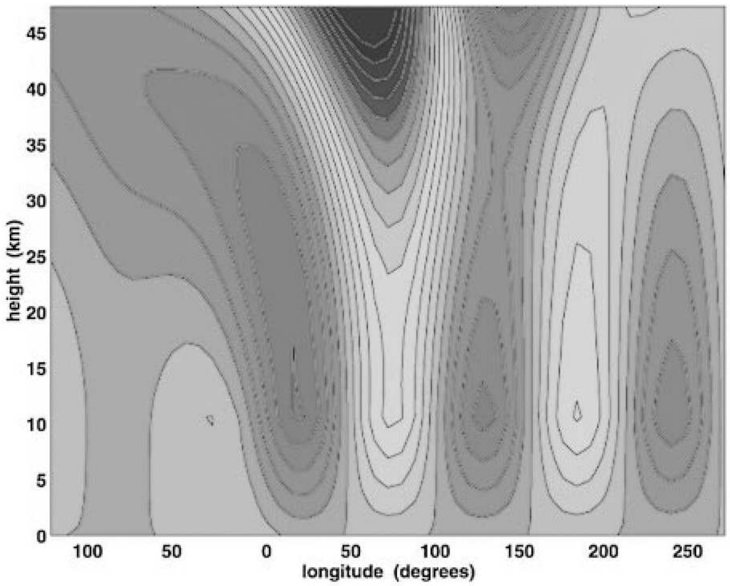

Figure 1.9: Streamfunction response to orography in a QG model on a β plane with uniform Brunt-Väisälä frequency, in which the mean zonal flow is linear in height below the tropopause (at 10 km) and uniform above the tropopause. The orography and the solution are assumed to be independent of latitude. The orography is centered at 0° longitude. Adapted from Fig.4 of Held *et al.*(2002).

By using linearized QG model on a β plane with the zonal-mean flows being linear in height below the tropopause and uniform above the tropopause, Held (1983) shows the two-dimensional (x-z) response of streamfunction to a localized topographic source as a delta function by integrating 1.3 [4] (Fig. 1.9). The response shows that an eastward and upward propagating wave train into the stratosphere of large scale and only eastward propagating wave train with its maxima around the tropopause of small scale are observed separately. This result is consistent with the condition of vertical propagation (1.9), which indicates that only large-scale wave components can propagate upward into the stronger westerlies.

Plumb (1985) discussed localized sources of planetary waves in the wintertime NH troposphere including zonally-confined upward wave-activity propagation across the tropopause,

[4] In actual, a damping term equivalent to 5 days is added.

by deriving his wave-activity flux with log-pressure coordinate as

$$\vec{F} = \frac{p}{2} \begin{pmatrix} v^{*2} - \psi^* v_x^* \\ -u^* v^* + \psi^* u_x^* \\ \frac{f_0 R_a}{N^2 H_0}(v^* T^* - \psi^* T_x^*) \end{pmatrix}, \tag{1.39}$$

which expresses three dimensionally propagating wave packets on zonally-symmetric basic state. This is an extension of the conventional E-P flux (1.21). He suggested that the orographic effect of the Tibetan plateau and diabatic heating and/or interaction with transient eddies in the western North Atlantic and North Pacific Oceans and Siberia are important for the generation of upward propagating planetary waves into the stratosphere.

Randel (1988) presented a statistical signature of wave packets in the wintertime stratosphere propagating upward and eastward from localized tropospheric origins in the Southern Hemisphere (SH) by using one-point correlation in which base points were set near the tropopause (Fig. 1.10). Especially in October (right column), a wave train that consists of a sequence of positive and negative correlations propagates eastward and upward with time that can be known from the fact that maxima of correlations move upward and downward correlations with time.

Nishii and Nakamura (2004b) found that the breakdown of the SH polar vortex in late September 2002 that led to the collapse of the ozone hole, associated with a major SSW event observed for the first time in the SH, was associated with amplification of a Rossby wave train in the stratosphere (Fig. 1.11a). The formation of this wave train was contributed to by upward and eastward wave activity propagation as a form of a wave train (Fig. 1.11b), which was excited by a blocking flow configuration over the South Atlantic (denoted by H in Figs. 1.11b and c). This work was the first to pinpoint the wave source of stratospheric planetary waves that amplified during a SSW event. In the study of Nishii and Nakamura (2004b), zonally-propagating Rossby wave packets in the stratosphere were diagnosed by

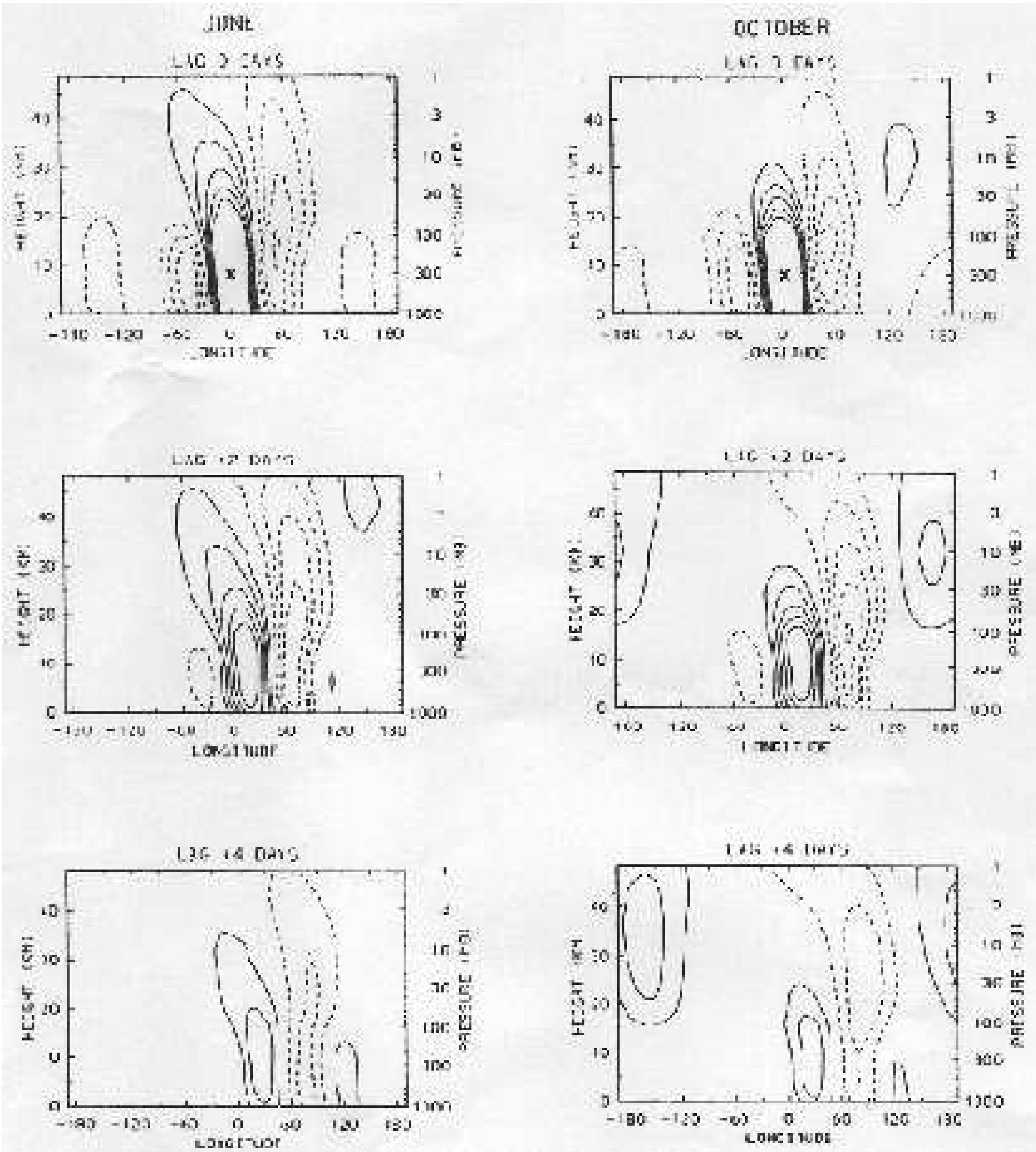

Figure 1.10: Longitude and height sections of height correlation coefficients with respect to 300-hPa, for time lags of 0 (top), +2 (middle), and +4 (bottom) days, for June (left column) and October (right column). Contours for ± 0.075, ± 0.150,..,. The base grid of correlations are shown by x. Note that a wave train propagating from the troposphere to stratosphere. Adapted from Fig. 11 of Randel (1988).

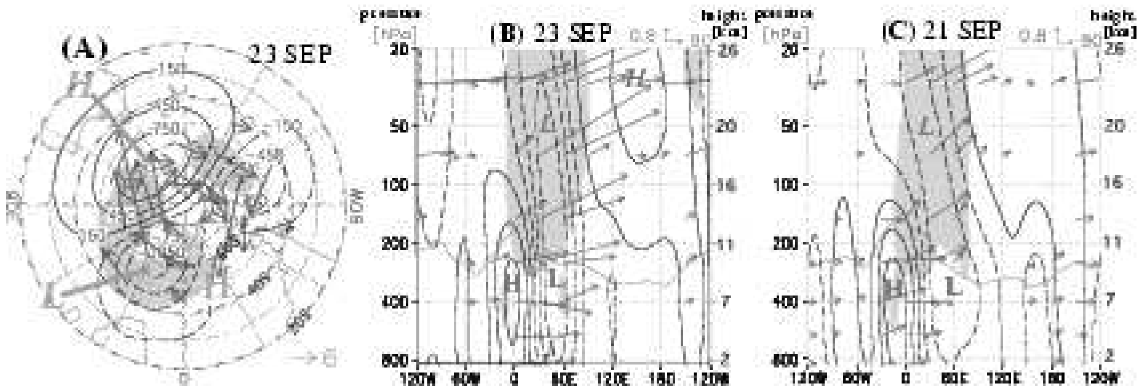

Figure 1.11: (a) 5-day mean map of the zonally-asymmetric component of 20-hPa height (m) for 23 September, 2002. Contour lines : wave-associated cyclonic (dotted) and anticyclonic (solid) eddies. Arrows: horizontal component of 20-hPa wave-activity flux (Plumb 1985) with scaling (unit: $m^2\ s^{-2}$) at the lower-right corner. Shading: the upward flux component across the 100-hPa surface exceeding 0.04 ($m^2\ s^{-2}$). (b, c) As in (a), but for zonal sections at 50°S for (b) 23 and (c) 21 September. Height anomalies are normalized by pressure. Thick line : tropopause. Arrows : Zonal and vertical components of the wave-activity flux (Plum 1985), with scaling ($m^2\ s^{-2}$) at the upper-right corner. Shading: the upward flux component exceeding 0.04 ($m^2\ s^{-2}$). Adapted from Fig. 2 of Nishii and Nakamura (2004b).

wave-activity flux formulated by Plumb (1985). It is noteworthy in Fig. 1.11b, that in association with upward wave packet propagation, or more precisely, wave-activity propagation (denoted by arrows and yellow shading), phase lines are tilted westward with height, which is consistent with the discussion on (1.15) $\sim$ (1.17).

1.4.2 Zonally asymmetric behavior of wave packets in the stratosphere

In those aforementioned studies, planetary waves in the stratosphere are regarded as deviations from the zonal-mean circulation field, i.e., zonally-symmetric field, on which characteristics of the wave propagation depend. In constant, another framework in which circulation fields are decomposed into fast and slowly varying components that are regarded as wave and basic state components, respectively, is common in studies on a tropospheric circulation. In this framework, wave disturbances can propagate zonally as wave packets and their propagating characteristics depend on the zonally-asymmetric field, which modulates a wave component as persistent deviations from the zonal-mean state. Therefore, wave packets are part of the entire planetary waves.

One may raise a question whether propagation of a stratospheric Rossby wave can depend on zonally-asymmetric basic state. In the work of Randel (1988) stated above (Fig. 1.10), 36 correlation patterns obtained for every 10° in longitude were averaged without considering their differences. The data period for this study was only 8 years from 1979 to 1986. Now we re-examine his work especially on the longitudinal dependence of wave propagation characteristics. The data set used here has been provided by the cooperative project of the JRA-25 long-term reanalysis by the Japan Meteorological Agency (JMA) and Central Research Institute of Electric Power Industry (CRIEPI). The data have been provided on a regular 2.5°×2.5° latitude-longitude grid at 23 pressure levels of 1000, 925, 850, 700, 600, 500, 400, 300, 250, 200, 150, 100, 70, 50, 30, 20, 10, 7, 5, 3, 2, 1 and 0.4 hPa levels. Since the production of this data set has not yet been completed, the data from 1980 to 1999 are used in this study. A low-pass digital filter with a cut-off period of 8 days has been imposed on the data time series to remove high-frequency fluctuations associated with migratory, synoptic-scale disturbances. Then its 31-day running mean is removed from the data to obtain submonthly fluctuations.

Figure 1.12 shows one-point correlation maps based on the reference time series at 400-hPa, (60°S, 90°W) over the eastern Pacific in August. On the lag of -3 day, a wave train confined in the troposphere is observed. Then downstream (eastward) of the base point, negative signal elongated upward into the stratosphere for the lag of 0 day. On the lag of +3 day, a wave train, which consists of positive (around 80°W), negative (around 100°W) and positive (around 60°E) correlations, is propagating eastward and upward into the stratosphere. On the contrary, no significant signal is not observed in the stratosphere in the corresponding correlation maps based on the time series at 400-hPa, (60°S, 90°E) over the Indian Ocean (Fig. 1.13). This different behavior of the wave propagation between over the Indian Ocean and eastern Pacific suggests that the characteristics of wave propagation depend on the longitudinal direction. This results indicate that a zonally-asymmetric basic state is important

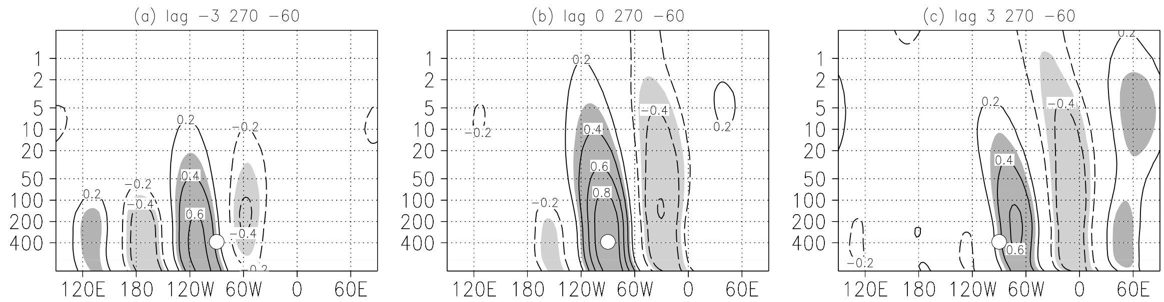

Figure 1.12: (a) Zonal cross section along 60°S latitude of one-point correlation maps based on 400-hPa, 90°W-60°S grid with -3 lag day in August. Solid and dashed contours denote positive and negative. Contour interval is 0.2 and zero lines are omitted. Heavy and lightly shading denotes positively and negatively significant signal over 95% level, respectively. The degree of freedom is estimated as such one month is equivalent to two. The reference grid is pointed by a circle. (b) The same as in (a) but for lag 0 day. (c) The same as in (a) but for lag 3 day.

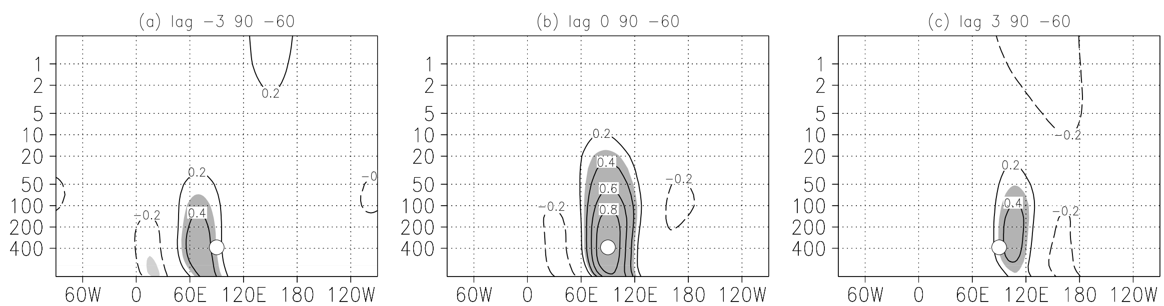

Figure 1.13: (a) The same as in Fig. 1.12a but for 90°E and 60°S grid. (b) The same as (a) but for lag 0 day. (c) The same as (a) but for lag -3 day.

for Rossby wave packet propagation even in the stratosphere.

1.4.3 Stratospheric wave packets propagating in zonally asymmetric basic state

Applying a framework that a wave packet propagation depends on a zonally-asymmetric basic state to the stratospheric planetary waves, Nakamura and Honda (2002; hereafter referred to as NH02) showed that tropospheric circulation anomalies in February over the North Atlantic emit a quasi-stationary Rossby wave train upward into the lower-stratospheric PNJ over the Eurasian continent.

Nishii and Nakamura (2004a; hereafter referred to as NN04) analyzed dynamical characteristics of submonthly geopotential height fluctuations observed in the SH lower stratosphere during late winter and early spring of 1997. They showed that those fluctuations were often associated with zonally-confined Rossby wave trains that had originated from quasi-stationary tropospheric anomalies. The upward and eastward propagation of those wave trains was found sensitive to the zonally-asymmetric PNJ structure, which can be regarded as an important factor for the zonally-asymmetric distribution of the activity of the submonthly fluctuations observed in the SH lower stratosphere.

1.4.4 A wave-activity flux defined for zonally asymmetric basic fields

In the studies of NH02 and NN04, a wave-activity flux formulated by Takaya and Nakamura (2001; hereafter referred to as TN01) was used to represent three-dimensional propagation of quasi-stationary Rossby waves in the zonally-inhomogeneous westerlies. This is an extension of Plum's (1985) wave-activity flux (1.39) into a zonally-asymmetric basic state. Its expression in the logarithm pressure coordinate may be given as

$$\vec{W} = \frac{p}{2|\vec{U}|}\begin{pmatrix} U(v'^2 - \psi' v'_x) + V(-u'v' + \psi' u'_x) \\ U(-u'v' + \psi' u'_x) + V(u'^2 + \psi' u'_y) \\ \frac{f_0 R_a}{N^2 H}\{U(v'T' - \psi' T'_x) + V(-u'T' - \psi' T'_y)\} \end{pmatrix}, \tag{1.40}$$

where a prime $()'$ denotes perturbation from time-mean field, (U,V) the geostrophic basic-flow velocity, p the normalized pressure and N the Brunt-Väisälä frequency defined for the basic flow. This flux is also written as;

$$\vec{W} = \vec{C}_g M, \tag{1.41}$$

where M denotes the wave-activity pseudomomentum. This is an extension of (1.28) to three-dimensional wave packet propagation. The wave-activity pseudomomentum is a linear combination of two quantities, one is proportional to wave enstrophy and the other to wave energy, as;

$$M = \frac{p}{2}\left(\frac{q'^2}{2|\vec{\nabla}_H Q|} + \frac{e}{|\vec{U}| - C_p}\right) \tag{1.42}$$

where $\vec{\nabla}_H$ denotes a horizontal gradient operator, Q signifies quasi-geostrophic PV of the basic flow, e wave energy and C_p wave phase speed. The first term of the right hand side of (1.42) is equivalent to wave-activity density defined in (1.25), and the second term is equivalent to pseudomomentum (Uryu 1974). These two quantities are equivalent if the perturbations (i.e. anomalies) are replaced with deviations from the zonal mean (i.e. eddies) and then zonally averaged (TN01). Since the first term is related to the square of ψ' (maximum at a wave loop) the second term to the squares of u' and v' (maximized at a wave node), they are 90° out of phase. M and hence $\vec{W}$ are independent of wave phase if the wave has a sinusoidal form. Moreover, $\vec{W}$ is parallel to the local three-dimensional group-velocity vector or, more precisely, the "wave-activity velocity" (Harnik 2002). Hence $\vec{W}$ is suited for representing a "snapshot" of a propagating Rossby wave packet. M and $\vec{W}$ satisfy conservation relation;

$$\frac{\partial M}{\partial t} + \vec{\nabla} \cdot \vec{W} = 0, \tag{1.43}$$

which is an extension of (1.24), showing that convergence (divergence) of $\vec{W}$ acts to increase (decrease) M locally. It is noteworthy that $\vec{W}$ applied to quasi-stationary anomalies embedded in a zonally-varying time-mean flow accounts only for a fraction of the corresponding flux associated with the entire field of planetary waves that can be evaluated by using Plumb's (1985) wave-activity flux (1.39). Thus, the vertical propagation of stationary Rossby wave trains can be either upward or downward depending on time and location, despite the general tendency that the wave-activity flux of the entire planetary waves is upward because they are forced in the troposphere.

1.4.5 A refractive index

As another useful tool for diagnosing wave propagation characteristics, a so-called refractive index (κ_s) [5] is used for representing mean-flow properties with respective to the propagation of stationary Rossby waves. This index is an extension of K defined in (1.14) on a meridional plane into a zonally-asymmetric basic flow, in a manner similar to those in Karoly (1983) and Hoskins and Ambrizzi (1993):

$$\kappa_s^2 = \frac{|\vec{\nabla}_H Q|}{|\vec{U}|} - \frac{f^2}{4N^2H_0^2}. \tag{1.44}$$

In this definition, $\vec{\nabla}_H$ denotes the horizontal gradient operator, Q, which signifies quasi-geostrophic PV of the basic flow. The derivation is referred to NN04.

As a extension of (1.37), a tendency in the direction of group velocity has the following relation with the gradient of κ_s in a zonal cross section assuming that variations of k is sufficiently small;

$$\frac{d_g\theta_{km}}{dt} = \frac{\kappa_s^2}{\kappa_s^2 - l^2}\vec{j}\cdot\vec{C}_g \times \vec{\nabla}\kappa_s, \tag{1.45}$$

where $\tan\theta_{km}$ is equal to the ratio of the vertical and zonal group velocity components, $\vec{j}$ denotes unit vector in the meridional direction positive northward. A similar relation holds for on the horizontal plane as well as the meridional plane. Hence, a wave packet tends to be refracted toward the gradient of the refractive index. A band of maxima of the index, if locally defined in the WKB sense, represents a localized waveguide of those waves if the band is associated with a westerly jet.

In the derivation of the wave-activity flux and refractive index κ_s, so-called "local coor-

[5] The ordinary refractive index for each zonal wave number (n_k) is equivalent to square root of $l^2 + m^2$ and the form is obtained from (1.13) and (1.14). Thus κ_s may be appropriate to be called as a "total wave number".

dinate rotation" technique is used (TN01 [6], NN04). (1.2) may be linearized as:

$$\frac{\partial q'}{\partial t} + \vec{U} \cdot \vec{\nabla}_H q' + \vec{u}' \cdot \vec{\nabla}_H Q = 0. \tag{1.46}$$

By using the "local coordinate rotation" technique, (1.46) is converted onto the local X-Y coordinate system with the X-axis taken in the direction of $\vec{U}$ and the Y-axis perpendicular to it (poleward if $Y > 0$) at a particular location. It follows that,

$$\frac{\partial q'}{\partial t} - \frac{\partial \Psi}{\partial Y}\frac{\partial q'}{\partial X} + \frac{\partial Q}{\partial Y}\frac{\partial \psi'}{\partial X} - \frac{\partial Q}{\partial X}\frac{\partial \psi'}{\partial Y} = 0. \tag{1.47}$$

Now, we consider a steady, nearly unforced basic flow,

$$\vec{U} \cdot \vec{\nabla}_H Q \approx 0, \tag{1.48}$$

which yields $\frac{\partial Q}{\partial X} \approx 0$ since the Y-component of the basic flow is zero. Thus (1.47) becomes,

$$\frac{\partial q'}{\partial t} + U\frac{\partial q'}{\partial X} + \frac{\partial Q}{\partial Y}\frac{\partial \psi'}{\partial X} = 0, \tag{1.49}$$

which corresponds to (1.3) that is linearized about the zonal-mean flow in x-y coordinate. The derivation of the wave-activity flux and refractive index are essentially the same as in the X-Y coordinate system as in the case of a zonally uniform basic state in the x-y coordinate system. It is important to note that the "local coordinate rotation" technique requires the WKB-type approximation in which variations in the basic state are sufficiently weak. In addition, (1.48) assumes an unforced time-mean flow, which strictly speaking, is not valid in the real atmosphere. Therefore, our argument on results obtained under these assumptions in the following chapters must be kept qualitative.

[6] In TN01, derivation of the wave-activity flux using this technique is presented as a second way.

1.4.6 An example of applying a wave-activity flux and refractive index to the zonally-asymmetric PNJ

As an example for an application of the wave-activity flux and refractive index (κ_s) to upward wave-activity propagation from the troposphere into the stratosphere, some results of NN04, which suggest importances of zonally-inhomogeneous westerly structure and zonally-localized wave sources on upward wave propagation in the SH stratosphere, are reviewed in this subsection.

Figures 1.14a and c, taken from NN04, show the meridional sections of the refractive index κ_s defined for 31-day mean, zonally-averaged field (1.14) with its maximum shaded and averaged periods are for (a) 16 June $\sim$ 16 July, 1997 (Period I) and for (b) 17 July $\sim$ 16 August, 1997 (Period II). Waveguide structures of maximum κ_s regions in the lower-stratosphere are well defined in both periods. Activity of zonally-averaged submonthly fluctuations, $Z_s = \sqrt{[\overline{z_*'^2}]}$, is shown in Figs. 1.14b and d are for Periods I and II. The activity of the tropospheric submonthly fluctuations, which are considered as a source of upward propagating wavy disturbances into the stratosphere, is nearly the same between the two periods. However, the stratospheric submonthly fluctuations are weaker in Period I. Simultaneously, the E-P flux (1.21), estimated with zonally-asymmetric components of submonthly fluctuations (arrows in Figs. 1.14a and c), is also weaker in Period I than Period II.

This paradoxical result motivated us toward further analysis in which the zonally-asymmetric basic filed and locally-confined wave propagation are taken into consideration. Figures 1.15a and c show 31-day mean 400-hPa westerly wind for Period I (16 June $\sim$ 16 July, 1997) and for Period II (17 July $\sim$ 16 August). Standard deviation of submonthly geopotential height fluctuations corresponding to Periods I and II are presented in Fig. 1.15b and d, respectively. In both periods, geopotential height fluctuations are particularly strong in the Southeastern Pacific and South Atlantic. However upward wave activity propagation over those regions is much weaker in Period I than in Period II.

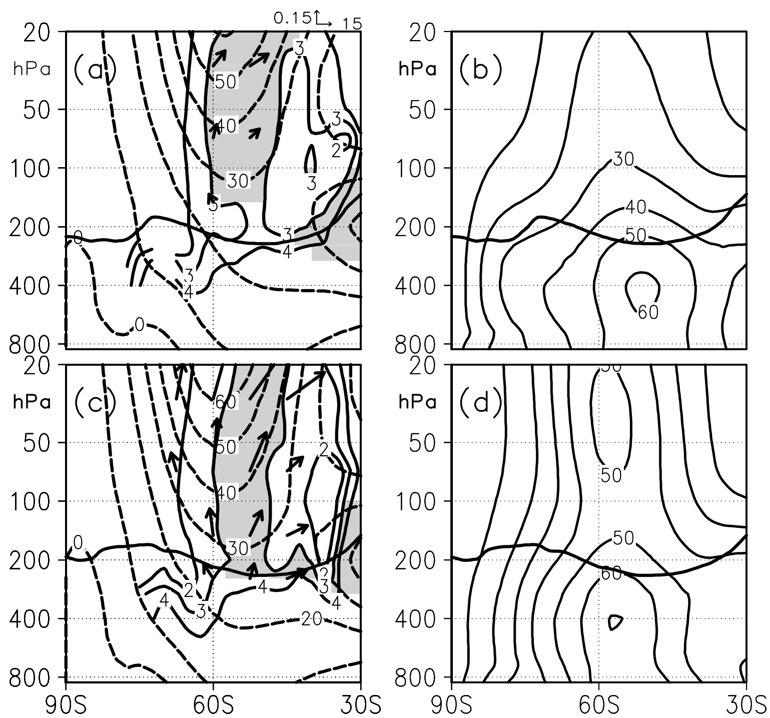

Figure 1.14: Meridional sections of (a) the zonal-mean U (dashed lines: every 10 ms^{-1}) and refractive index for stationary Rossby waves (κ_s) defined for the zonal-mean flow (solid line), superimposed on the E-P flux (arrow;scaling is at the right-upper corner; unit: m^{2}s^{-2}) for Period I (16 June $\sim$ 16 July, 1997). Shading indicates the regions for $\kappa_s \geq 3$ and $U \geq 35$ [ms^{-1}]. A heavy line indicates the tropopause defined by the NCEP. (b) As in (a), but for the standard deviation of submonthly geopotential height fluctuations normalized by pressure (contoured for every 10 m). (c, d) As in (a) and (b), respectively, but for Period II (17 July $\sim$ 16 August).

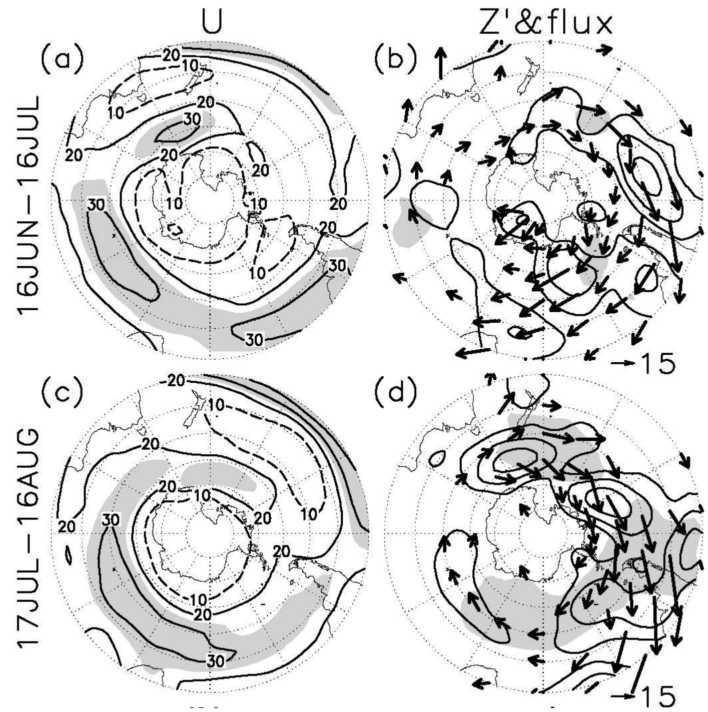

Figure 1.15: (a) Mean 400-hPa westerly wind speed (U: every 10 ms^{-1}; dashed for U=10 ms^{-1}; shaded for $U \geq 25$ ms^{-1}) and (b) standard deviation of submonthly fluctuations $\sigma(\psi')$ in 400-hPa geopotential height (contoured for; 80, 110 and 140 m) superimposed on the horizontal component of a mean wave-activity flux (arrows), for Period I (16 June $\sim$ 16 July, 1997). In (b), shading indicates the upward component of the mean wave-activity flux at the 150-hPa level exceeding 0.01 [m^{2}s^{-2}]. Scaling of the arrows (unit; m^{2}s^{-2}) is given near the lower-right corner of the panel. (c,d): Same as in (a,b), respectively, but for Period II (17 July $\sim$ 16 August).

This difference may be caused by difference in local waveguide structure over the Southeastern Pacific between the two Periods (Figs. 1.16c and f). In Period I, the PNJ does not fully develop right above the tropopause and the vertical waveguide structure is not well defined, which is likely to prevent wave activity associated with submonthly fluctuations from propagating upward into the stratosphere. In fact, 100-hPa westerlies are weak over that region associated with minima in κ_s (Figs. 1.16 a and b). In contrast, in Period II, the westerlies become stronger and 100-hPa κ_s is maximized in this regions. Correspondingly, waveguide structure well develops vertically across the tropopause over the Southeastern Pacific, which leads to the enhanced wave-activity propagation into the stratosphere (Fig. 1.16f).

Thus, it is suggested that mismatch in longitudinal position between the localized tropospheric wave forcing and the local well-defined vertical waveguide right across tropopause may lead to the paradoxical results in the analysis based on the conventional framework.

1.5 Downward injection of wave activity from the stratosphere into the troposphere associated with wave packet propagation

1.5.1 The purpose of this study

In the entire field of planetary waves, the upward propagating component should be dominant because most of them are forced in the troposphere. However, one can image that a PNJ with a substantial westerly vertical shear, even if it were zonally uniform, would act as a "prism" that allows only the k=1 component (or maybe also the k=2 component) included in the wave train to transmit farther upward. The rest of the wave activity, associated mainly with the higher harmonics ($k \geq 2$), would be refracted back into the troposphere as implied by (1.37) and its related discussion.

Figure 1.17 illustrates this "prism effect" of an idealized PNJ in a β channel based on the ray tracing method. The westerlies are assumed to be zonally symmetric with a uniform

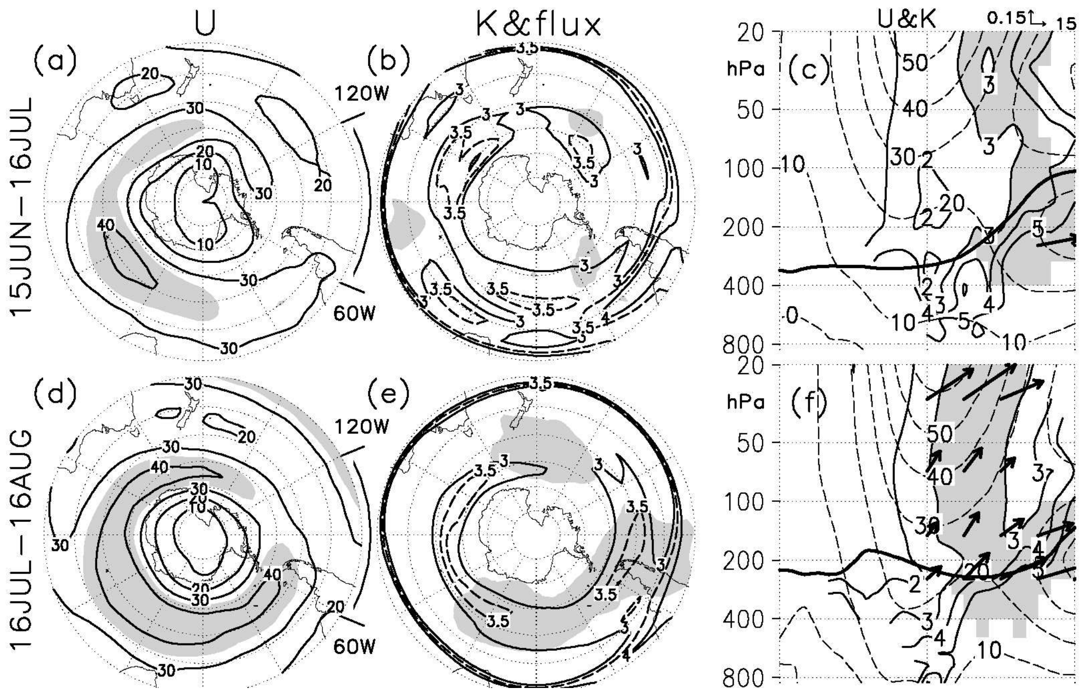

Figure 1.16: (a) Mean 100-hPa westerly wind speed (U: every 10 ms^{-1}; shaded for $U \geq 35$ ms^{-1}), (b) refractive index (κ_s) of stationary Rossby waves at the 100-hPa level, represented as the equivalent zonal wavenumber for each latitude, and (c) meridional section of κ_s (solid lines), U (dashed lines: every 10 ms^{-1}) and the meridional and vertical components of a mean wave-activity flux (arrows), all of which are averaged between 60°W and 120°W as indicated in (a), for Period I (16 June ∼ 16 July, 1997). In (b), shading is applied where the upward component of mean wave-activity flux exceeds 0.01 [m^{2}s^{-2}]. In (c), shading indicates the regions for $\kappa_s \geq 3$ and $U \geq 25$ [ms^{-1}], and scaling for arrows is given at the right-upper corner of the panel. A thick line the tropopause defined by the NCEP. (d,e,f): Same as in (a,b,c), respectively, but for Period II (17 July ∼ 16 August).

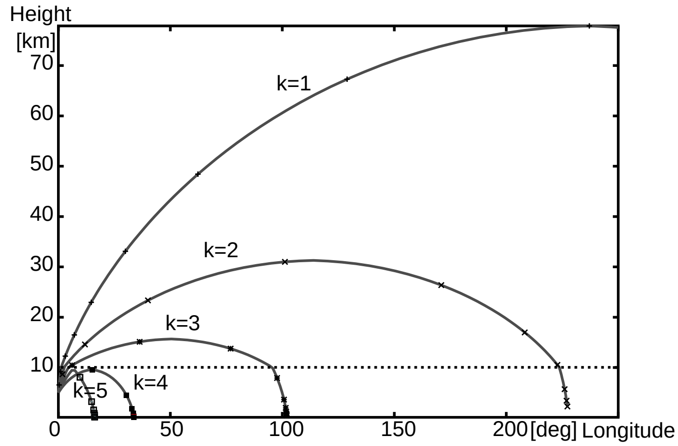

Figure 1.17: Ray tracing of stationary Rossby waves in a β channel at 60° S for individual zonal harmonics with zonal wavenumbers (k) 1 through 5 as indicated. The background westerlies are zonally homogeneous with a uniform vertical shear of 10 [m s^{-1}/10km] and no surface wind. Scale height (H) is fixed to 10 [km]. The "tropopause" is placed at the altitude of $z = H$, and the Brunt-Väisälä frequency is set to 0.02 [s^{-1}] and 0.01 [s^{-1}] above and below $z = H$, respectively. Distance between any pairs of symbols along each of the rays corresponds to the distance over which the ray can travel in a particular 24-hour period.

vertical shear and Brunt-Väisälä frequency in the stratosphere (above the 10-km altitude).

In contrast to PH03, in which downward propagation of Rossby wave activity occurred at a "reflecting surface" formated by anomalous negative vertical shear, downward wave-activity propagation illustrated in Fig. 1.17 is due to refraction of wave activity in the positively vertically sheared westerlies. Furthermore, unlike in PH03, where the downward propagation of the entire planetary waves is discussed, our primary focus is placed on a zonally confined wave packet that accompanies geographically localized circulation anomalies. The anomalies are only a fraction of the entire planetary waves that are modulated due to the superposition of those anomalies on the climatological wave field. This wave packet behavior is further discussed in Appendix A.

In such an idealized situation as depicted in Fig. 1.17, the upward as well as downward injection of Rossby wave activity across the troposphere can occur at any longitude. In reality, however, the upward injection exhibits an apparent geographical preference even in the SH in the presence of zonal asymmetries in the seasonal-mean westerlies (NN04). One would find a similar geographical preference also for the downward wave-activity injection, if it really occurs, across the tropopause.

In this study we show that wave activity associated with zonally-confined Rossby wave trains in the SH lower stratosphere can indeed propagate *downward*, contributing positively to the development of localized circulation anomalies in the troposphere. Localized in the zonal direction, the upward and downward wave-activity propagation associated with zonally-confined wave trains cannot be well depicted in the conventional framework of the zonal harmonic decomposition nor the Eliassen-Palm (E-P) diagnosis, which has characteristics as follows;

- The entire field at a given instance was decomposed into the zonally-symmetric component and deviations from it (i.e., eddies).
- The deviations are considered as planetary waves and often decomposed into zonal harmonics.
- Their propagation depends on the zonal-mean basic state.
- They propagate meridionally and vertically.
- A zonally-localized wave source can not be identified.
- Mathematically strict discussions can be made.

In contrast, those of the same framework as in NH02 and NN04 are;

- The entire field at a given instance was decomposed into the three-dimensional, zonally-asymmetric time-mean flow[7] and deviations from it (*i.e.*, anomalies).
- The anomalies are not decomposed into zonal harmonics and considered them as Rossby wave trains or packets.

[7] In this paper, we use the term "time-mean flow" to indicate seasonally varying flow whose time scales are much longer than those of the evolution of quasi-stationary circulation anomalies.

- Their propagation depends on the time-mean, zonally-asymmetric basic state.
- They propagate zonally as well as vertically and meridionally.
- A zonally-localized wave source can be identified.
- Mathematical strictness must be sacrificed to some extent.

Thus, in spite of loosing mathematical strictness, we will adopt the latter framework. Following those two studies of NH02 and NN04, we applied diagnostics suited for that framework.

1.5.2 Data set and analysis method

The data set used is a reanalysis data set of the U.S. National Centers for Environmental Prediction (NCEP) and the U.S. National Center for Atmospheric Research (NCAR) (Kalnay *et al.* 1996) from 1979 to 2003. The data have been provided on a regular $2.5^\circ \times 2.5^\circ$ latitude-longitude grid at each of the 17 standard pressure levels of 1000, 925, 850, 700, 600, 500, 400, 300, 250, 200, 150, 100, 70, 50, 30, 20, 10 hPa. A low-pass digital filter with a cut-off period of 8 days has been imposed on the four-time-daily data time series to remove high-frequency fluctuations associated with migratory, synoptic-scale disturbances. Seasonal evolution of the circulation is represented in the 31-day running-mean field, and the deviation of the low-pass-filtered field from the running-mean field corresponds to submonthly, quasi-stationary anomalies. Our choice of this filtering is to be discussed in Appendix B. Geopotential height anomalies have been multiplied by a factor (f_0/f) to mimic streamfunction-like anomalies (f: the Coriolis parameter; $f_0 = f(43^\circ S)$).

In order to depict three-dimensional group-velocity propagation of quasi-stationary Rossby wave trains both in the troposphere and lower stratosphere, a wave-activity flux of TN01 (1.40) is used. In this study, the 31-day running-mean field is regarded as the basic state in which quasi-stationary waves are embedded, and the low-pass-filtered anomalies are regarded as fluctuations associated with those waves.

For representing mean-flow properties with respective to the propagation of quasi-stationary waves, the refractive index κ_s defined as (1.44) is used and the all quantities have been evaluated on the basis of the 31-day running-mean field as in NN04. To keep consistency with WKB-type assumptions used in the derivation of the wave-activity flux of TN01, we use locally evaluated N. The terms that include vertical derivatives of N, which were included in the definition by Karoly and Hoskins (1982), have been neglected in our evaluation of κ_s, as in Chen and Robinson (1992), in recognition of the fact that vertical variations in N are generally small except in the immediate vicinity of the tropopause. Still, a discontinuity is present in κ_s across the tropopause, reflecting the corresponding discontinuity in N. The κ_s field has been smoothed by retaining only its zonal harmonic components of k=0$\sim$4, so as to be consistent with defining a waveguide structure for free stationary Rossby waves in the stratosphere.

It should be noted that the wave-activity flux and refractive index used in this study have been derived under WKB-type approximations of the sufficient slowness of zonal and time variations in the basic flow. Unlike in the troposphere, the validity of the approximations is not immediately obvious in the stratosphere, where only a few lowest zonal harmonics of planetary waves are allowed to propagate. One way to assess their validity in space may be through evaluating WKB parameters (Karoly and Hoskins 1982). For validity of WKB approximations change of wavenumbers must be sufficiently small, i.e.;

$$|\frac{\partial k^{-1}}{\partial x}| \ll 1, \qquad (1.50)$$

$$|\frac{\partial m^{-1}}{\partial z}| \ll 1. \qquad (1.51)$$

Since

$$\frac{\partial k^{-1}}{\partial x} = \frac{\frac{\partial \kappa_s}{\partial x}}{\kappa_s^2}(\frac{\kappa_s}{k})^3, \qquad (1.52)$$

$$\frac{\partial m^{-1}}{\partial z} = \frac{f}{N}\frac{\frac{\partial \kappa_s}{\partial z}}{\kappa_s^2}\left(\frac{\kappa_s}{\frac{f}{N}m}\right)^3, \tag{1.53}$$

(assuming that f/N variations are small) and the orders of κ_s/l and $\kappa_s/(f/Nm)$ are unity, a parameter

$$W_k = \frac{\frac{\partial \kappa_s}{\partial x}}{\kappa_s^2}, \tag{1.54}$$

for the zonal direction and another parameter

$$W_m = \frac{f}{N}\frac{\frac{\partial \kappa_s}{\partial z}}{\kappa_s^2}, \tag{1.55}$$

for the vertical direction may be reasonable indices (Karoly and Hoskins 1982). However, we do not have any appropriate method to estimate the validity of the WKB-type assumptions for time variations. As argued in NH02 and NN04, hence, the validity of the assumptions in our application may be justified *only a posteriori in a qualitative sense* by assessing a degree of localization of the wave-activity flux and its geographical correspondence with localized waveguide structure as revealed by the refractive index. Therefore, our argument in the rest of the study must be kept qualitative.

The structure of this dissertation is as follows. In Chapter II, case studies of upward and downward wave-activity propagation across the tropopause observed over the SH in late winter of 1997 are presented. Then the climatology and interannual variations of localized wave-activity propagation across the tropopause and its influences on the stratospheric and tropospheric circulations are explored in Chapter III. General discussions and concluding remarks are presented in Chapter IV.

Chapter 2

Case studies in SH late winter of 1997

2.1 Introduction

Figure 2.1a shows the vertical (net) component of the monthly-mean 100-hPa wave-activity flux associated with the low-pass-filtered submonhtly fluctuations averaged zonally along 60°S circle, which is considered to be an adequate indicator for wave-activity propagation across the tropopause. Figure 2.1b shows the corresponding monthly mean, but for the 100-hPa wave-activity flux. As a zonal average, the upward wave-activity propagation into the stratosphere dominates over the downward wave-activity injection. Nishii and Nakamura (2004a, hereafter referred to as NN04) showed that the upward wave-activity injection in the 1997 winter was in the form of zonally-confined wave trains. Meanwhile, the downward injection of wave activity was more active than in any other years from 1979 to 2003, the period in which the data set is available. As a typical example for depicting downward wave-activity injection across the tropopause and its influence on the local tropospheric circulation, we show a few cases observed in late winter of 1997 in the SH. Many of the results presented in this chapter have been published in Nishii and Nakamura (2005).

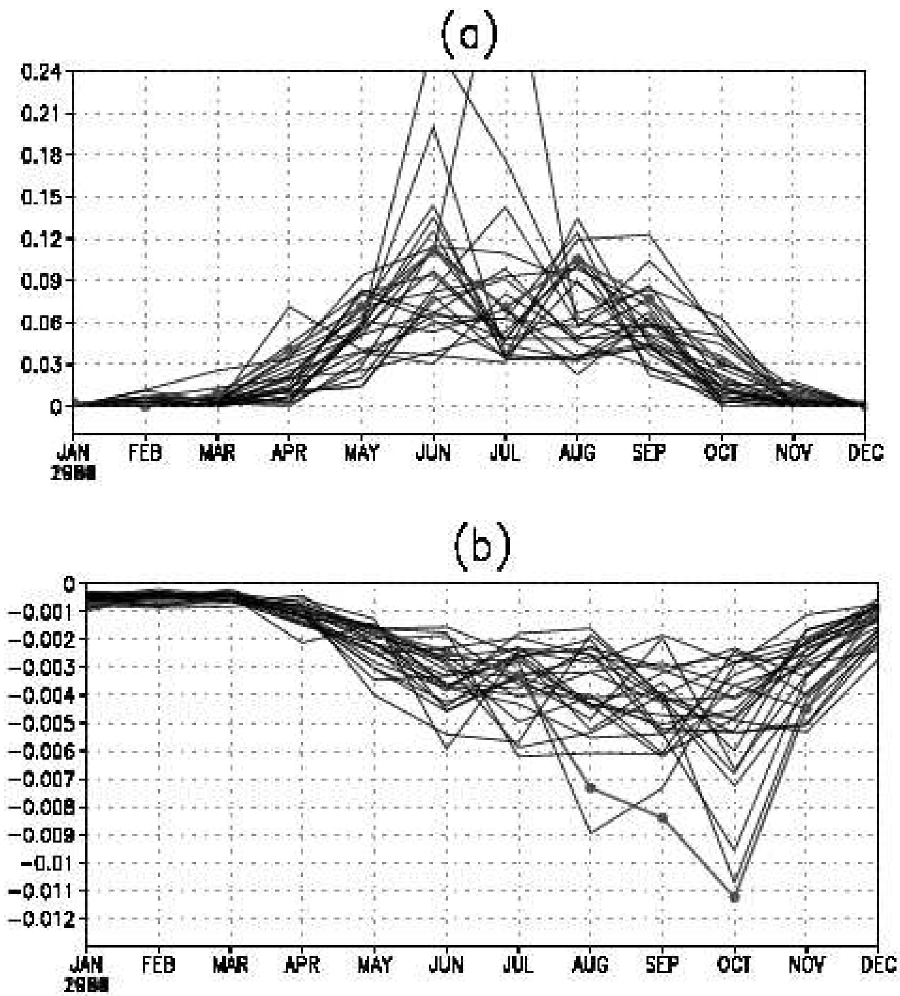

Figure 2.1: (a) Time series of zonal-mean monthly-mean vertical component of wave activity flux of TN01 at 100-hPa level along 60°S from 1979 to 2003. The unit is [m^2 s^{-2}]. A thick line with open circle denotes that of 1997. (b) The same as in (a) but for monthly mean of daily value of only negative (downward) component of wave activity flux. Note that the range of the vertical axes are different between (a) and (b).

2.2 An event of large-scale cyclogenesis in August 1997

2.2.1 Mechanisms of the cyclogenesis

As a typical example of a lower-stratospheric Rossby wave train influencing the tropospheric circulation, an event of large-scale cyclogenesis that occurred around 10 August of 1997 off the Antarctic coast to the south of Australia is investigated in this section. The quasi-stationary nature of the cyclogenesis is apparent in unfiltered sea-level pressure maps shown in Figs. 2.2a-c. Over the 5-day period centered at 10 August, the cyclone center exhibited its eastward phase migration of only ∼2000 km, which is substantially slower than a typical migration speed of an extratropical cyclone. In the NCEP/NCAR reanalysis data, the surface cyclone center deepened below 960 hPa on that day. The surface cyclogenesis was associated with the intensification of upper-tropospheric cyclonic anomalies (denoted by a square in Figs. 2.2d-f) within the subpolar jet (SPJ [1] ; see also Fig. 2.7a). The centers of the surface cyclone and the cyclonic anomalies aloft (the former is also denoted by a square in Figs. 2.2a-c) almost coincided with one another, indicative of their nearly equivalent barotropic structure typical for low-frequency tropospheric anomalies over the ocean (Blackmon *et al.* 1979). An incoming wave-activity flux into the cyclonic anomalies from the tropospheric anticyclonic anomalies upstream was modest (Figs. 2.2d-f). The barotropic feedback forcing from migratory synoptic-scale transient eddies ($\left(\frac{\partial Z}{\partial t}\right)_{HFT}$) on the cyclonic anomalies was evaluated in a manner described in Nakamura *et al.* (1997);

$$\left(\frac{\partial Z}{\partial t}\right)_{HFT} = \frac{f_0}{g}\nabla^{-2}\left[-\vec{\nabla}\cdot\left(\overline{\vec{v}'\zeta'}+\overline{\vec{v}\zeta'}+\overline{\vec{v}'\zeta}\right)\right],$$

where over bar and primes denote the 8-day low-pass- and high-pass-filtered quantities, respectively. ζ is the relative vorticity, f_0 the Coriolis parameter at 43°S ($\simeq \times 10^{-4}\mathrm{s}^{-1}$). $\left(\frac{\partial Z}{\partial t}\right)_{HFT}$ was quite weak around developing cyclonic anomalies when compared with the

[1] It is also referred to as a polar-front jet.

observed height tendency (Fig. 2.3) [2].

In the lower stratosphere (50 hPa), strong quasi-stationary anticyclonic anomalies were observed over the Indian Ocean during the same period (Figs. 2.2g-i). They were located slightly upstream of the developing tropospheric cyclonic anomalies of interest. This vertical structure is well depicted in zonal-height sections along 60° S in Figs. 2.2j-l [3] In the lower stratosphere (between the 200 and 50-hPa levels), phase lines of the streamfunction anomalies exhibited an apparent *eastward* tilt with height between the stratospheric anticyclonic anomalies upstream (around 100° E) and the tropospheric cyclonic anomalies downstream (around 130°E, indicated with a square in Figs. 2.2j-l), suggestive of downward propagation of quasi-stationary Rossby wave activity. Our wave-activity flux diagnosis reveals that the downward injection of wave activity across the tropopause was indeed pronounced within the upstream half of the tropospheric cyclonic anomalies of interest [4]. Especially on 8 August (Fig. 2.2j), when the cyclonic anomalies began to develop, the flux was dominantly downward below and slightly downstream of the stratospheric anticyclonic anomalies, extending downward into the mid- and lower troposphere. On 10 August (Fig. 2.2k), the flux was still dominantly downward except in the lower troposphere.

For an assessment of the importance of the downward injection of wave activity relative to its horizontal injection for a particular cyclogenesis of interest, the vertical and horizontal convergence of the wave-activity flux was evaluated separately (Figs. 2.4a and b, respectively). The vertical and horizontal convergence was found comparable in magnitude around

---

[2] $\left(\frac{\partial Z}{\partial t}\right)_{HFT}$ represents geopotential height tendency due solely to vorticity flux convergence associated with the migratory transient eddies. Since the f_0 is a constant, $\left(\frac{\partial Z}{\partial t}\right)_{HFT}$ is equivalent to a stream-function-like tendency. This quantity tends to overestimate the net effect of those eddies because it does not include the effect of eddy heat flux that acts to offset the barotropic feedback (Lau and Nath, 1991). In other words, the barotropic feedback sets an upper bound of the net transient eddy effect, and therefore the smallness of the former implies the primary importance of the low-frequency dynamics.

[3] In all the vertical sections in Figs. 2.2, 2.5, 2.12, 2.17, the wave-activity flux is weighted by pressure as in (1.40).

[4] Those anomalies were slowly moving eastward. Strictly speaking, the wave-activity flux plotted in those figures thus represents group-velocity propagation relative to the slowly-moving wave phase (TN01). Since the group velocities of those wave packets are much larger than their phase velocities, the flux nevertheless depicts the essential features of the observed wave packet propagation (Figs. 2.2d-j).

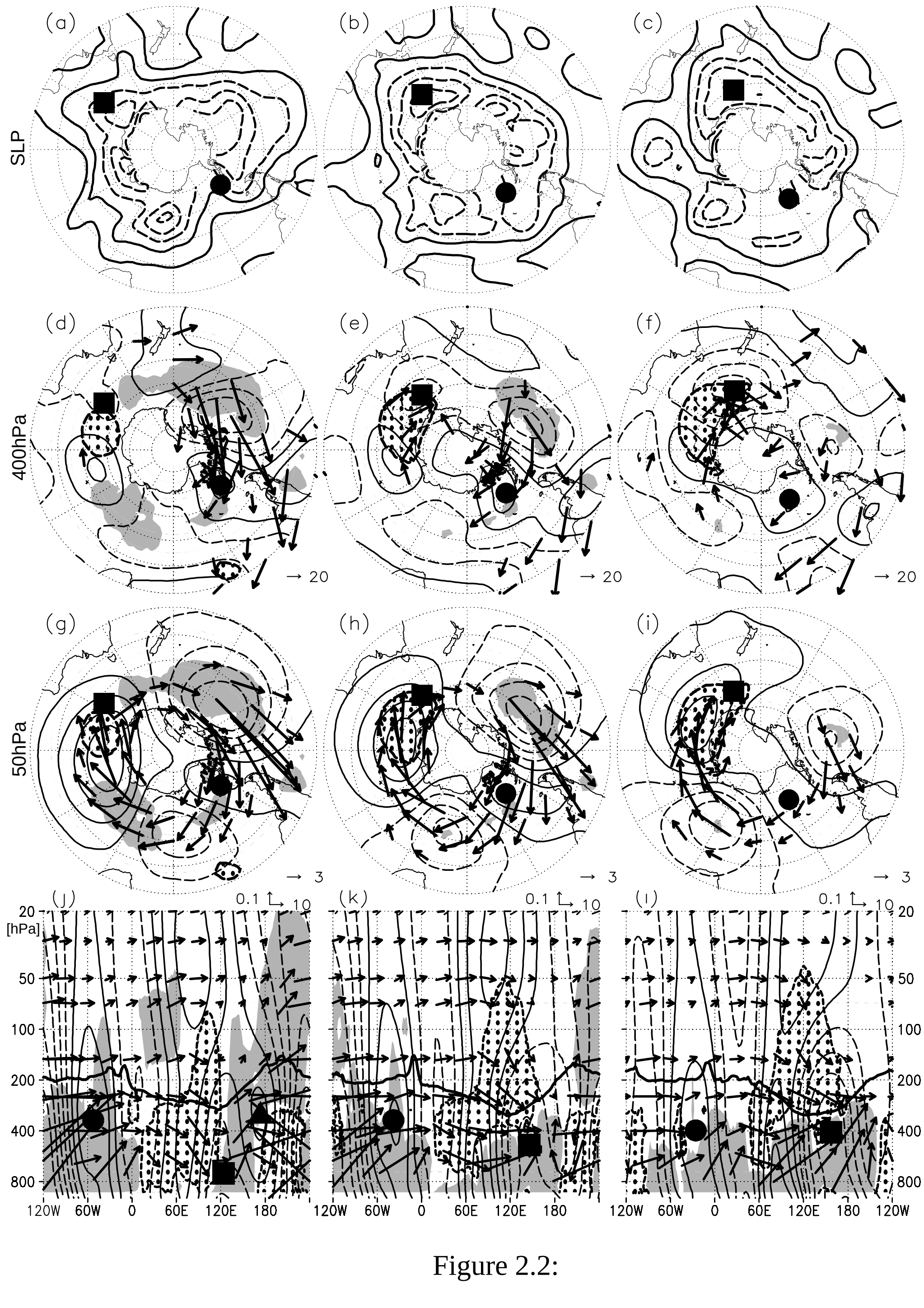
(a)
(b)
(c)
SLP
(d)
(e)
(f)
400hPa
→ 20
(g)
(h)
(i)
50hPa
→ 3
(j)
(k)
(l)
0.1
10
20
[hPa]
50
100
200
400
800
120W
60W
0
60E
120E
180

Figure 2.2:

Figure 2.2: Continued; (a-c) Maps of unfiltered sea-level pressure for (a) 8, (b) 10 and (c) 12 August, 1997. Solid lines are for 1005 and 1020 hPa, and dashed lines for 960, 975 and 990 hPa. (d-f) As in (a-c), respectively, but for 8-day low-pass-filtered geopotential height anomalies (contoured for ±50, ±150 and ±250 m), and the horizontal component of an associated wave-activity flux (arrows) at the 400-hPa level. Solid and dashed lines represent anticyclonic (positive) and cyclonic (negative) anomalies, respectively. Scaling for the arrows is given at the lower-right corner of each panel [Unit: m^2 s^{-2}]. Shading and stippling indicate the upward and downward components, respectively, of the wave-activity flux at the 150-hPa level whose magnitude exceeds 0.03 [m^2 s^{-2}]. A square indicates the 400-hPa cyclonic anomaly center associated with the surface cyclone of interest, as also plotted in (a-c). A circle and triangle denote the two 400-hPa anticyclonic anomaly centers referred to in the text (also in other panels). (g-i) As in (d-f), respectively, but for 8-day low-pass-filtered 50-hPa geopotential height anomalies (contoured for ±60, ±180, ±300 and ±420 m), and the horizontal component of an associated wave-activity flux at the 50-hPa level (arrow). (j-l) Zonal sections for 60°S of geopotential height anomalies (contoured for ±30, ±90, ±150 and ±210 m) and an associated wave-activity flux (arrows). Scaling for the arrows is given near the upper-right corner of each panel [Unit: m^2 s^{-2}]. Shading and stippling indicate the upward and downward components, respectively, of the wave-activity flux whose magnitude exceeds 0.03 [m^2 s^{-2}]. The anomalies have been normalized with pressure. The 5-day mean tropopause defined by the NCEP is indicated with a thick solid line.

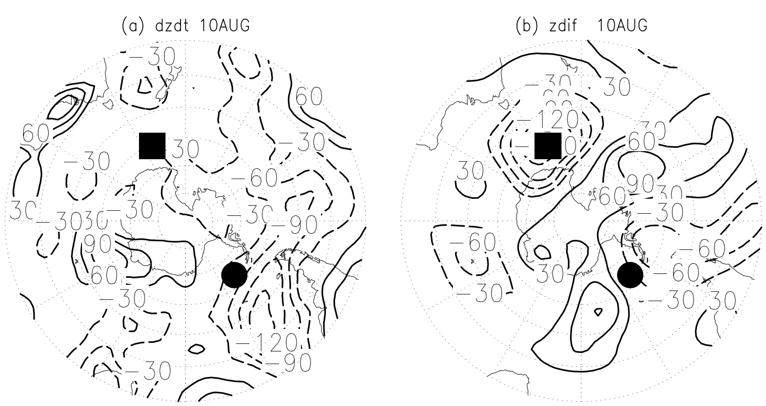

Figure 2.3: (a) Anomalous 250-hPa feedback forcing on the geopotential height from the vorticity flux due to high-frequency (under about 8 days) transient eddies on 10 August 1997. The contour interval is 30 [m/day] and zero lines are omitted. (b) Observed 250-hPa geopotential height tendency on 10 August 1997.

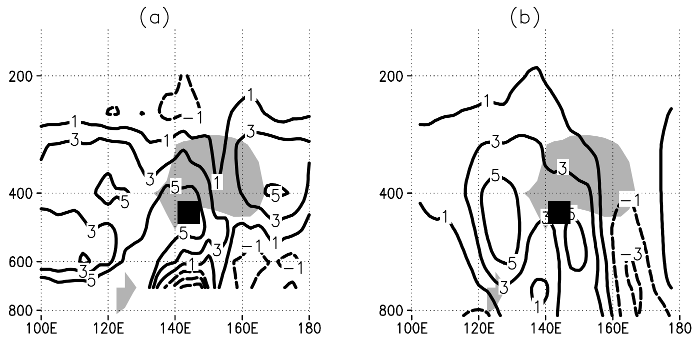

Figure 2.4: Zonal sections for 60°S over a longitudinal sector [100°E∼180°] of (a) vertical and (b) horizontal convergence of a wave-activity flux (contoured for −1, 1, 3, 5 [m s^{-1}/day]), respectively, for 10 August 1997. Shading denotes the time tendency of M defined in TN01 larger than 5 m s^{-1}/day. The tendency was evaluated from anomaly data by centered differencing. In (a) and (b), solid and dashed lines represent the flux convergence (positive) and divergence (negative), respectively. A square denotes the center of the cyclonic anomalies of interest.

the cyclonic anomalies near the tropopause. Therefore, both contributed to the increase in wave-activity pseudomomentum M associated with the amplification of the cyclonic anomalies, but the vertical convergence appears to correspond to the increase in M slightly better than the horizontal convergence. Figure 2.4 thus suggests that the downward wave-activity injection from the lower-stratospheric anomalies was, *at least*, as important as the horizontal injection from the upstream tropospheric anomalies in the particular large-scale cyclogenesis.

It should be noted that, on 12 August (Fig. 2.2l), the upward wave-activity flux was dominant in the mid- and lower troposphere in and around the cyclonic anomalies of interest, while the flux was still downward across the tropopause converging into them. In the lower troposphere, the upward flux was hinted as early as 10 August (Fig. 2.2k). The upward flux is consistent with a slight westward phase tilt with height found in the lower-tropospheric portion of the cyclonic anomalies (Figs. 2.2k-l), indicative of a contribution from baroclinic processes to the amplification of the cyclonic anomalies. In fact, the anomalies developed above an intense oceanic frontal zone (the Antarctic Polar Frontal Zone) along the Antarctic

Circumpolar Current that accompanies sharp surface temperature gradient (Nakamura and Shinpo 2004). It is thus conjectured that the upper-tropospheric cyclonic anomalies whose development had been initiated by the downward wave-activity injection from the lower stratosphere (Fig. 2.2d) induced the thermal advection across the near-surface baroclinic zone, rendering the anomalies slightly baroclinic (c.f. Nakamura and Fukamachi 2004). This baroclinic structure must be favorable for the further amplification of the anomalies within the tropospheric subpolar jet. Nevertheless, Figs. 2.2 and 2.4 suggest that the downward propagation of the Rossby wave train from the stratosphere contributed substantially to the initial development of the cyclonic anomalies of interest.

2.2.2 Evolution of a lower-stratospheric wave train

A few days before the tropospheric cyclogenesis of interest, the aforementioned anticyclonic anomalies developed at the 50-hPa level over the South Indian Ocean, downstream of the accompanying cyclonic anomalies over the South Atlantic (Fig. 2.5b). At that level, the horizontal wave-activity flux was predominantly eastward across those two anomaly centers both located at $\sim 60°$S. It is thus suggested that these anticyclonic and cyclonic anomalies were associated with a quasi-stationary Rossby wave train propagating along the lower-stratospheric PNJ. The flux was strongly divergent in the upstream portion of the cyclonic anomalies, where the flux was predominantly upward across the 150-hPa level. By August 4 (Fig. 2.5b), another cyclonic anomalies developed over the South Pacific with a wave-activity flux diverging downstream. Again, the wave-activity flux was strongly upward across the 150-hPa level in the upstream portion of these cyclonic anomalies.

The vertical structure of the two wave trains on 4 August is elucidated in a zonal-height section in Fig. 2.5c. The lower-stratospheric anticyclonic anomalies over the South Indian Ocean, from which part of the associated wave activity was injected downward into the tropospheric cyclonic anomalies under amplification (denoted by a square as in Figs. 2.2j-l), developed as a component of the lower-stratospheric Rossby wave train that had emanated

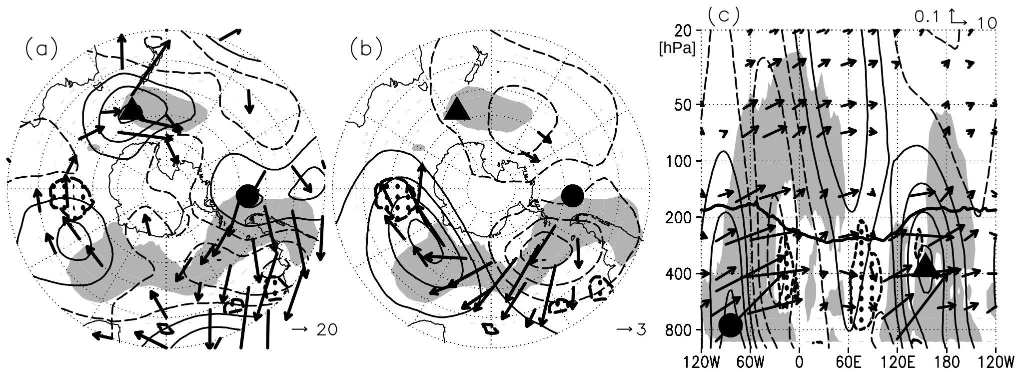

Figure 2.5: (a-c) As in Figs. 2.2(d, g, j), respectively, but for 4 August.

from a tropospheric anticyclonic ridge located as far upstream as around the Drake Passage (90° ∼60°W, denoted by a circle in Fig. 2.5c). Associated streamfunction anomalies exhibited an apparent westward tilt of phase lines with height, which is consistent with the upward emanating wave-activity flux associated with the wave train. The other wave train was found to emanate from another anticyclonic ridge located southwest of New Zealand (indicated with a triangle in Figs. 2.2j and 2.5c). Again, the wave train exhibited an obvious westward phase tilt. The latter wave train appears to reinforce the former. Barotropic feedback forcing from migratory eddies contributed positively to the amplification of each of those blocking ridges (Fig. 2.6). Wave activity that had emanated eastward from the blocking near New Zealand and then propagated along the SPJ across the South Pacific acted to reinforce the blocking ridge around the Drake Passage (Figs. 2.2d, 2.5a and 2.7a).

2.2.3 Waveguide structure

It is evident in Figs. 2.2g-i that the eastward wave-activity propagation at the 50-hPa level tended to be confined to a latitudinal band between 50°S and 60°S, which corresponds to the prominent PNJ at that level (Fig. 2.7c). The upward wave-activity injection into the stratosphere also tended to be confined to the same latitudinal band along the bottom of the stratospheric PNJ (Fig. 2.5b). Both at the 50- and 150-hPa levels, the refractive index (κ_s), defined locally for stationary Rossby waves through the formula (1.44), exhibits

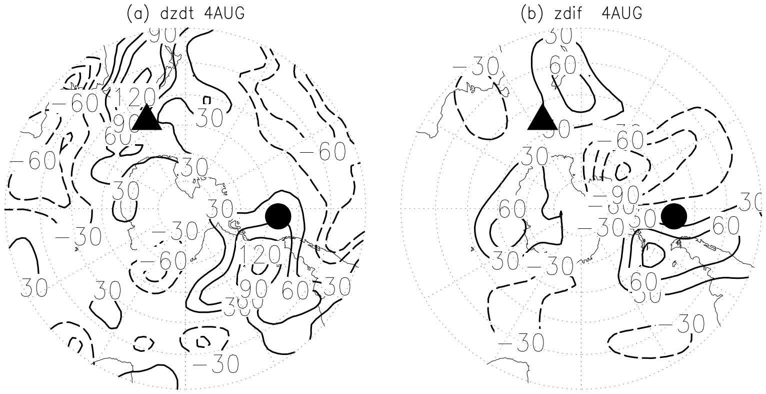

Figure 2.6: (a) The same as in Fig. 2.3a but on 4 August 1997. (b) The same as in Fig. 2.3b but on 4 August 1997.

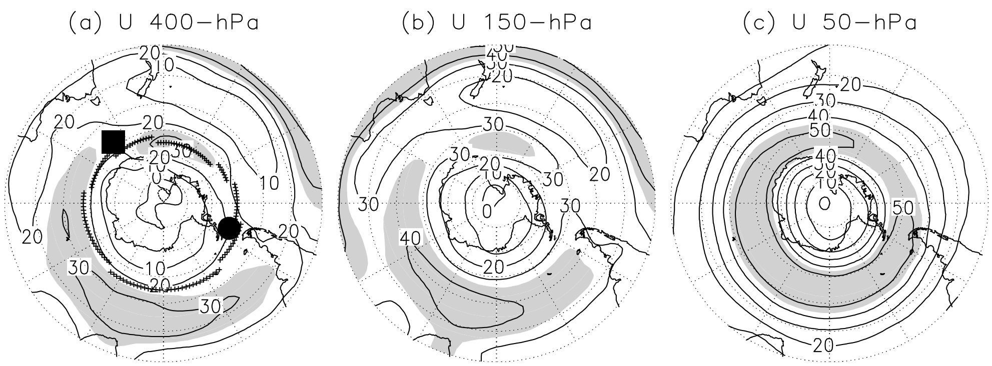

Figure 2.7: Mean westerly wind speed (U; contoured for every 10 m s^{-1}) for the 31-day period centered at August 10 at the (a) 400-hPa, (b) 150-hPa and (c) 50-hPa levels. Shading: (a) $U \geq 25$ [m s^{-1}], (b) $U \geq 35$ [m s^{-1}], (c) $U \geq 45$ [m s^{-1}]. A line of small crosses in (a) indicates the 50-hPa PNJ axis plotted in (c). A circle and square indicate the same 400-hPa anomaly centers on August 10 as plotted in Fig. 2.2.

a zonally-elongated band of local maxima extending along the PNJ axis from around the Drake Passage to the region south of New Zealand across the South Atlantic and Indian Ocean (Fig. 2.8). This waveguide is also evident in a zonal-height section of κ_s along 60°S (Fig. 2.9b). Around the tropopause level, the waveguide structure appears to be somewhat distorted within a longitudinal sector of κ_s minima over the South Atlantic between 20°W and 40°E, in association with the equatorward displacement of the tropospheric SPJ relative to the PNJ axis (Fig. 2.7a). This sector is located just downstream of the tropospheric blocking ridge of interest (indicated by a circle in Figs. 2.7-2.9). In the lower stratosphere, the waveguide with relatively large κ_s extended zonally along the PNJ above those κ_s minima. The anticyclonic ridge of interest developed at the exit of the Pacific SPJ (denoted as a circle in Figs. 2.7-2.9), located right below the entrance of the stratospheric PNJ (Figs. 2.7, 2.8 and 2.9a). It is conjectured that, in the presence of this particular waveguide structure, wave activity that had emanated from the anticyclonic ridge propagated selectively upward into the stratosphere (Fig. 2.5c), leading to the formation of the wave train along the PNJ. The rest of the wave activity emanated from the ridge was dispersed mainly equatorward over the South Atlantic (Figs. 2.2d-f).

The downward wave-activity propagation across the tropopause occurred into the developing cyclone of interest, as the leading edge of the wave train approached the PNJ exit around 120°E (Figs. 2.2j-l). Below that exit, κ_s was particularly large toward the tropospheric SPJ (Fig. 2.9b). This region acted as a localized vertical waveguide or a "chimney" through which the wave activity could be injected downward into (or could have emanated upward from) the tropospheric cyclonic anomalies. The well-defined entrance and exit of the PNJ as evident in Fig. 2.7c were apparently a manifestation of the k=1 component of the persistent lower-stratospheric planetary waves.

2.2.4 Validity of WKB approximation

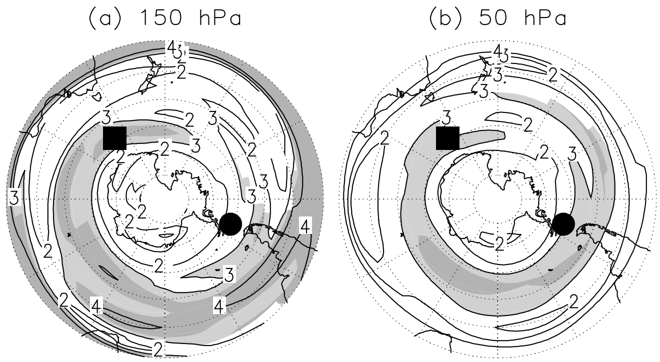

Figure 2.8: Maps of the refractive index κ_s for stationary Rossby waves represented as the "equivalent zonal wavenumber" for each latitude (i.e. κ_s divided by the earth radius and cosine of each latitude) at the (a) 150-hPa and (b) 50-hPa levels, both based on the mean circulation over the 31-day period centered at 10 August, 1997. Light and heavy shading indicates regions where $\kappa_s \geq 3$ and 3.5, respectively, and $U \geq 25$ [m s^{-1}]. A circle and square indicate the same 400-hPa anomaly centers on August 10 as plotted in Fig. 2.2.

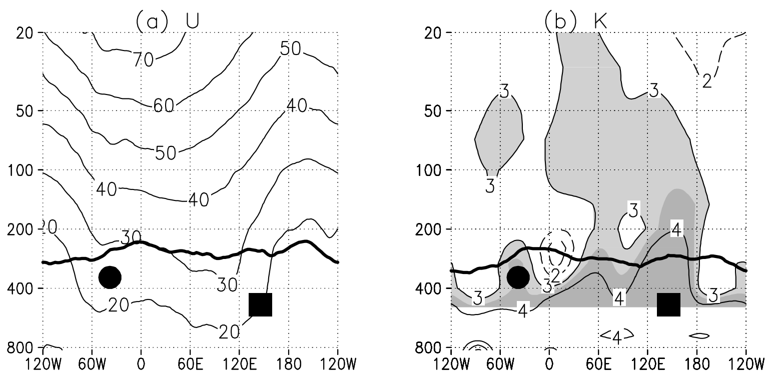

Figure 2.9: Zonal sections for 60°S of (a) westerly wind speed (U; every 10 m s^{-1}) and (b) refractive index (κ_s) for stationary Rossby waves, both based on the mean circulation in the 31-day period centered at 10 August, 1997. κ_s is represented as the equivalent zonal wavenumber for this latitude circle. Shading conventions in (b) are the same as in Fig. 2.8. Heavy lines represent the tropopause. A circle and square indicate the same anomaly centers on August 10 as plotted in Fig. 2.2.

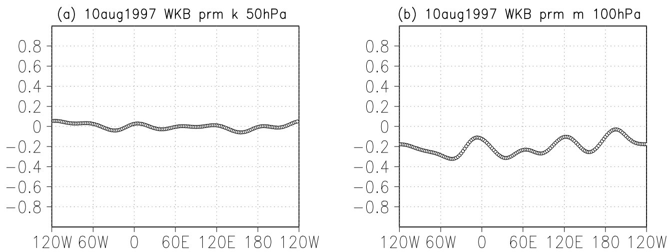

Figure 2.10: WKB parameters defined as (1.54) and (1.55) for the (a) 50-hPa and (b) 100-hPa levels, respectively evaluated for 10 August 1997.

As stated in the preceding chapter, our diagnosis through the wave-activity flux and refractive index is based on a WKB-type assumption that the fluctuations were slowly varying both in space and time compared to the time-mean basic state. To assess the validity of this WKB-type approximation, the WKB parameters defined as (1.54) and (1.55) are evaluated for the 50-hPa and 100-hPa levels, respectively (Fig. 2.10). Their absolute values are sufficiently less than unity at every longitude, which suggests the validity of the WKB-type approximation both in the zonal and vertical directions.

As another assessment of the WKB-type assumption validity, the zonal and vertical group velocities were estimated in three different ways. Our first estimation of the zonal group velocity was based on a Hovmöller diagram of 50-hPa height anomalies along the 60°S circle by tracing cyclonic and anticyclonic anomaly centers alternatively toward downstream (Fig. 2.11). The estimated 50-hPa eastward group velocity is about 17 [m/s], since the peak time of the cyclonic anomaly center at 40°W was on 0400UTC 4 August and that of the anticyclonic anomaly center at 85°E was 2300UTC 8 August. The estimation for the vertical component is based on the fact that the peak time of the anticyclonic anomalies in the lower-stratosphere (50 hPa, about 18 [km] above the sea level) was on 9 August and that of the cyclonic anomalies in the upper troposphere (400 hPa, altitude of about 6 [km]) was on 12 August, which suggests that it took for the wave packet about 3 days to propagate downward from the lower stratosphere to troposphere. The mean vertical group velocity thus estimated is about 0.05 [m/s] (4 [km/day]).

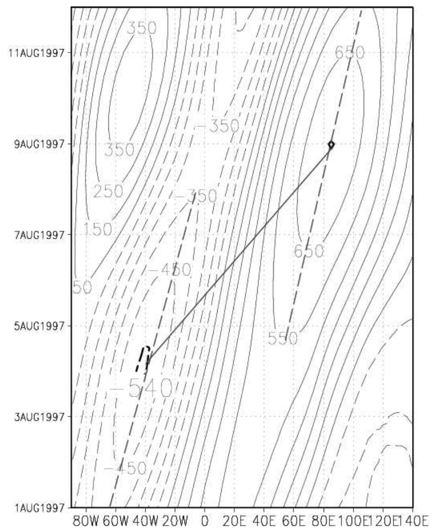

Figure 2.11: Hovmöller diagram of 50-hPa height anomalies [m] along the 60°S circle from 3 to 11 August. Solid and dashed lines denote positive and negative anomalies, respectively. Thick solid and dashed lines denotes 730 [m] and -540 [m], respectively. The estimations of the zonal group velocity and the phase speeds are based on a red solid line and blue dashed lines, respectively.

In our second estimation, group velocity was estimated as the ratio of wave-activity flux and wave-activity pseudomomentum (TN01; Harnik 2002) based on (1.41). However, the quantity M defined as (1.42) is highly noisy because it contains a term that is the ratio of squared PV fluctuations and basic-state PV gradient. Hence we estimated M by averaging another term in (1.42) that includes wave energy

$$E = \frac{p}{2}\left(\frac{e}{|\vec{U}| - C_p}\right) \tag{2.1}$$

over half wave length. This procedure can be justified because those two terms in (1.42) are equivalent, equally contributing to M over half a wavelength to eliminate the phase dependency of M (TN01). In the calculation, the phase speed was assumed to be zero due to its smallness (about 4 [m/s] as estimated from the phase lines in Fig. 2.11), when it is compared to the background westerlies about 50 [m/s] (Fig. 2.7c). We estimated the 50-hPa eastward group velocity from the ratio of the intensity of the wave-activity flux $|\vec{W}|$ and $2E$

averaged between 30°W and 90°E along the 60°S circle[5] on 7 August, which spans over half a wavelength (Figs. 2.2k). The eastward group velocity is thus estimated as 19 [ms^{-1}]. The 100-hPa vertical group velocity was estimated similarly, but averaged between 60°E and 150°E where downward wave-activity flux was prominent is about -0.027 [m/s] (2.3 [km/day]).

In the third estimation, we used the dispersion relation under assumption that the meridional wavenumber is nearly zero ($l \sim 0$) in recognition of the fact that $\vec{W}$ was nearly eastward along the PNJ and confined meridionally to it (Figs. 2.2g-i). The zonal group velocity (C_{gx}) for stationary Rossby waves may be written as an expansion of (1.15) as follow;

$$C_{gx} = \frac{2U^2k^2}{|\vec{\nabla}_H Q|}, \tag{2.2}$$

On the basis of Fig. 2.9b, the 50-hPa eastward group velocity averaged between 30°E and 150°E along 60°S circle is estimated as 8 [m/s] and 34 [m/s] for the k=1 and k=2 components, respectively. The zonal wavenumber corresponding to the observed 50-hPa eastward group velocity, which is 17 [m/s] in our first estimation, is k=1.5. The estimation of the vertical group velocity was not performed due to the difficulty in a quantitative estimation of meridional and vertical components of wavenumber.

These estimations of the group velocity are qualitatively consistent, which justifies the validity of the WKB-type assumption assumed in our diagnosis. Randel (1987) discussed the vertical propagation of the planetary waves by using a cross correlation analysis. He found that it takes 4 and 1-2 days for k=1 and k=2 components, respectively, to reach the stratosphere (10 hPa, 30 [km]) from the upper troposphere (300 hPa, 10 [km]). His result suggests that the mean vertical group velocities for k=1 and k=2 components are about 5 [km/day] and 10-20 [km/day], which is consistent with our results.

[5]Taking an adequate averaging span, the contribution of E and the counterpart term to M is theoretically identical. Thus E must be doubled for using E instead of M.

2.3 A blocking event in September 1997

As our another example of downward wave-activity injection across the tropopause, we briefly refer to a blocking event that occurred south of New Zealand in late September of 1997 (denoted by a square in Figs. 2.12d-f). As evident in Fig. 2.12f, the blocking anticyclonic anomalies were relatively shallow, confined mostly to the troposphere. Cyclonic anomalies located upstream, in contrast, were deeper, extending into the stratosphere. Rossby wave activity was injected into the developing ridge horizontally in the upper troposphere from another anticyclonic anomalies farther upstream over the South Indian Ocean through the tropospheric cyclonic anomalies (Fig. 2.12d). At the same time, part of wave activity propagating eastward along the lower-stratospheric PNJ was injected downward across the tropopause into the blocking ridge developing to the south of New Zealand (Figs. 2.12e-f). Consistently, phase lines of the streamfunction anomalies associated with the ridge exhibited a distinct eastward tilt with height (Fig. 2.12f).

As indicated in Fig. 2.12f, the quasi-stationary Rossby wave train with deep structure observed on 24 September originated from another tropospheric cyclonic anomalies located farther upstream over the South Atlantic (denoted by a circle in Fig. 2.12). The cyclonic anomalies had remained rather shallow, confined mostly to the troposphere for the past several days. On 20 September (Fig. 2.12c), the cyclonic anomalies were situated below the anticyclonic anomalies in the stratosphere over the South Atlantic (60°W∼0°). While weak downward injection of wave activity occurred across the tropopause into the upstream portion of the cyclonic anomalies (Figs. 2.12a-c), wave activity emanated more strongly upward into the stratospheric anomalies from the downstream portion of the tropospheric anomalies (Figs. 2.12a-f). This upward wave-activity injection occurred where the stratospheric PNJ partially overlapped with the tropospheric SPJ (Figs. 2.12g-h). It should be noted that distinct downward injection of wave activity into the blocking ridge of our primary interest did not occur until the leading edge of the stratospheric wave train reached a "chimney" (vertical

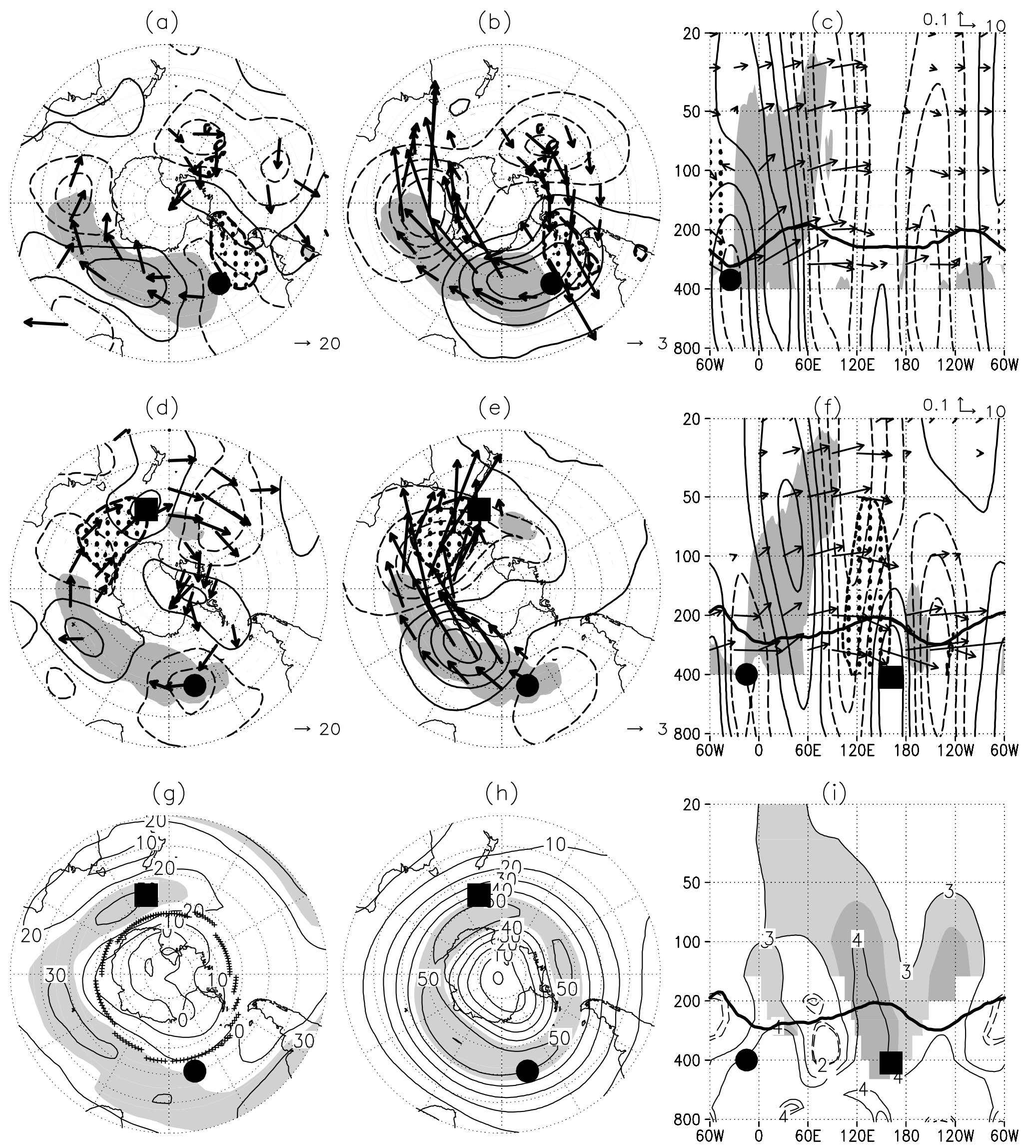

Figure 2.12: (a-c) Same as in Figs. 2.2d, g and j, respectively, but for 20 September, 1997. (d-i) Same as in Figs. 2.2d, 2.2g and 2.2j, 2.7a, 2.7c and 2.9b, respectively, but for 24 September 1997.

waveguide) in the exit region of the PNJ to the south of Australia, which was overlapped with the tropospheric SPJ. The "chimney" was marked with local maxima of κ_s ($\geq$3.5) extending from the 70-hPa level downward below the tropopause (Fig. 2.12i).

The validity of WKB-type approximation was assessed in the same way as in the August case. The WKB parameters (1.54) for the 50-hPa level and (1.55) for the 400-hPa level are presented in Figs. 2.13a and b, respectively, which show sufficient smallness of their absolute values. The zonal group velocity estimated from a Hovmöller diagram along the 60°S circle of 50-hPa height anomalies around 22 September is about 70 [m/s] (Fig. 2.14), as estimated from the fact that the group velocity propagation occurred from the anticyclonic anomaly center at 5°W to the cyclonic anomaly center at 105°E over 25hours. The zonal group velocity estimated from ratio of the zonal wave-activity flux component and $2E$ (2.2) on the 50-hPa level averaged between the anticyclonic anomaly center at 10°W and the cyclonic anomaly center at 90°E along 60°S circle on 22 September is about 52 [m/s]. Taking the zonal phase speed of about 10[m/s] (Fig. 2.14) into consideration, this estimation based on the wave-activity flux is about 62 [m/s]. The 50-hPa height anomalies on 50-hPa level observed on 24 September were dominated by the k=3 component (Fig. 2.12e). The zonal group velocities based on the dispersion relation on the 50-hPa level averaged between 10°W and 90°E along the 60°S circle are about 9, 35 and 77 [m/s] for zonal wavenumber k=1, 2 and 3 components, respectively. Those results are consistent with each other in a qualitative sense. Meanwhile, the downward group group velocity estimated from the ratio of the vertical component of the wave-activity flux and $2E$ averaged between 90°E and 150°E along 60°S on 25 September is -0.028 [m/s] ([2.3 [km/day]). Since the peak time of the tropospheric blocking was about 4 days after (on 26 September) the peak time of the stratospheric cyclonic anomaly center, the downward group velocity estimated is about -0.035 [m/s] (3 [km/day]).

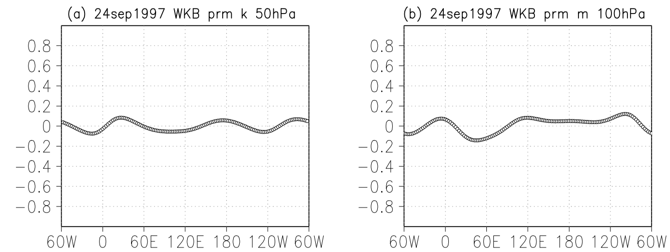

Figure 2.13: The same as in Fig 2.10 but for 24 September 1997.

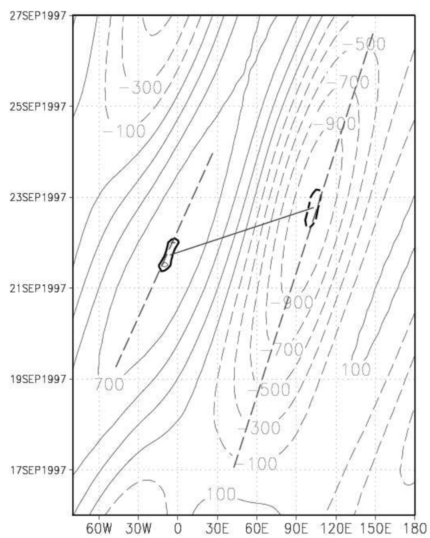

Figure 2.14: The same as in Fig. 2.11 but from 16 to 27 September. Thick solid and dashed lines denotes 895 [m] and -1080 [m], respectively.

2.4 Stratospheric wave trains in late winter of 1997

In the preceding sections two examples were presented in which downward wave-activity injection from lower-stratospheric Rossby wave trains appeared to contribute toward the amplification of large-scale quasi-stationary anomalies in the SH troposphere. In those examples, the stratospheric wave trains propagating along the PNJ had originated from another tropospheric anomalies located far upstream. In this section, we show that such upward and downward injection of quasi-stationary Rossby wave activity across the tropopause was observed over the SH rather frequently during late winter and early spring of 1997.

Figure 2.15 shows Hovmöller diagrams of low-pass-filtered geopotential height anomalies at the (a) 50-hPa and (b) 400-hPa levels averaged between 50°S and 60°S. Shading and stripping indicate the upward and downward wave-activity injection, respectively, across the 150-hPa level. As discussed in NN04, formation of a zonally propagating quasi-stationary wave train occurred frequently in the lower stratosphere in conjunction with enhanced upward wave-activity injection across the 150-hPa level (Fig. 2.15a). One may notice that the event of the lower-stratospheric wave train examined in our first example was one of the earliest among such events as observed in the particular season. Though less frequently than the upward propagation, the downward wave-activity injection across the 150-hPa level did occur occasionally just downstream of an eastward propagating wave train at the 50-hPa level. The downward wave-activity injection tended to be observed right over or slightly upstream of quasi-stationary 400-hPa height anomalies from which the wave-activity flux diverged eastward (arrows in Fig. 2.15b). In many of those occasions including the two examples shown in the preceding sections, Rossby wave trains that had originated from the tropospheric circulation anomalies propagated zonally in the lower stratosphere, and they were then refracted back into the troposphere to form another wavetrains downstream.

Figure 2.16 also summarizes the activity of quasi-stationary submonthly fluctuations in the lower stratosphere and upper troposphere, an associated three-dimensional flux of sta-

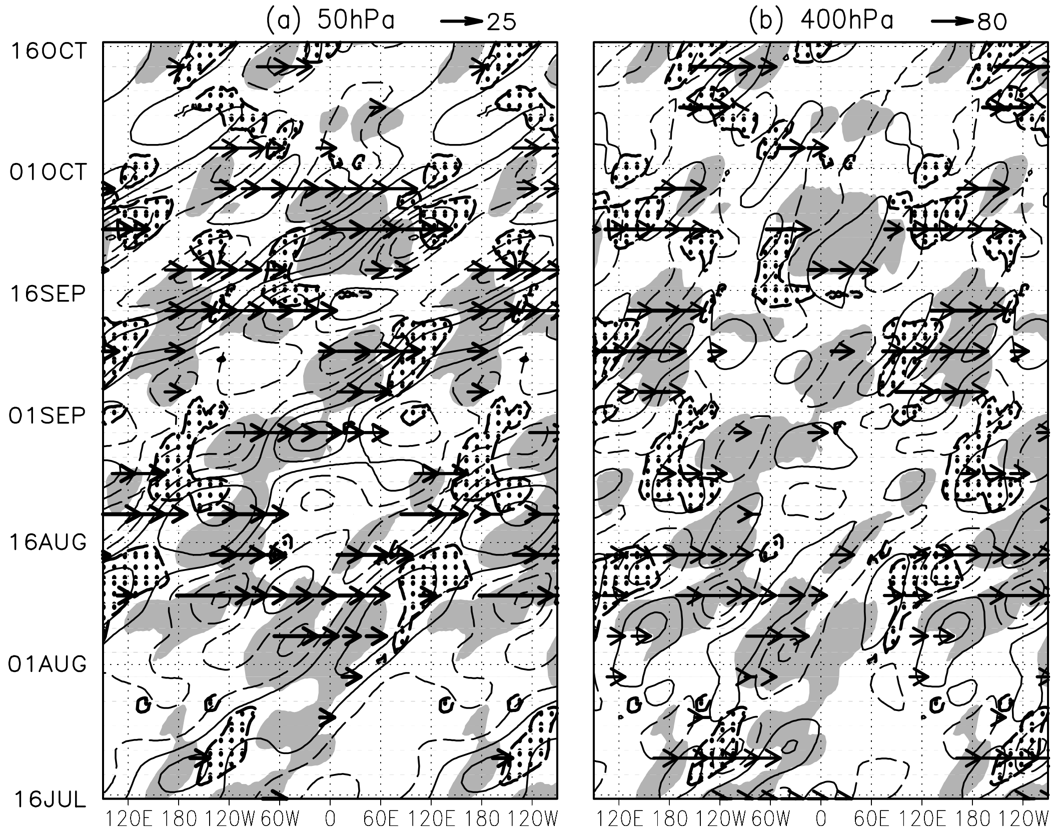

Figure 2.15: Zonal-time sections for our analysis period (16 July $\sim$ 16 October, 1997) of geopotential height anomalies and the zonal component of a wave-activity flux (arrows), based on the meridional averaging between 55°S and 60°S at the (a) 50-hPa and (b) 400-hPa levels. Solid and dashed lines indicate anticyclonic and cyclonic height anomalies, respectively. Contours are drawn for (a) ±150, ±450, ±750, ±1050 and ±1350 m, and for (b) ±100, ±300 and ±500 m. Scaling for the arrows is given at the upper-right corner of each panel (unit: $m^2\ s^{-2}$). Shading and stippling indicate the upward and downward components, respectively, of the wave-activity flux across the 150-hPa level whose magnitude exceeds 0.03 [$m^2\ s^{-2}$].

tionary Rossby waves and the time-mean structure of the westerly jets for the three 31-day periods of 17 July-16 August, 17 August-16 September and 16 September-16 October in 1997. Again, shading and stippling denote the upward and downward injection of wave-activity across the 150-hPa level. As pointed out by NN04 and confirmed by comparing the left and right columns of Fig. 2.16, the upward wave-activity propagation tended to be pronounced in regions below the lower-stratospheric PNJ where the tropospheric sub-monthly fluctuations were particularly strong. In good agreement with Fig. 2.15, downward wave-activity injection into the troposphere was pronounced right below or slightly down-stream of local maxima of 50-hPa submonthly height fluctuations (Figs. 2.16a, d and g), located right above or slightly upstream of the local maxima of the tropospheric submonthly fluctuations (Figs. 2.16c, f and i). This result is suggestive of the significant influence of stratospheric Rossby-wave anomalies that can be exerted on the development of tropospheric quasi-stationary anomalies. As consistent with Fig. 2.15, the downward wave-activity injection occurred mainly to the south of Australia and in the central South Pacific (Figs. 2.16c and f), both along the tropospheric SPJ (Fig. 2.16b and e). After mid-September (Fig. 2.16i), the downward injection weakened in the central South Pacific, while it was enhanced around the Drake Passage, which is also along the SPJ, located just downstream of the exit of the secondary PNJ core that formed over the eastern South Pacific (Fig. 2.16h). Still, the region south of Australia remained as the primary region of the downward wave-activity injection. In this region, the downward injection from the stratosphere was so dominant that the wave-activity flux across the 150-hPa level was pointing *downward* even as the *net* over each of the 31-day periods (Fig. 2.16a, d and g). In the two other regions, the upward wave-activity propagation into the stratosphere dominated over the downward injection, which rendered the net wave-activity flux at the 150-hPa level weakly upward in all of the three periods (Figs. 2.16a, d and g). In each of those regions of active downward wave-activity injection, a local "chimney" structure with vertically extending κ_s maxima is apparent in association with the overlapping of the stratospheric PNJ and tropospheric SPJ (Fig. 2.17).

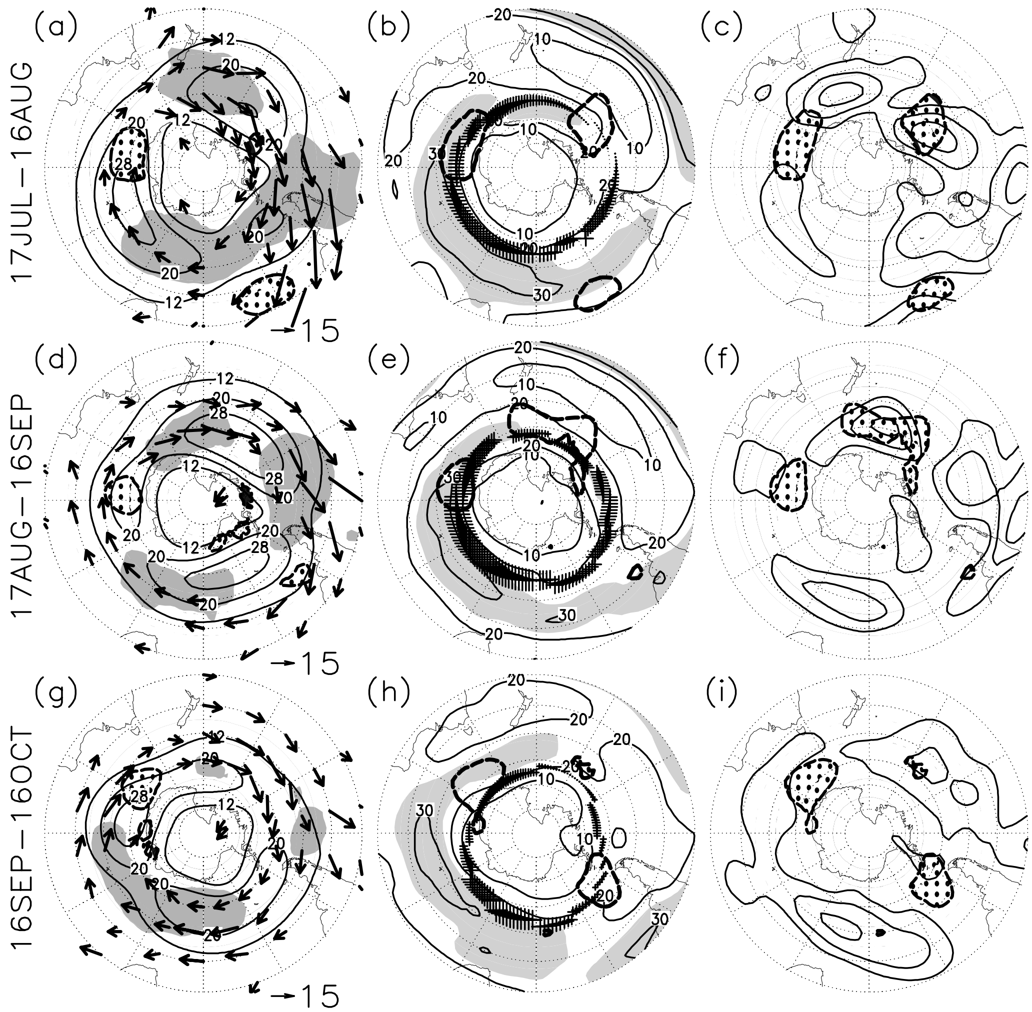

Figure 2.16: (a) Standard deviation of submonthly low-pass-filtered fluctuations in 50-hPa geopotential height (contoured for 120, 200 and 280 m), and the horizontal component of a time-mean 50-hPa wave-activity flux (arrows). Scaling for the arrows is indicated at the lower-right corner. Shading and stippling are applied to the regions where the vertical component of the 31-day mean *net* wave-activity flux is upward or downward, respectively, at the 150-hPa level, exceeding 0.01 [m^2 s^{-2}] in strength. (b) Mean 400-hPa westerly wind speed (contour interval: 10 m s^{-1}). Small crosses superimposed mark the 50-hPa PNJ axis (their size is proportional to the corresponding local wind speed). Dashed lines surround the regions where the 31-day mean downward wave-activity flux (but not the net flux) at the 150-hPa level was stronger than 0.01 [m^2 s^{-2}] in magnitude. (c) Standard deviation of submonthly low-pass-filtered fluctuations in 400-hPa geopotential height (contoured for 80, 110 and 140 m). Stippling is applied where the 31-day mean downward wave-activity flux as in (b) at the 150-hPa level exceeds 0.01 [$m^2 s^{-2}$] in magnitude. The periods for (a-c), (d-f) and (g-i) are for 17 July $\sim$ 16 August, 17 August $\sim$ 16 September and 16 September $\sim$ 16 October, respectively.

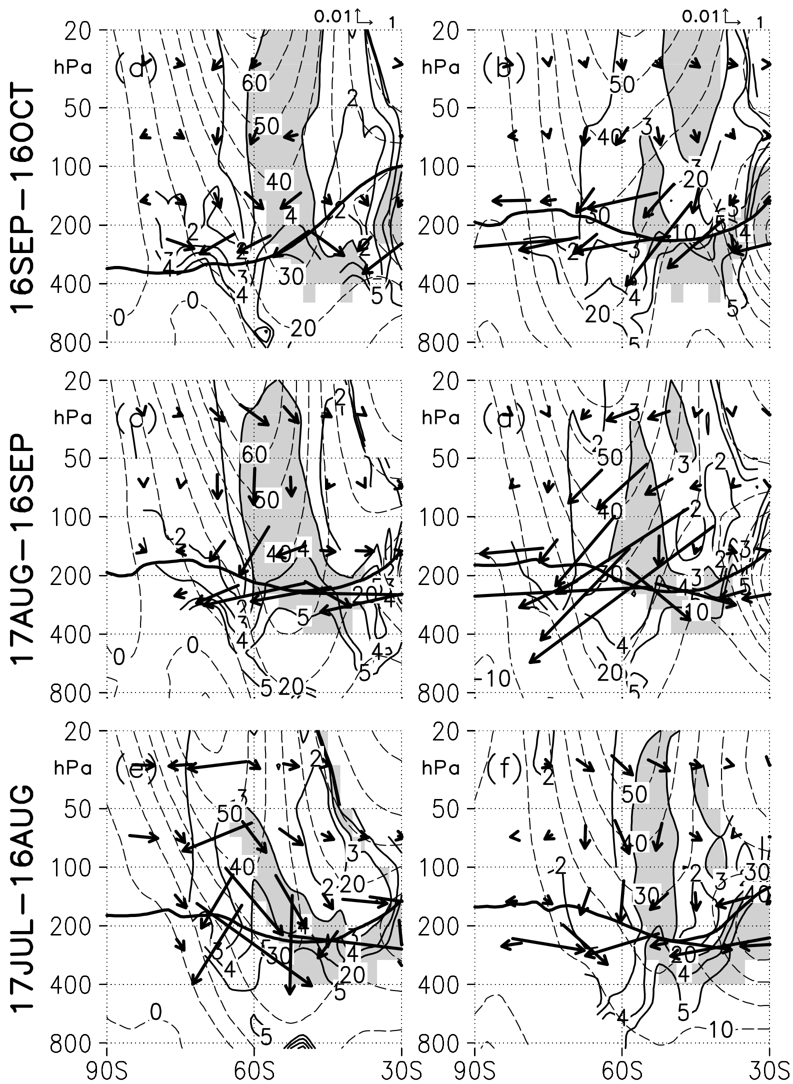

Figure 2.17: (a) Meridional section of κ_s (solid lines), U (dashed lines for every 10 [m s^{-1}]) and the meridional and vertical components of a mean wave-activity flux (arrows), all of which are averaged between 80°E and 140°E for 17 July $\sim$ 16 August. Shading indicates the regions for $\kappa_s \geq 3$ and $U \geq 25$ [m s^{-1}], and scaling for arrows is given at the right-upper corner of the panel. A thick line indicates the tropopause defined by the NCEP. The wave-activity flux was included in the averaging only when the flux was pointing downward. (b): Same as in (a), but averaged between 110°W and 150°W. (c): Same as in (a), but averaged between 80°E and 120°E for 17 August $\sim$ 16 September. (d): Same as in (a), but averaged between 160°E and 130°W for 17 August $\sim$ 16 September. (e): Same as in (a), but averaged between 110°E and 150°E for 16 September $\sim$ 16 October. (f): Same as in (a), but averaged between 40°W and 70°W for 16 September $\sim$ 16 October.

2.5 Concluding remarks

In our case study of the SH circulation in 1997, we have presented several pieces of evidence that wave activity associated with a zonally propagating quasi-stationary Rossby wave train along the lower-stratospheric PNJ that has emanated from quasi-stationary tropospheric anomalies developing at a particular location can, in some occasions, be injected downward into the troposphere, contributing to the development of another tropospheric anomalies at a distant location. In one of our examples, the downward propagation of Rossby wave activity across the tropopause contributed to large-scale quasi-stationary cyclogenesis to the south of Australia. In our another example, such downward wave-activity propagation contributed to the formation of a blocking ridge in nearly the same region.

For a quasi-stationary Rossby wave packet that consists mainly of the k=1, 2 and 3 components, the stratospheric PNJ with a large wind speed and tight PV gradient acts as a better waveguide than the tropospheric SPJ does. Therefore, Rossby wave activity, once injected into the lower-stratospheric PNJ, propagates eastward through the PNJ nearly twice as fast as it would through the SPJ, thus effectively transferring wave activity downstream. During the August event (from 6 to 10 August), amplitudes of k=1 to k=3 component are about 390 [m], 350 [m] and 200 [m], respectively (Fig. 1.2, presented in p. 3). Thus the k=3 component, which constituted the zonally-confined, “beam-like” wave packet in the lower stratosphere, accounted for nearly 20% of the amplitude of the whole height anomalies along the PNJ at the 50-hPa level.

At this stage, we are not quite certain whether wave-activity injection across the tropopause alone could trigger the development of the tropospheric anomalies of interest in our examples. Circulation anomalies initiated in the SPJ by tropospheric processes would amplify through downward injection of Rossby wave activity across the tropopause if another anomalies with the opposite sign are or have already been present slightly upstream in the exit of the lower-stratospheric PNJ. It should be stressed that, as mentioned in the introduction, our argument must remain qualitative because of the WKB-type assumptions implicit in our particular diagnosis tools whose validity is not immediately obvious in the stratosphere. Nevertheless, our examples, especially the first one, suggest a potential importance of the downward propagation of a Rossby wave train from the stratosphere at the early stage of the development of large-scale tropospheric anomalies.

It has been shown in this chapter that zonal asymmetries in the time-mean westerlies are important, even over the SH, for zonal and vertical propagation of Rossby wave trains. Specifically, the vertical overlapping of the stratospheric PNJ with the tropospheric SPJ is of particular importance in the local formation of a vertical waveguide across the tropopause through which a quasi-stationary Rossby wave train can propagate upward or downward. If such a cross-tropopause "chimney" forms around the exit region of the lower-stratospheric PNJ, downward wave-activity injection will be possible through which a stratospheric Rossby wave train can contribute to the large-scale cyclogenesis or blocking formation in the troposphere. This is likely the reason why downward wave-activity injection into the troposphere during late winter of 1997 occurred most frequently to the south of Australia, where the overlapping of the PNJ exit and the SPJ was observed throughout the season. The location of such a "chimney" must be sensible to the three-dimensional structure of planetary waves included in the time-mean flow. We thus conjecture that the seasonal and interannual changes in positions of the PNJ exits could result in the modulation of the downward propagation of quasi-stationary Rossby wave activity into the troposphere, which will be a topic of the next chapter.

Chapter 3

Climatology and interannual variability of vertical wave-activity propagation

3.1 Introduction

In the preceding chapter, we have shown that both upward and downward wave-activity propagation across the tropopause occurred in association with the local amplification of submonthly fluctuations in the stratosphere and troposphere in the Southern Hemisphere (SH) winter of 1997. In this chapter, we show that such vertical propagation of submonthly wave-train-like anomalies were also observed in other years over the SH winter. The distribution and magnitude of vertical wave-activity propagation are found substantially different from one winter to another. The results obtained in the preceding chapter suggest that the wave-activity propagation is rather sensitive to the configuration of the stratospheric polar-night jet (PNJ) and the tropospheric subtropical jet (SPJ) structures. One may conjecture that interannual variations in the vertical wave-activity propagation may occur in association with those of PNJ and SPJ.

The most dominant mode of interannual variability in the tropospheric circulation over the Southern Hemisphere (SH) is called "Southern Hemisphere annular mode (SAM)" [1] (Thompson and Wallace 2000) or "high latitude mode (HLM)" (e.g., Kiladis and Mo 1999),

[1] SAM is also referred to as Antarctic Oscillation (AAO)

which is characterized by a zonally-symmetric out-of-phase relationship of geopotential height anomalies between the polar region and the mid latitudes. The circulation anomalies associated with the SAM, characterized by north-south fluctuations in position of the zonal-mean westerly jet about 50°S, are sustained by a positive feedback from momentum flux of migratory transient eddies (Limpasuvan and Hartmann 1999; Lorenz and Hartmann 2001). In winter, the SAM related anomalies are extended into the stratosphere and show the barotropic structure over both the stratosphere and troposphere (Thompson and Wallace 2000). The second mode is characterized by a wave train that extends southeastward from the central to the southeast Pacific then turns northeastward to South America. The third mode represents a zonal wavenumber 3 (k=1) pattern with its maximum amplitude between 50°S and 60°S (e.g., Kiladis and Mo 1999). The second and third modes are considered to be linked to El Niño/Southern Oscillation (ENSO) and referred to as Pacific South American (PSA) patterns (Vera *et al.* 2004 and references therein).

Fewer studies have been done on interannual variations in the SH stratosphere than the NH stratosphere due to the limited availability of hemispheric reliable data until recently. The interannual variations has been studied mainly from a viewpoint of anomalous seasonal march of the zonal-mean zonal wind and E-P flux propagation. In SH late winter and spring, the core of the zonal-mean PNJ moves poleward and also downward from the upper stratosphere into the lower stratosphere. Interannual variability of the zonal-mean PNJ is related to the year-to-year differences in the timing of the jet core shift associated with anomalous E-P flux upward from the troposphere (Shiotani *et al.* 1993; Kuroda and Kodera 1998; Hio and Yoden 2005). The descent of the zonal-mean zonal wind anomalies are regard as being associated with the SAM, of which variability is extending over the stratosphere and troposphere (e.g. Thompson *et al.*2005). On the other hand, there is another viewpoint that the stratospheric variability is associated with the polar-night jet oscillation (PJO) and it interacts with the tropospheric SAM in winter (e.g. Kuroda and Kodera 2001).

Hio and Hirota (2002) found through the EOF analysis that the interannual variability in the zonally asymmetric components of the SH mid-stratospheric circulation in late winter (September and October) can be decomposed into two components, one is amplification of the stationary k=1 component and the other is a longitudinal phase shift of k=1 component. They also found that the interannual variations in the stratosphere are associated with those in the tropospheric subpolar and subtropical jets.

In this chapter, we begin our discussion by showing the climatological distribution of vertical wave-activity propagation in late winter (August and September) and its relation to the climatological distributions of submonthly fluctuations and the climatological westerly jet structure. Their interannual variations are then discussed. Meridional heat flux at the 100-hPa level associated with upward wave-activity propagation and its interannual variation are known to be maximized from August to November (Randel 1988; Randel and Newman 1999). In normal years, breakdown of the stratospheric polar vortex associated with the final warming occurs from October to November. During the final warming, the rapidly changing circulation can not be decomposed unambiguously into the submonthly fluctuations and seasonally-varying basic state as was shown in the last chapter. As a measure of the local intensity of submonthly fluctuations, the root-mean square of low-pass-filtered height anomalies over a given months is used. At the most of the locations, the monthly mean of the vertical component of the wave-activity flux is typically positive, masking the downward wave-activity propagation, if exists. We therefore evaluated the upward and downward wave-activity propagation across the tropopause separately by summing up the positive and negative values of the vertical component separately within a given month then dividing them by the numbers of days in the particular months. NCEP/NCAR reanalysis data set from 1979 to 2003 is used for this calculation.

3.2 Climatological distribution of late winter of the SH

In late winter (August-September) of the Southern Hemisphere (SH), the maximum cores

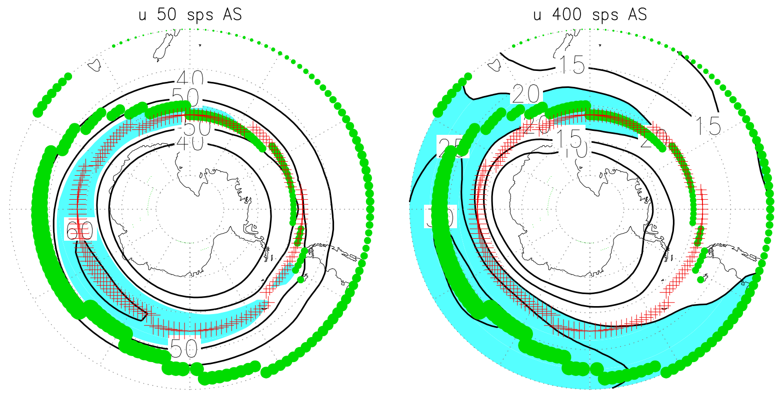

Figure 3.1: (a) Climatological mean of zonal wind at the 50-hPa level in August and September from 1979 to 2003 (contoured for 40, 50 and 60 m/s). Southward from 40°S is shown. (b) Same as (a) but for 400-hPa level (contoured for 15, 20, 25 and 30 m/s). In both panels, red crosses and green dots show axes of 50-hPa and 400-hPa westerlies jets, respectively.

of the stratospheric PNJ and tropospheric SPJ are both observed over Indian Ocean (Fig. 3.1), but the axis of the PNJ is shifted poleward of that of SPJ. Their axes are overlapped over the Pacific and Atlantic Oceans, where both the upward and downward components of the 100-hPa wave-activity flux are pronounced (Figs. 3.2a and b). This supports the hypothesis proposed in the preceding chapter that overlapping of the PNJ and SPJ leads to the formation of a vertical waveguide ("chimney") through which the wave activity can effectively propagate vertically across the tropopause. Due to the pronounced upward injection of wave activity from below, lower-stratospheric submonthly fluctuations are also the strongest over the Pacific and Atlantic Oceans (Figs. 3.3a and b).

3.3 Interannual variations over the SH

Distribution of the climatological-mean downward wave-activity flux differs substantially from that in late winter of 1997 shown in preceding chapter, which means large year-to-year variations in the downward wave-activity propagation over the SH. To examine the interannual variations in local downward wave-activity propagation and related anomalous time-mean westerlies, the area averaged monthly-mean downward wave-activity flux across

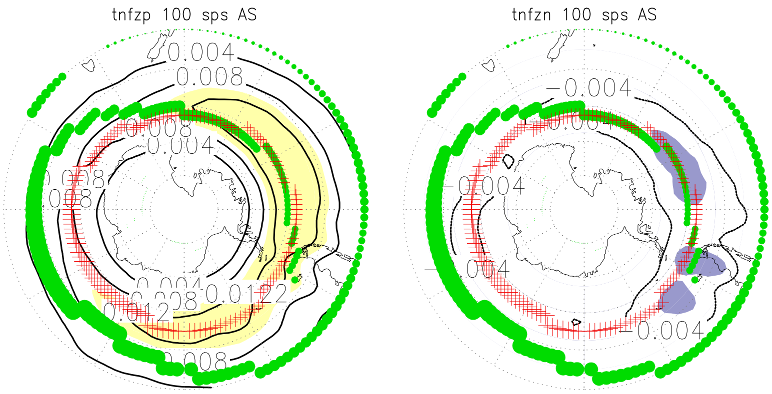

Figure 3.2: (a) Upward component of time-mean wave-activity flux at 100-hPa level (contoured for 0.004, 0.008 and 0.0012 m^2s^{-2}). Yellow shading indicates regions where the flux is larger than 0.006 [m^2s^{-2}]. (b) Same as (a) but for downward component (contoured for -0.004 m^2s^{-2}). Purple shading indicates regions where the flux is less than -0.006 [m^2s^{-2}]. Red crosses and green dots are the same as in Fig. 3.1).

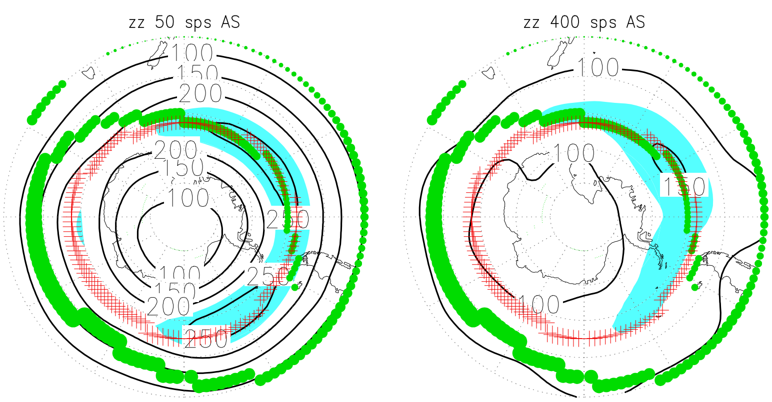

Figure 3.3: (a) Standard deviation of submonthly low-pass-filtered fluctuations in 50-hPa geopotential height (contoured for 100, 150, 200 and 250 [m]). Light blue shading denotes regions where the standard deviation is more than 220 [m]. (b) Same as (a) but for 400-hPa geopotential height (contoured for 100 and 150 m). Light blue shading denotes regions where the standard deviation is more than 120 [m]. Red crosses and green dots in (a) and (b) are the same as in Fig. 3.1).

the 100-hPa level are used for classifying active and inactive downward wave-activity propagation months over indicated areas. Then composite maps of the wave-activity flux, westerlies and rms of submonthly height fluctuations are made for each of the categories. Significance of the difference between the two groups are estimated with Student t statistic.

3.3.1 South of Australia

Wave propagation statics over are between 120°E to 180° and between 55°S to 65°S, where downward wave-activity injection is prominent in 1997 late winter, are discussed in this subsection. Five months (8 months) when the area averaged magnitudes of the 100-hPa downward wave-activity flux exceeds 0.009 [m^2s^{-2}] (is less than 0.001 [m^2s^{-2}]) have been selected as months of active (inactive) downward wave-activity injection. The active months thus selected are Sep. 1983, Sep. 1988, Aug. 1997, Sep. 1997 and Aug. 2003 and the inactive months are Aug. 1979, Aug. 1980, Aug. 1985, Aug. 1987, Sep. 1990, Sep. 1992, Aug. 1998 and Sep. 2001.

Figure 3.4a shows difference composite maps of the monthly-mean downward wave-activity flux between the two groups. In the active months, downward wave-activity injection from the stratosphere is prominent to the south of Australia and New Zealand, whereas upward wave-activity propagation into the stratosphere is enhanced over the southeastern Pacific and over from the southeastern Atlantic to the southwestern Indian Ocean. Consistently with this enhanced upward wave-activity injection, submonthly fluctuations in the lower stratosphere are enhanced along the PNJ in all longitude in the active downward wave-activity injection months downstream of the enhanced upward wave-activity injection (Fig. 3.5a). The enhancement of submonthly fluctuations in the troposphere occurs over the Atlantic, Indian Ocean, the southwestern Pacific, where the downward wave-activity injection from the stratosphere is intensified.

Associated with the variations of the downward wave activity propagation to the south of Australia, the stratospheric PNJ axis over the Indian Ocean is shifted poleward with the

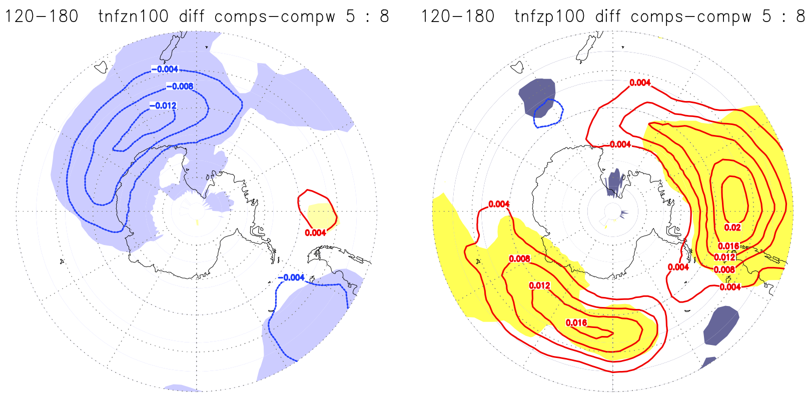

Figure 3.4: (a) Difference of composite map for monthly-mean downward wave-activity flux between "active" and "nonactive" downward wave-activity propagation months to the south of Australia. Red and blue line denote positive and negative, respectively (contour interval is 0.004 [m^2s^{-2}] and a zero line is omitted). Enhanced downward wave activity is indicated by the blue line. Yellow and purple shading denotes the difference is positively and negatively significant at 90% level. (b) The same as (a) but for monthly-mean upward wave-activity flux.

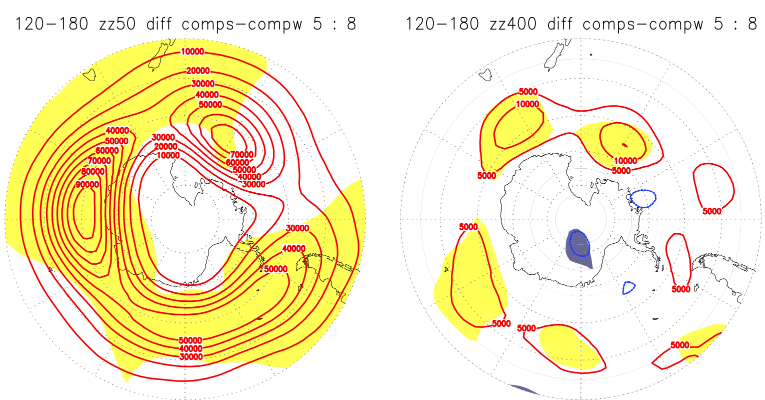

Figure 3.5: (a) Difference of composite map for variance of 50-hPa anomalous geopotential height defined in each months between active and nonactive downward injection months. The yellow and purple shading denotes the difference is positively and negatively significant by 90% with Student t-test. (b) The same as (a) but for 400-hPa level.

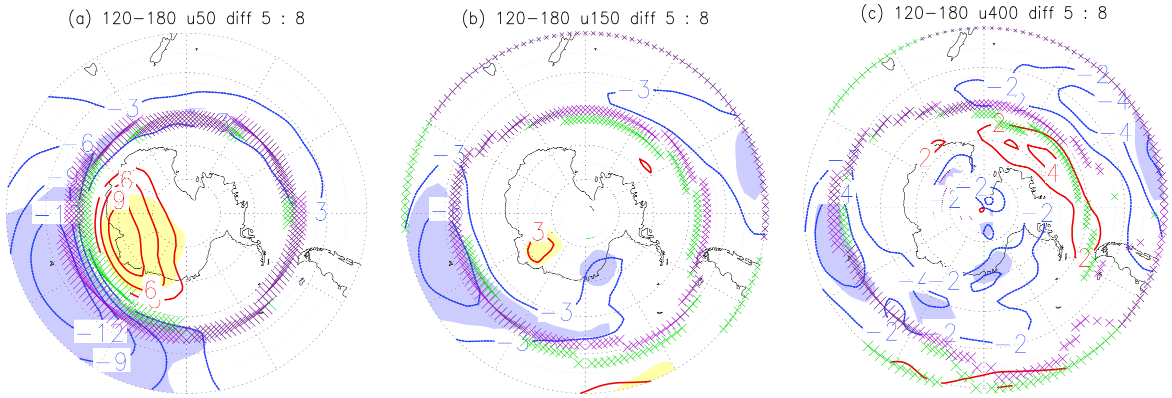

Figure 3.6: (a) The same as in Fig. 3.5 but for the 50-hPa monthly mean westerlies. Green and purple crosses denote westerly axes for the active downward months and inactive downward months, respectively. (b) The same as in (a) but for 150-hPa level. (c) The same as in (a) but for 400-hPa level.

wind speed of its poleward side being stronger and of its equatorward side being weakened (Fig. 3.6a). Near the tropopause and tropopause (Figs. 3.6b and c), wind speed is decreased significantly at the equatorward of jet axes over the Indian Ocean. In the poleward side of the jet axis, although not significant, tendency of stronger wind speed is observed.

Figure 3.7 shows vertical cross sections of the refractive index (κ_s), defined in (1.44), along 150°E based on the active and inactive composites. Along that meridian, the enhancement in downward wave-activity injection is prominent in the active months. In the active months, maxima in κ_s observed between 55°S and 60°S ($\kappa_s \geq 0$) in the stratosphere extend downward into the upper troposphere (Fig. 3.7a), while the stratospheric maxima in κ_s are disconnected from the tropospheric maxima in the inactive months (Fig. 3.7b). In other words, the "chimney" structure tends to be better established in the active months than in the inactive months, reflecting the jet structure. More specifically, the stronger vertical curvature of the westerly jet just above the tropopause contribute to the increasing κ_s in the active months (Fig. 3.7c).

To show the influence of the enhanced downward wave-activity injection on the tropospheric circulation in a more specific manner, one-point correlation of anomalous geopoten-

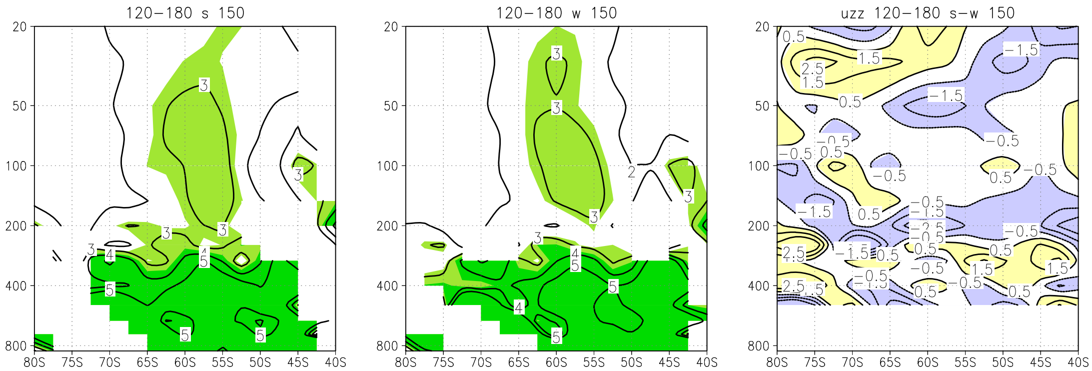

Figure 3.7: (a) Meridional section along 150°E of the refractive index (κ_s) composited for the months of active downward wave-activity injection to the south of Australia. The contour interval is 1. Light and heavy green shading denote the region where the refractive index is more than 2.8 and 3.5. The definition of active and inactive months is refereed to text. (b) The same as in (a) but for the months of inactive wave-activity injection. (c) Meridional section along 150°E of the composite difference in a composited vertical curvature of the mean westerlies jet. The negative curvature contribute to increasing κ_s as known from (1.38). The contour interval is 5.0×10^{-8} [$\mathrm{m}^{-1}\mathrm{s}^{-1}$]. Yellow and purple shading denote regions where the vertical curvature is more than 2.5×10^{-8} [$\mathrm{m}^{-1}\mathrm{s}^{-1}$] and less than -2.5*$10^{-8}$ [$\mathrm{m}^{-1}\mathrm{s}^{-1}$].

tial height field is constructed with 400-hPa height anomaly at (140°E, 55°S) as the reference time series. The grid point is in the region where the downward wave-activity injection is enhanced across the tropopause and submonthly fluctuations in the troposphere tend to be enhanced to its downstream during active months. The evaluation is based on the JRA25 data from 1979 to 2000. Figure 3.8 shows zonal cross sections of the one-point correlation for the “active” and “inactive” months. For the “active” months (Figs. 3.8a and b), a center of negative correlation is evident for the lag of -1 day in the lower stratosphere upstream (at ∼120°E) of the reference grid point, and another center of positive correlation farther upstream (at ∼120°E), indicative of a wave train along the stratospheric PNJ. Between the stratospheric domain of the negative correlation and the tropospheric domain of the positive correlation around the reference grid point, correlation contours are tilted eastward with height, suggestive of downward Rossby wave-activity injection to the tropospheric anomalies developing around the reference points from stratospheric anomalies that had developed earlier. For the “inactive months”, in contrast, significant correlation is confined to the tro-

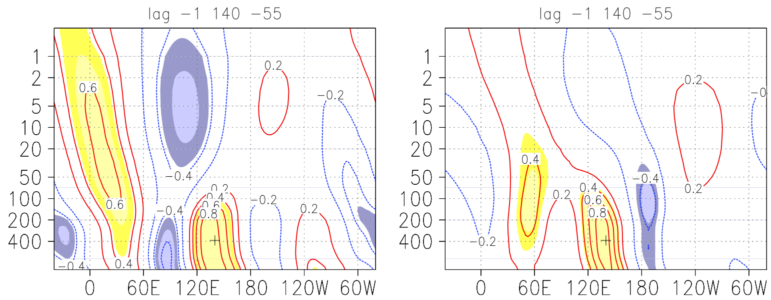

Figure 3.8: (a) Zonal cross section along 55°S latitude of one point correlation maps based on 400-hPa, 140°E-55°S grid with -1 lag day using active downward wave-activity injection months defined in the text. Red and blue contours denote positive and negative. Contour interval is 0.2 and zero lines are omitted. Yellow and purple shading denotes positively and negatively significant signal over 95% level, respectively. (b) The same as in (a) but for using nonactive downward wave-activity injection months.

posphere and no significant anomaly is present in the stratosphere (Figs. 3.8c and d).

3.3.2 Over the South Atlantic

Interannual variability in the downward wave-activity injection across the tropopause is also strong over the South Atlantic, where the climatological mean downward wave-activity injection is prominent (Fig. 3.2a). A relationship similar to that discussed in the preceding subsection is found between anomalous structure of the westerly jet streams and the anomalous vertical wave-activity injection, through the sample composite analysis as applied earlier. The area average of 100-hPa monthly-mean downward wave-activity flux from 30°W to 60°W in longitude and from 50°S to 60°S in latitude was used for selecting the months of “active” and “inactive” downward wave-activity injection across the tropopause. A particular month was selected as the “active” (“inactive”) months when the are-averaged flux was stronger than 0.01 [m^2s^{-2}] (weaker than 0.0015 [m^2s^{-2}]). In this manner, five months (Aug. 1988, Sep. 1990, Sep. 1991, Aug. 1992, Sep. 1996) have been selected as the “active” months and another five months (Aug. 1984, Aug. 1989, Aug. 2000, Aug. 2001, Sep. 2003) for “inactive” months. When composited for the “active months”, the downward wave-activity flux over the South Atlantic and the upward wave-activity flux over

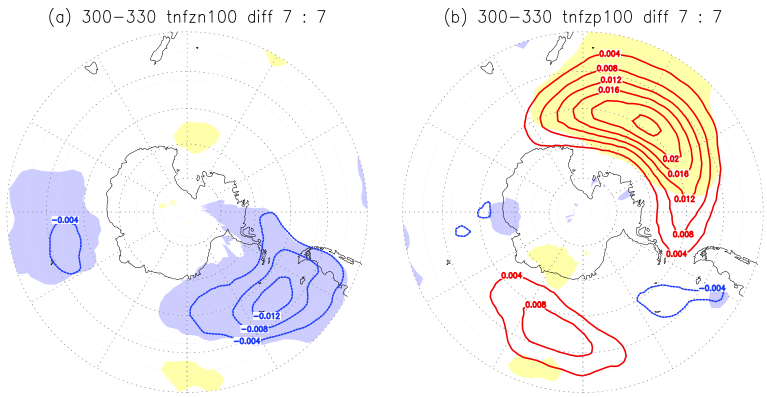

Figure 3.9: (a) The same as in Fig. 3.4a but for over the South Atlantic. (b) The same as Fig. 3.4b but for over the South Atlantic.

the central Pacific both at the 100-hPa level tend to be more prominent than in the “inactive” months (Fig. 3.9). Over south America, located upstream (downstream) of the region of enhanced downward (upward) wave-activity propagation across the troposphere, the axis of the lower-stratospheric PNJ shifts slightly poleward in the “active” months (Fig. 3.10). The tropospheric SPJ tends to strengthen at its mean axis and weakens at the equatorward side especially over the South Atlantic, where the downward wave-activity injection into the troposphere is augmented (Fig. 3.9a), and its upstream over the South Pacific enhancement of the tropospheric submonthly fluctuations is apparent particularly over the South Pacific, where the upward wave propagation is stronger (Fig. 3.9b). Though slightly less apparent, the enhancement in the tropospheric variability is also observed in the Southeastern Atlantic (Fig. 3.11), slightly downstream of the region of the enhanced downward wave-activity injection (Fig. 3.9b).

Figures 3.12a and b show meridional sections of κ_s along 320°E. In active downward wave-activity injection months, the maximum of κ_s is observed around 100-hPa level, which is not in inactive downward wave-activity injection months. This maximum is contributed to by both vertical and meridional curvatures as shown in difference composite of them (Figs. 3.12b and c).

One-point correlation maps have been constructed for low-pass-filtered submonthly height

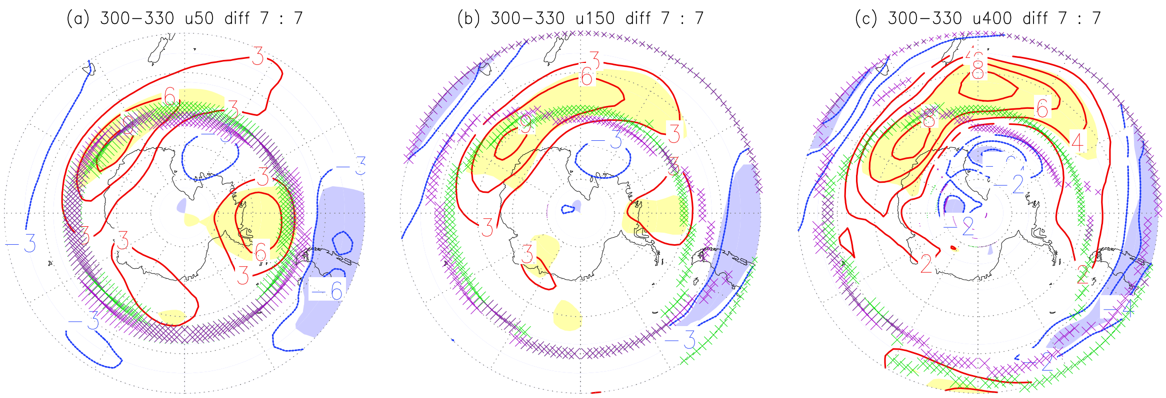

Figure 3.10: (a) The same as in Fig. 3.6a but for composite map over the South Atlantic. (b) The same as in (a) but for the 150-hPa level. (c) The same as in (a) but for the 400-hPa level.

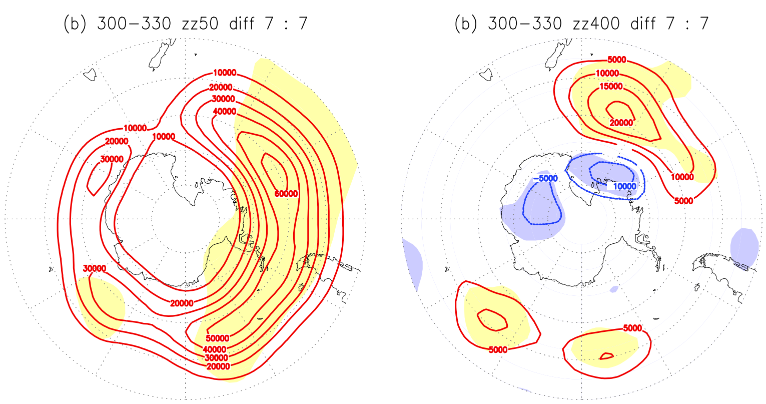

Figure 3.11: (a) Same as in Fig. 3.5a but for over the South Atlantic. (b) The same as Fig. 3.5b but for over the South Atlantic.

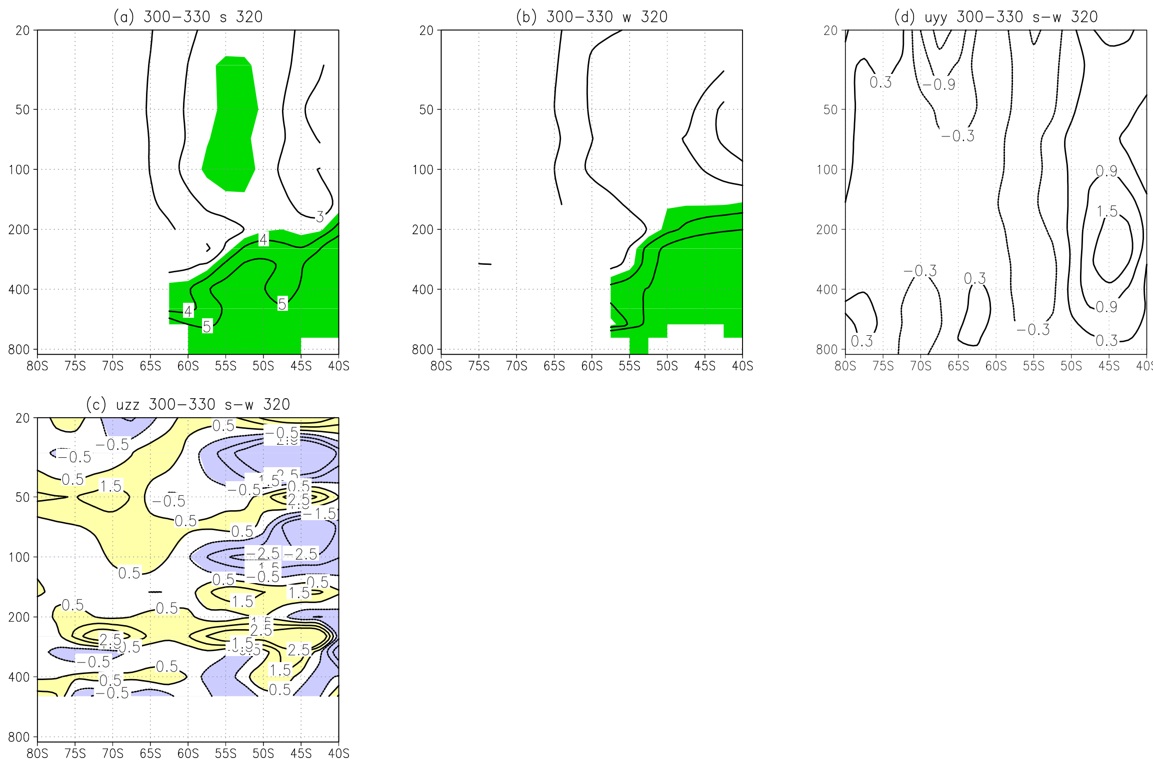

Figure 3.12: (a) Same as in Fig. 3.7a but for a composite map for "active" months over the South Atlantic and meridional cross section along 320°E. Shading denotes where κ_s is over 3.5. (b) The same as in (a) but for the months of inactive wave-activity injection. (c) Same as in Fig. 3.7a but for a composite map for "active" months over the South Atlantic and a meridional cross section along 320°E. (d) Same as in (c) but for meridional curvature. The contour is for -1.5, -0.9, -0.3, 0.3, 0.9, 1.5 $\times$ 10^{-11} [$m^{-1}s^{-1}$]. The negative meridional curvature contribute to increasing κ_s as known from (1.38).

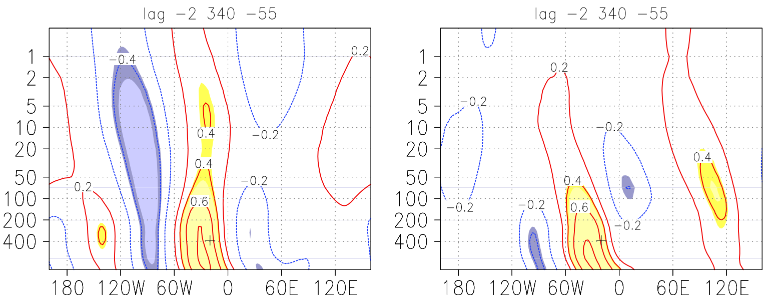

Figure 3.13: (a) The same as in Fig. 3.13a but for the base point is at 20°W-55°S grid with -2 lag day using active downward wave-activity injection months defined in the text. (b) The same as in (a) but for using nonactive downward wave-activity injection months.

anomalies with the reference time series at (20°W, 55°S) at the 400-hPa level. For the "active" months, significant negative correlation is apparent in the lower stratosphere upstream of the tropospheric reference point over the South Atlantic with the lag of -2 days (Fig. 3.13a). In the correlation maps, contour lines are tilted eastward with height upstream of the reference point, which suggests that the downward wave-activity injection tends to occur across the tropopause. In the corresponding correlation map for the "inactive" months (Fig. 3.13b), in contrast, no signal is found upstream in the stratosphere.

3.3.3 Influence of SAM

In the preceding subsections, it is suggested that the westerly jet structure variations are important to determine downward wave-activity injection across the tropopause. As noted in the first section, interannual variations associated with SAM is large in the troposphere. Circulation variations associated with SAM are also observed in the wintertime stratosphere (Thompson and Wallace 2000). Thus the interannual variations of wave-activity propagation associated with SAM is expected through the PNJ and SPJ structure changes.

In this study, the SAM is defined as the leading empirical orthogonal function (EOF) of anomalies in 850-hPa height in August and September. The region of poleward of 20°S were used for our EOF analysis, where the local height anomalies have been weighted by the square root of cosine of latitude (Thompson and Wallace 2000 [2]). This leading EOF can account for 22% of the total variance of the monthly 850-hPa height anomalies. The positive and negative SAM events were defined by using the corresponding principal component (PC) time series normalized by its standard deviation. A month with PC under -0.6 (over +0.6) was regarded as a positive (negative) event of SAM. Composite maps were made for monthly-mean geopotential height, westerlies, variances of submonthly height fluctuations and their associated wave-activity flux. The 13 positive SAM events selected are Aug. 1982, Sep. 1982, Sep. 1985, Sep. 1986, Aug. 1987, Sep. 1990, Aug. 1993, Sep. 1993, Aug. 1994, Sep. 1995, Sep. 1997, Aug. 1998 and Sep. 2001, and 13 negative SAM events are Aug. 1980, Sep. 1980, Aug. 1981, Sep. 1981, Sep. 1983, Aug. 1984, Aug. 1986, Sep. 1988, Sep. 1994, Aug. 1996, Sep. 1996, Sep. 2000 and Sep. 2002.

Figures 3.14a and b show the difference composite maps of 850-hPa and 50-hPa height anomalies, respectively, between the positive and negative events of SAM. A seesaw pattern between the polar region and lower latitudes is evident both in the troposphere and the lower stratosphere. In association with SAM, the SPJ in the lower stratosphere and the tropospheric PNJ are also changing (Fig. 3.15). In the positive phase of SAM, the PNJ and SPJ tend to strengthen around the 60°S circle, especially over the South Indian Ocean, south of Australia and the Southwestern Pacific. They also strengthen slightly while shifting its axis poleward over the Drake passage. Corresponding to the poleward shift of the PNJ axis, downward wave-activity flux tends to be more active over the Drake Passage during the positive SAM events than during negative SAM events (Fig. 3.16). In fact, a one-point correlation map of the submonthly height anomalies for positive SAM months based on the reference time-series at (30°W, 70°S), 400-hPa level displays significant negative correlation in the lower stratosphere with the lag of -2 days upstream of the reference grid point (Fig. 3.17a), while such negative correlation is missing for the corresponding map for the negative SAM months (Fig. 3.17b). However, despite the significant changes in the PNJ and SPJ almost at every

[2] In Thompson and Wallace (2000), SAM is defined using all year or cold months (May to October).

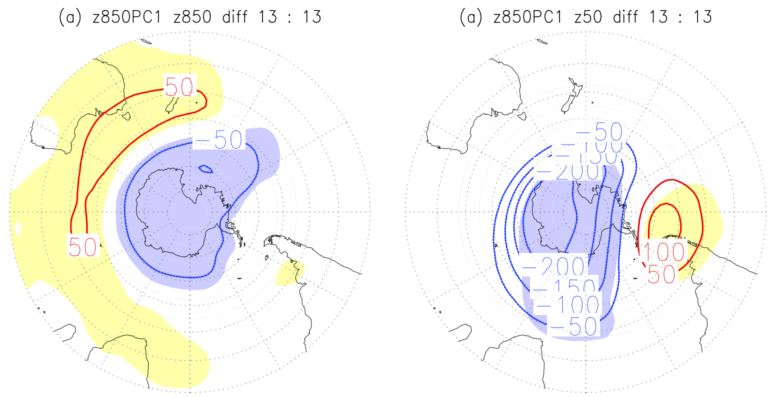

Figure 3.14: (a) Difference composite maps (poleward of 20°) of monthly-mean 850-hPa geopotential height between the positive and negative SAM months as defined in the text. Contour interval is 50 [m] (zero line is omitted) and red and blue line denote positive and negative difference, respectively. Yellow and purple shading is applied where the significance of the positive and negative differences exceeds the 90% confidence level. based on Student t-static. (b) Same as in (a) but for 50-hPa height.

longitude associated with SAM (Fig. 3.15), the anomalous downward wave-activity flux is weaker than that shown in the previous sections, and its influence on the vertical propagation of wave-like submonthly fluctuations can not be observed downstream of the the anomalous downward wave-activity flux, over the South Atlantic (Fig. 3.18b). In addition, prominent changes of submonthly fluctuations in the stratosphere is not observed (Fig. 3.18a). It is therefore concluded that the dominant variability in the PNJ and SPJ associated with SAM exerts only limited influence on the vertical propagation of submonthly wave-like fluctuations across the tropopause, which tends to be more sensitive to local changes in the PNJ and SPJ.

3.3.4 Influence of ENSO

a. Definition of the El Niño and La Niña years

To address the ENSO influence on vertical wave-activity propagation associated with submonthly fluctuations, a composite analysis as in the preceding sections was applied separately to El Niño and La Niña months that had been selected for August and September on

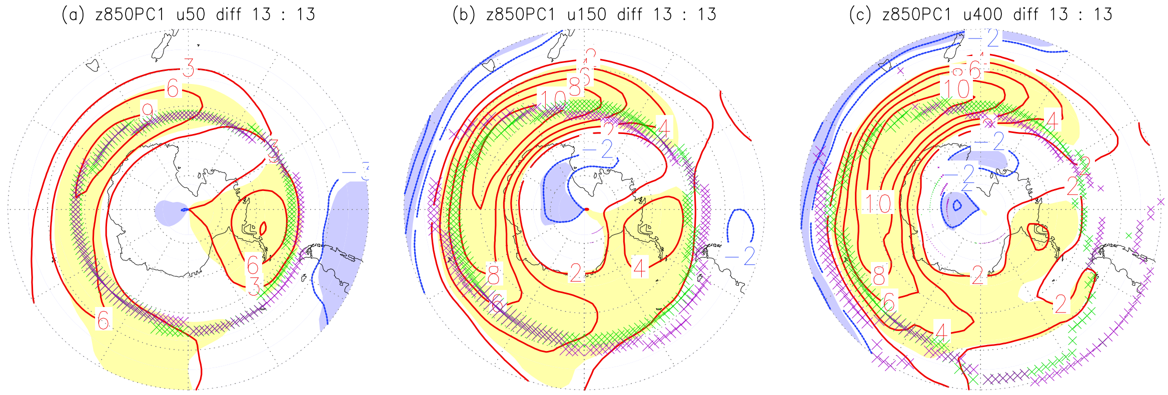

Figure 3.15: (a) Same as in 3.14 but for 50-hPa zonal wind (poleward of 40°S). Contour interval is 2 [m/s] and zero line is omitted. (b) Same as in (a) but for 50-hPa zonal wind with contour interval of 3 [m/s].

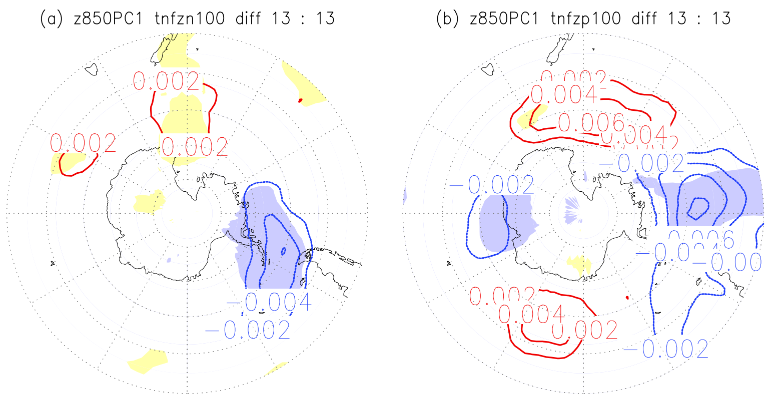

Figure 3.16: Same as in 3.14 but for 100-hPa (a) downward and (b) wave-activity flux with contour interval of 0.002 [m^2s^{-2}.

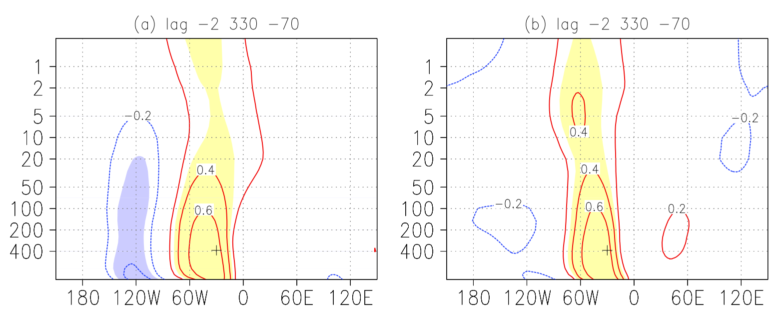

Figure 3.17: Same as in Fig. 3.13a but for (a) positive and (b) SAM months. Reference time series are used at 400-hPa, 30°W-70°S.

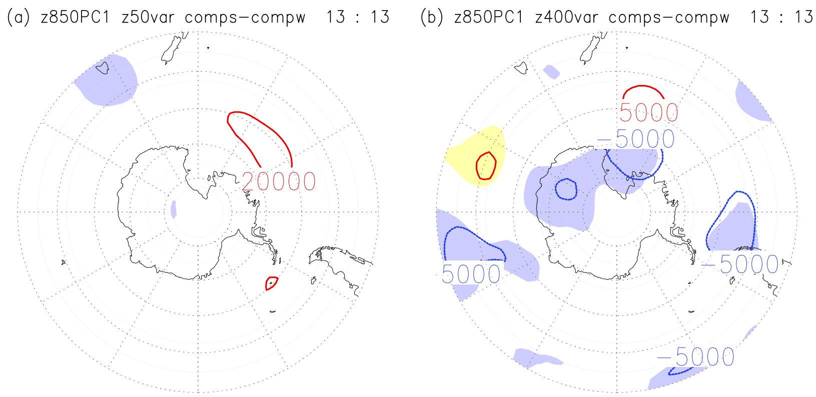

Figure 3.18: The same as in 3.14 but for 400-hPa submonthly height variance. The contour interval is 5000 [m^2] and zero line is omitted.

the basis of the Japan Meteorological Agency (JMA) definition. El Niño (La Niña) periods are defined when 5-month moving averaged sea surface temperature (SST), averaged between 90°W and 150°W and between 4°N and 4°S in the equatorial Eastern Pacific, exceeds (is below) the climatological SST [3] by 0.5°C successively for more than 6 months. Thus, 14 El Niño months have been selected for August and September of 1982, 1983, 1987, 1991, 1993, 1997 and 2002, and 6 La Niña months for August and September of 1985, 1988 and 1999. The other 30 months have been categorized as neutral months. The degree of freedom used in our statistical tests is estimated not by the number of months but by the number of years, taking the interannual nature of ENSO into consideration. It has been shown that a typical circulation anomaly pattern in the troposphere during the El Niño event is not the perfect mirror image of that during a La Niña event, especially in winter (e.g., Kiladis and Mo 1999). Thus we made composite maps separately for each of those groups and then diagnosed their differences between the El Niño and neutral months (EN-n) and between the La Niña and neutral months (LN-n).

b. Mean circulation anomalies associated with ENSO

[3] The climatological SST is obtained for 30 years from 1961 to 1990.

Before discussing on the ENSO related modulations in the vertical wave-activity propagation associated with submonthly fluctuations, we study the ENSO influence on the monthly-mean circulation in the stratosphere as well as in the troposphere[4]. Figures 3.19 and 3.20 show the EN-n and LN-n composite maps of monthly-mean geopotential height, respectively, in the stratosphere and troposphere. The associated wave-activity flux defined in TN01 is presented in Figs. 3.21 and 3.22. In the estimation of the wave-activity flux (1.40), fluctuations were considered as the composite difference (i.e., EN-n and LN-n) and the basic state was taken as the composite circulation fields for the neutral months. Thus the El Niño and La Niña related circulation anomalies are considered as waves propagating on the zonally-asymmetric basic state that would be typically observed in the August and September period in a non-ENSO year. In the El Niño months, the wave-activity flux in the troposphere shown by arrows in Fig. (3.21b) reveals two wave trains, one is propagating southeastward over the south of Australia, and the other propagating southeastward over the South Eastern Pacific and then northeastward over the South Atlantic. In the La Niña months of the troposphere (Fig. 3.22b), a wave train that consists of anticyclonic anomalies to the south of Australia and over the Drake Passage, and negative anomalies over the Ross Sea is prominent in the troposphere (Fig. 3.22b). Those tropospheric anomaly patterns associated with El Niño and La Ninã are consistent with Figs. 8.4 and 8.5 of Kiladis and Mo (1999).

For the El Niño months in the lower-stratosphere (Fig. 3.19a), the persistent anticyclonic anomalies over the Drake Passage are statistically significant, showing an equivalent barotropic structure from the troposphere to the lower stratosphere (Figs. 3.19b and c). The upward wave-activity flux from the troposphere through the upstream portion of the anticyclonic anomalies and the eastward wave-activity flux through the anomalies in the lower stratosphere suggest that the lower-stratospheric anticyclonic anomalies are part of the wave train propagating upward the Australian region (Fig. 3.21a). A zonal cross section along 70°S (Fig. 3.23) confirms that the stratospheric anticyclonic anomalies over the Drake Pas-

[4]We could not fi nd any previous study on ENSO influence on the stratospheric circulation in the SH.

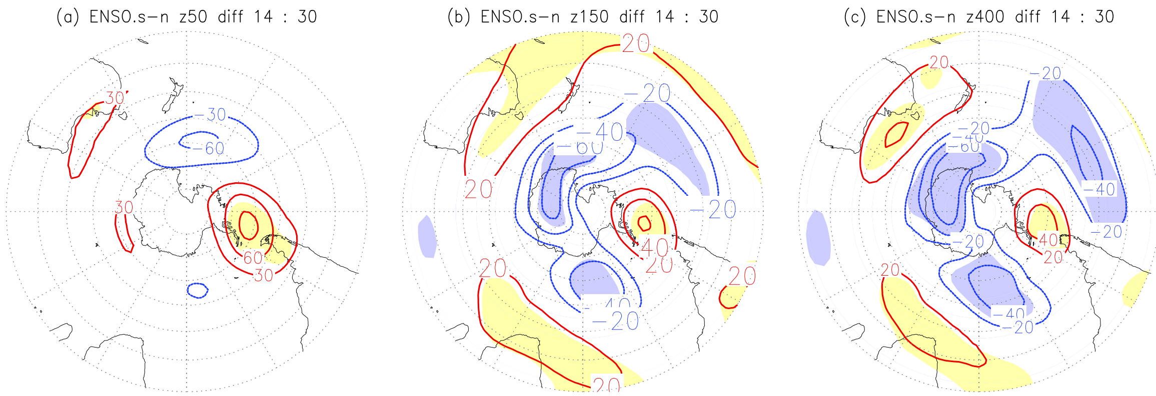

Figure 3.19: (a) A composite difference map of monthly-mean 50-hPa geopotential height between El Niño and neutral months (EN-n). Red and blue contours denotes positive and negative anomalies with intervals of 30 [m]. Zero contour is omitted. Yellow and purple shading is applied where the difference is significant positively and negatively, respectively. Note that southward of 20° S is shown. (b) The same as in (a) but for the 150-hPa level with contour intervals of 20 [m]. (c) The same as in (b) but for the 400-hPa level.

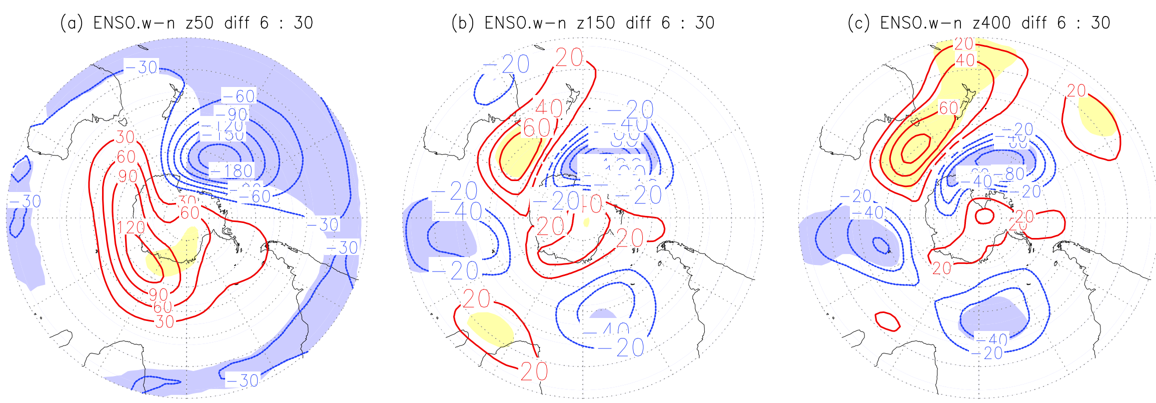

Figure 3.20: (a) The same as in 3.19a but for difference between La Niña and neutral months (LN-n). (b) The same as in (a) but for the 150-hPa level and with intervals of 20 [m]. (c) The same as in (b) but for the 400-hPa level.

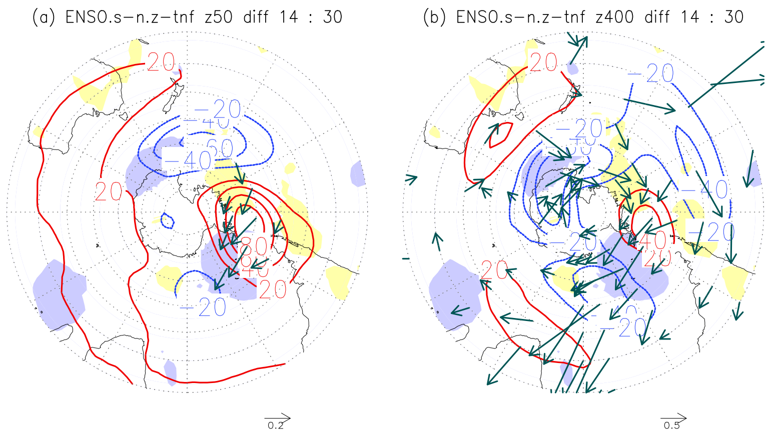

Figure 3.21: (a) Contours are the same as in Fig. 3.19a for El Niño months (EN-n). A wave-activity flux (TN01) associated with the monthly anomalies shown in Fig. 3.19 is superimposed with green arrows [m^2s^{-2}], and scaling for the arrows is given at the right-lower corner of the panel. Yellow and purple and shading denote where the vertical component of the 100-hPa wave-activity flux (TN01) exceeds 0.0005 [m^2s^{-2}] in magnitude positively and negatively, respectively. (b) The same as in (a) but for the 400-hPa level. The contour interval is 30 [m] and the shading is the same as in (a).

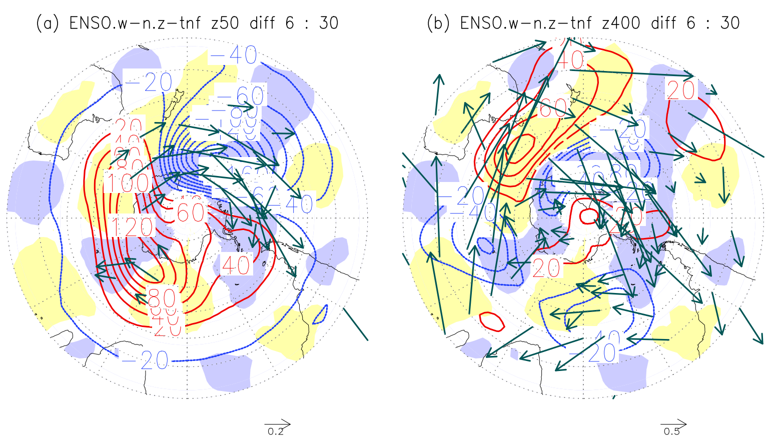

Figure 3.22: (a) The same as in Fig. 3.21a but for the La Ninã months (LN-n). (b) The same as in Fig. 3.21b but for LN-n.

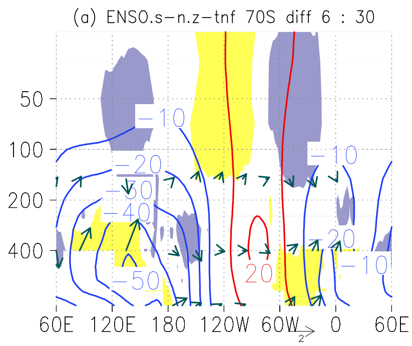

Figure 3.23: A zonal cross section of geopotential height anomaly composited along 70°S for the El Niño months (EN-n). Height anomalies are normalized with square root of pressure. The wave-activity flux associated with monthly anomalies is presented with arrows [m^2s^{-2}] and scaling for the arrows is given at the right-lower corner of the panel. Yellow and purple shading denotes vertical components of the wave-activity flux above 0.005 [m^2s^{-2}] and under -0.005 [m^2s^{-2}].

sage (around 90°W) are associated with the weak upward wave-activity flux from the tropospheric cyclonic anomalies upstream.

In contrast, the La Ninã-related persistent circulation anomalies in the lower stratosphere are characterized by a pair of significant cyclonic (negative) anomalies over the South Pacific and significant anticyclonic anomalies over the South Indian Ocean (Fig. 3.20a). In the lower-stratosphere (Fig. 3.22a), wave-activity propagation from the anticyclonic anomalies to cyclonic anomalies is evident along the PNJ. The upward wave-activity flux across the tropopause is evident in the downstream portion of the anticyclonic anomalies to the south of Australia, from which the eastward wave-activity flux is divergent through the cyclonic anomalies downstream (Fig. 3.22a). A zonal cross section along 55°S shows the upward wave-activity propagation from the deep anticyclonic anomalies around 120°E in the troposphere into the deeper cyclonic anomalies over the eastern Pacific in the lower stratosphere (Fig. 3.24). The upward flux and stratospheric anomalies tend to be much stronger than in the El Niño months. The composited analysis above suggests that remote influence of ENSO in the wintertime extratropical SH is not only in the troposphere as shown in the previous studies but also extending into the lower stratosphere in the form of the stationary Rossby

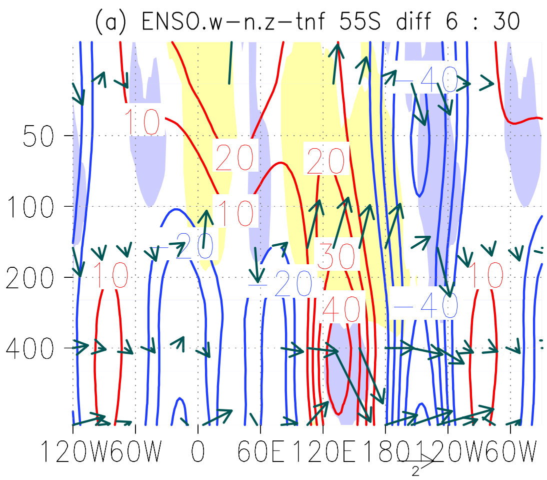

Figure 3.24: The same as in Fig. 3.23 but for the La Niña months (LN-n) and along 55°S circle.

waves, especially in La Niña years. The robustness of the stratospheric anomalies, however, may not be particularly high, especially for the La Niña composite based only on the three events.

c. Changes of monthly-mean westerly jet structures and vertical wave-activity propagation associated with submonthly fluctuations

The above-mentioned ENSO-associated monthly-mean anomalies modify the structure of the monthly-mean westerlies, which can influence activity and propagation of submonthly fluctuations. In the El Niño years, the PNJ tends to be enhanced over the Antarctic coast around 90°E and to the south of Drake Passage (Fig. 3.25a), indicating the shift of the PNJ axis in the regions. The westerlies are slightly enhanced also around the tropopause and troposphere over those regions (Fig. 3.25b and c). In addition , the tropospheric SPJ is intensified also to the south of Australia and from the South Atlantic to the southeastern Indian Ocean (Fig. 3.25c). Associated with the shift of the stratospheric PNJ axes, downward wave-activity injection into the troposphere is enhanced significantly over the southern Indian and the South Pacific (3.26a). Upstream of each of those regions, upward wave-activity propagation into the stratosphere is more active than in the neutral months over the South Atlantic

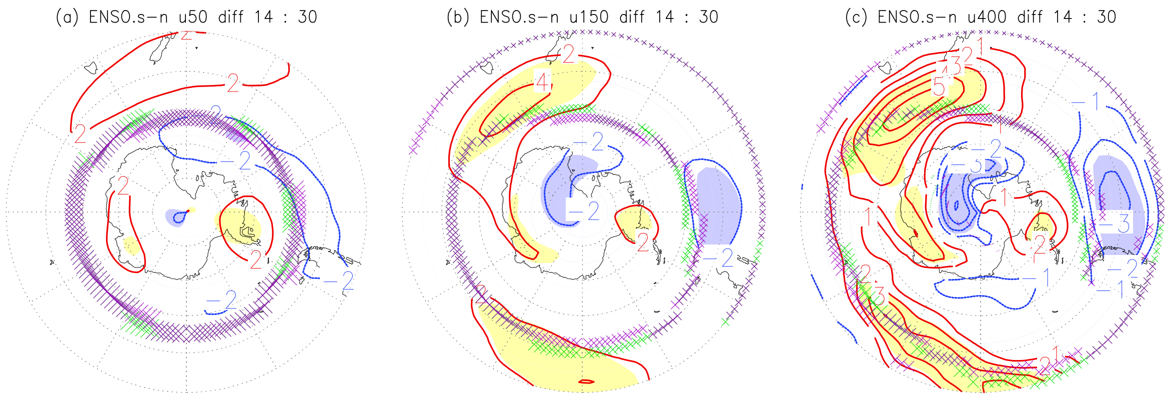

Figure 3.25: (a) The difference of 50-hPa monthly-mean westerlies composite map between El Niño and neutral months. The contour interval is 2 [m/s] and red and blue denote positive and negative values, respectively. Yellow and light purple shading denotes the significant differences positively and negatively at the 90% confidence level diagnosed by the Student t statics. Green and purple crosses show axes of westerlies jets in El Niño and neutral months, respectively. (b) The same as in (a) but for 150-hPa level. (b) The same as in (a) but for 400-hPa level.

and the Southwestern Pacific (Fig. 3.26b), where the tropospheric SPJ is intensified up to the tropopause level (Fig. 3.25). Associated with the upward wave-activity propagation into the stratosphere, the lower-stratospheric submonthly fluctuations over the southern Indian Ocean and the South Pacific are strengthened substantially (3.27a). However, the activity of tropospheric submonthly fluctuations is not changed significantly even in the downstream of downstream regions of the prominent downward wave-activity injection (Fig. 3.27b). Therefore, the enhancement of submonthly fluctuations in the lower stratosphere is not due to corresponding enhancement in the tropospheric activity, but rather it is due to the changes in the vertical waveguides as a remote influence of El Niño.

In the La Niña years, the PNJ is weakened over the Ross Sea, around 150°W (Fig. 3.28a). Although insignificantly, the PNJ tends to be enhanced over the Antarctic coast around 90°E. In the troposphere, the SPJ is strengthened to the south of Australia and New Zealand and its axis is shifted equatorward over the Southeastern Pacific, where the westerlies are weakened above the Antarctic coast (Fig. 3.28c). Figure 3.29a shows that downward wave-activity injection across the tropopause is enhanced over the Southwestern Pacific, much more strongly

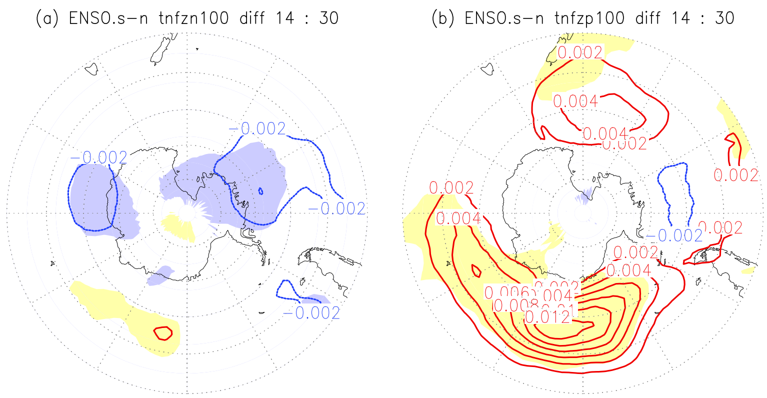

Figure 3.26: (a) The difference of 100-hPa monthly-mean downward wave-activity flux between El Niño and neutral months. The contour interval is 0.001 [m^2s^{-2}] and red and light blue denote positive and negative values, respectively. Yellow and purple shading denotes the significant difference positively and negatively at 90% confidence level diagnosed by the Student t statics. (b) The same as in (a) but for 100-hPa monthly-mean upward wave-activity flux.

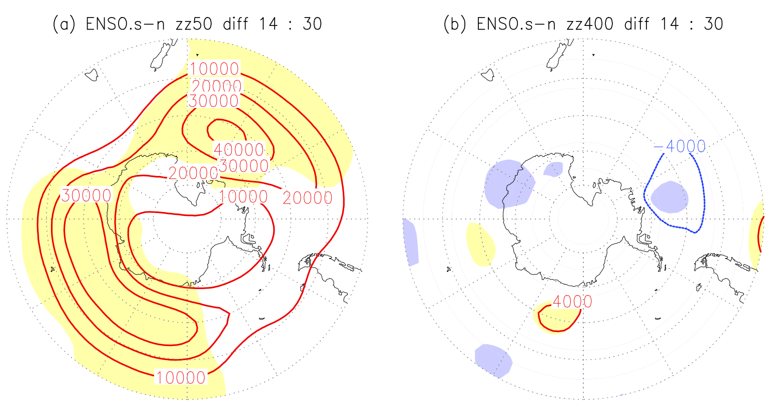

Figure 3.27: (a) The difference of 50-hPa submonthly height variance between El Niño and neutral months. The contour interval is 10000 [m^2] and red and blue denote positive and negative, respectively. Yellow and purple shading denotes the significant difference positively and negatively at 90% level diagnosed by Student t statics. (b) The same as in (a) but at 400-hPa level and the contour interval is 4000 [m^2].

in the months of El Niño. The enhancement is associated with the stronger PNJ. Enhanced upward wave-activity injection across the tropopause is observed over the South Pacific, downstream of the region of the enhanced downward wave-activity injection (Fig. 3.29b). submonthly fluctuations in the lower stratosphere are enhanced where upward wave-activity propagation in the stratosphere is enhanced over the South Pacific (Fig. 3.30a). In the troposphere, submonthly fluctuations are enhanced over the South Pacific just around the region of the enhanced downward wave-activity injection across the tropopause (Fig. 3.30a). The enhancement of the tropospheric submonthly fluctuations associated with the downward wave-activity injection over the Southwestern Pacific in the La Niña winters is confirmed by a one-point correlation map based on the reference time-series at (30°W, 50°S), the 400-hPa level with the lag of -1 day, where negative correlation is observed in the stratosphere upstream of the tropospheric reference grid point (Fig. 3.31a). Contrastingly, in the neutral months, no such negative correlation is observed in the stratosphere (Fig. 3.31b). In good correspondence to Pacific, the enhanced downward wave-activity injection, κ_s shows a belt of maxima extending vertically from the lower-stratosphere into the troposphere between 60°S and 65°S, (200-hPa to 300-hPa level) in the La Niña months (Figs. 3.32a), whereas such vertical waveguide structure is less obvious in the neutral months (Figs. 3.32b). A difference composite map of the meridional curvature of westerlies between La Niña and neutral months shows that the larger κ_s is due to the larger meridional curvature of the westerlies associated with enhanced the SPJ (Fig. 3.32c).

3.4 Discussion

In this chapter, we have shown that in association with enhancement of downward wave-activity injection, the PNJ axes tend to shift poleward upstream of the region of downward wave-activity injection. To confirm the influence of the PNJ axis shift on the downward wave-activity injection, composite analysis is done for months when the monthly-mean PNJ

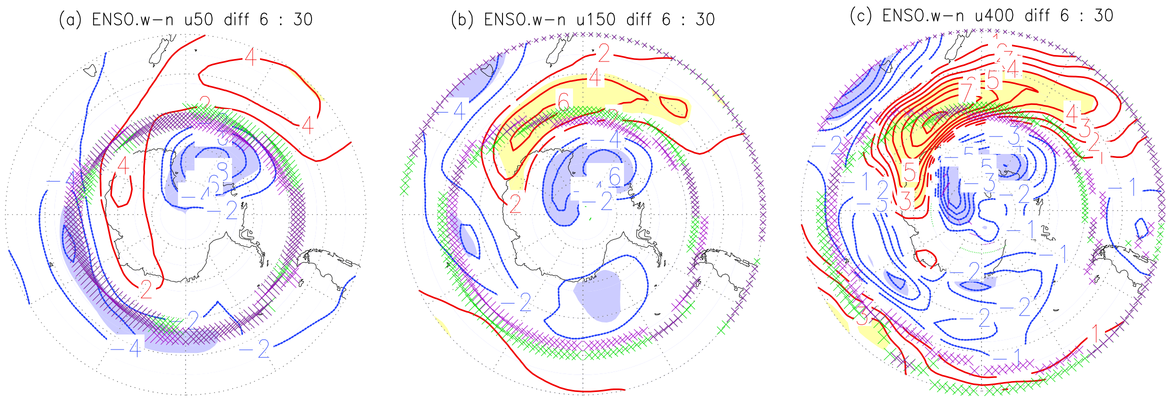

Figure 3.28: (a) The same as in Fig. 3.25a but for difference of 50-hPa monthly-mean westerlies composite map between La Niña and neutral months. (b) The same as (a) but for 150-hPa level. (b) The same as (a) but for 400-hPa level.

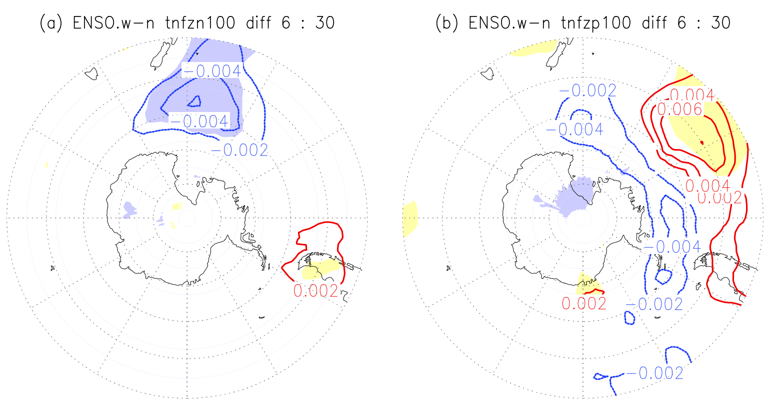

Figure 3.29: (a) The same as in Fig. 3.26a but for difference between La Niña and neutral months. (b) The same as in (a) but for 100-hPa monthly-mean upward wave-activity flux.

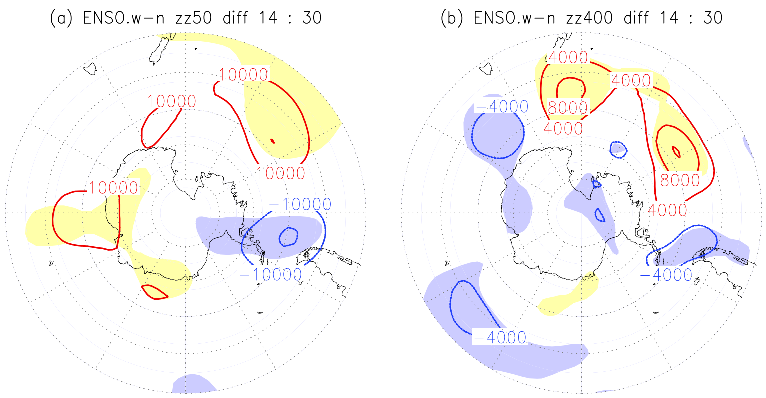

Figure 3.30: (a) The difference of 50-hPa submonthly height variance between La Niña and neutral months. The contour interval is 10000 [m^2] and red and blue denote positive and negative, respectively. Yellow and purple shading denotes the significant difference positively and negatively at 90% level diagnosed by Student t statics. (b) The same as in (a) but at 400-hPa level and the contour interval is 4000 [m^2].

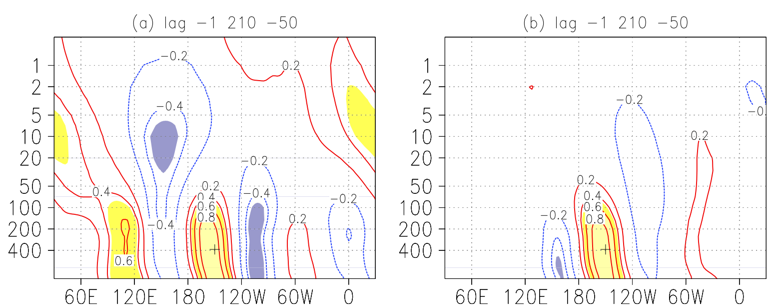

Figure 3.31: Same as in Fig. 3.13a but for (a) La Niña and (b) neutral months and at the lag of -1 day. Reference time series are used at 400-hPa, 30°W-50°S.

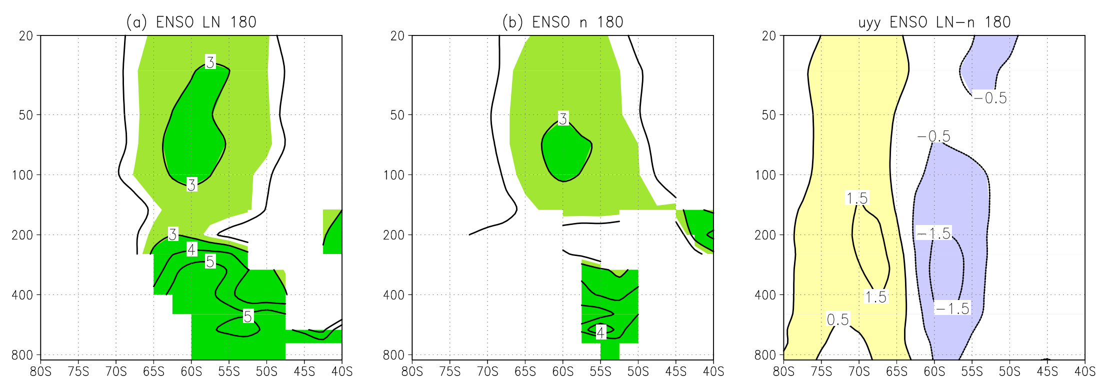

Figure 3.32: (a) Same as in Fig. 3.12a but for La Niña months and for 180^{κ}_{s} in longitude. Heavy and light shading denotes for 3.5 and 3. (b) Same as in (a) but for neutral months. (c) Same as in 3.12d but for difference composite maps between La Niña months and neutral months.

axes of particular longitudinal regions shift poleward and equatorward, respectively. In section 3.3.1, interannual variability of the downward wave-activity injection to the south of Australia was discussed. There, the downward wave-activity injection was shown to be enhanced associated with the poleward shift of the PNJ axis upstream (from 50°E to 80°E). Thus, September months are categorized when the monthly-mean PNJ axis, zonally averaged over the longitudes (from 50°E to 80°E) was shifted poleward (65°S; 1988 and 62.5°S; 1996 and 2002) and equatorward (55°S; 1980, 1985, 1987, 1994 and 2000). August months are not used in this analysis since the PNJ axis stays either at 55°S or 57.5°S, i.e., within 2.5° in latitude, corresponding to the interval of the NCEP/NCAR reanalysis data.

Figure 3.34a shows a difference composite map of 50-hPa westerlies between the "poleward-shifted-axis" and "equatorward-shifted-axis"Septembers. The PNJ axis shifted poleward with enhanced westerlies over the eastern Antarctic coast and weakened westerlies in the midlatitudes. Similar anomaly pattern is also observed around the tropopause level and in the troposphere (Figs. 3.34b and c). Thus, the axes of the westerly jets over the Eastern Hemisphere shift poleward in the stratosphere and troposphere. Associated with this jet axis shift, the downward wave-activity injection across the tropopause is observed over the South Indian Ocean (Fig. 3.35a) and the upward wave-activity injection is observed upstream of the region of the enhanced downward wave-activity injection (Fig. 3.35b). With the upward wave-activity injection from below, stratospheric submonthly fluctuations are enhanced over the Southwestern Indian Ocean (Fig. 3.36a) The enhanced region of the tropospheric submonthly fluctuations covers from the Southeastern Atlantic to the Indian Ocean, which suggests that the tropospheric fluctuation may be a source of the enhanced upward wave-activity flux and the downward wave-activity injection may contribute to the development of the tropospheric fluctuations. Meridional cross sections along 100°E of a composite refractive index κ_s for months when the PNJ axis shifts poleward and equatorward, respectively (Figs. 3.37a and b). In the former months, a belt of κ_s maxima across the tropopause is more obvious, connecting the troposphere and stratosphere, than in equatorward-shifted months.

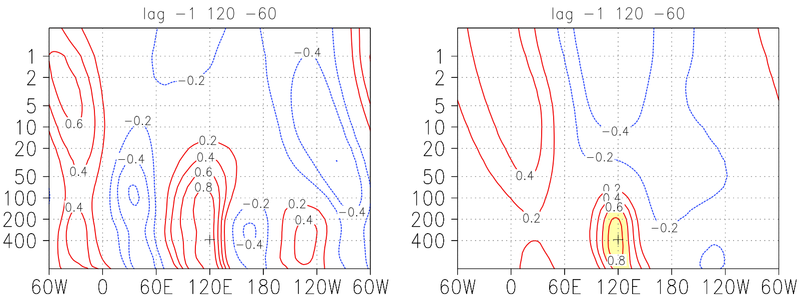

Figure 3.33: (a) The same as in Fig. 3.13a but for along 60°S latitude cross section and the base point is at 120°E-60°S grid with -1 lag day for the “poleward-poleward-shift-axis” months. (b) The same as in (a) but for “poleward-poleward-shift-axis” months.

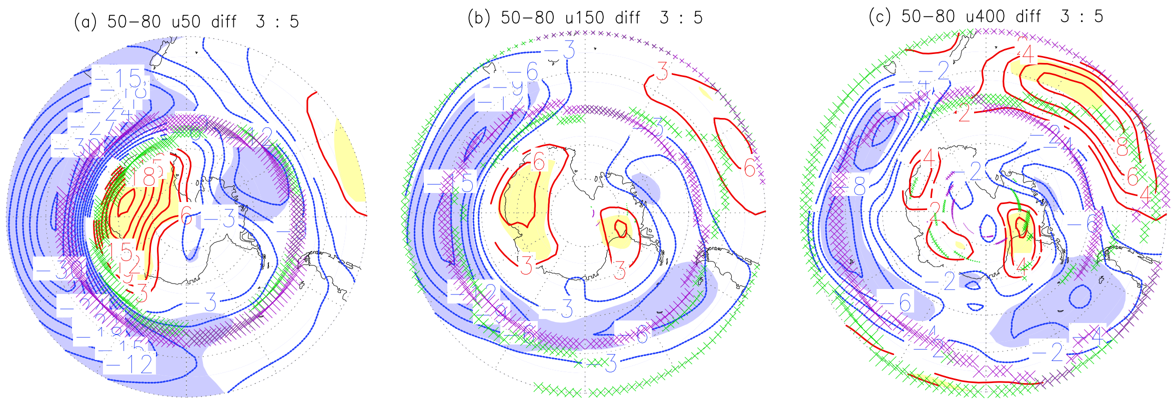

Figure 3.34: (a) The same as in Fig. 3.6a but for composite between composite maps for September between the “poleward-shifted-axis” and “equatorward-shifted-axis” year. (b) The same as in (a) but for 150-hPa westerlies. (c) The same as in (a) but for 400-hPa westerlies.

This maxima in κ_s is associated with the minima of the vertical curvatures of monthly-mean westerlies at 55°S around the 150-hPa level.

One-point correlation maps have been constructed for submonthly height anomalies with the reference time series at (120°E, 60°S) on the 400-hPa surface. For the poleward-shift-axis September, negative correlation in the lower stratosphere is found, though not quite significantly, upstream of the tropospheric reference point over the Indian Ocean with the lag of -2 days (Fig. 3.33a). We consider that this rather significance is due to the small number of sample months (2). It is interesting to note that, although all the signals are insignificant, positive and negative correlations are found farther upstream of the lower-

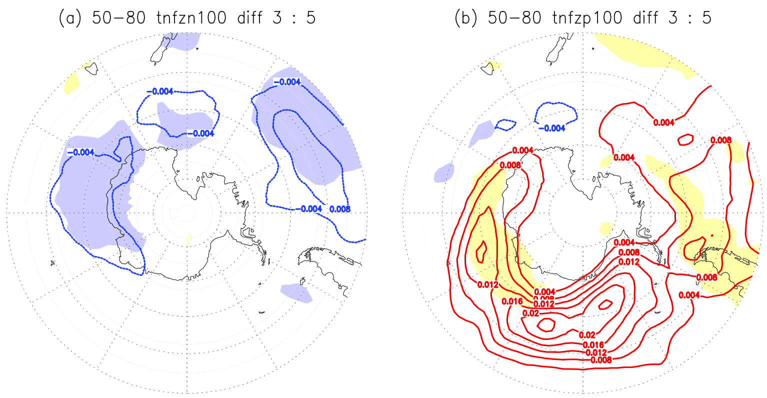

Figure 3.35: (a) The same as in Fig. 3.4a but difference between composite maps for "poleward-shift-axis" months and "equatorward-shift-axis" months. (b) As in (a), but for the 100-hPa monthly-mean upward wave-activity flux.

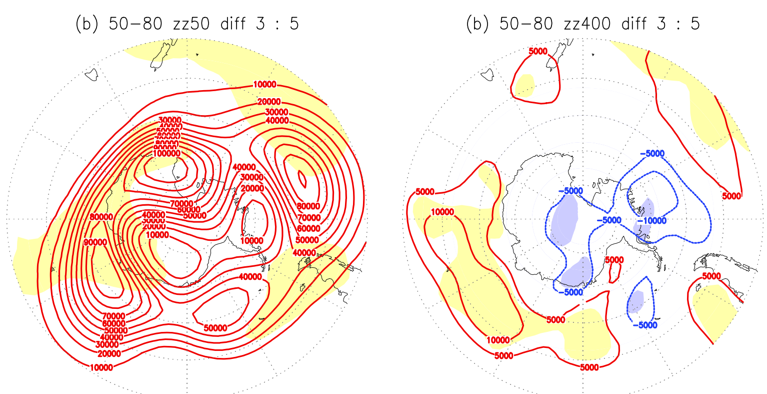

Figure 3.36: (a) The same as in Fig. 3.5a but difference between composite maps for "poleward-shift-axis" months and "equatorward-shift-axis" months. (b) As in (a), but for the 400-hPa level.

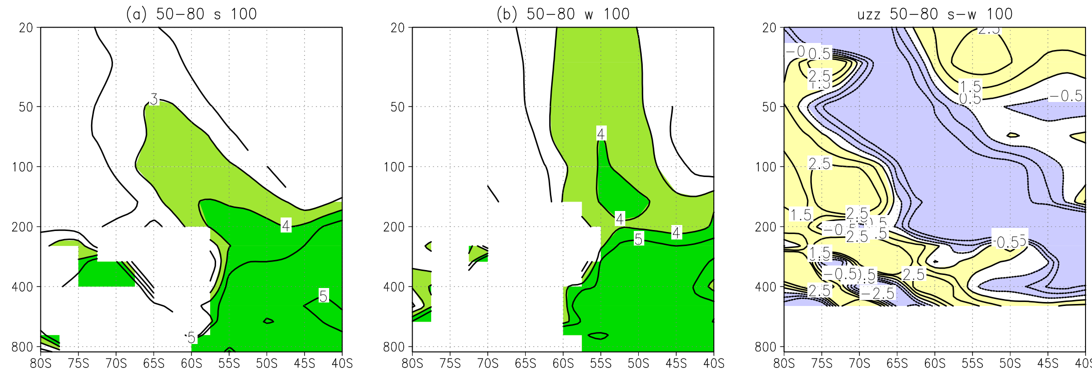

Figure 3.37: (a) Meridional section along 100°E of the refractive index (κ_s) composited for the months of the "poleward-shift-axis". Australia. The contour interval is 1. Light and heavy green shading denote the region where the refractive index is more than 3 and 4. The definition of active and inactive months is refereed to text. (b) The same as in (a) but for the months of the "equatorward-shift-axis". (c) Meridional section along 100°E of the difference composite map of a vertical curvature of the mean westerlies jet between "poleward-shift-axis" and "equatorward-shift-axis". The negative curvature contribute to increasing κ_s as known from (1.38). The contour interval is 5.0×10^{-8} [$m^{-1}s^{-1}$]. Yellow and purple shading denote regions where the vertical curvature is more than 2.5×10^{-8} [$m^{-1}s^{-1}$] and less than -2.5*11^{-8} [$m^{-1}s^{-1}$].

stratospheric negative correlation, suggestive of a wave train emanated over the Southeastern Pacific propagating eastward and upward in the stratosphere and then refracted back to the troposphere. In the equatorward shift PNJ axis months, no negative correlation is found in the lower stratosphere upstream of the tropospheric reference point is not observed. These results confirm that the meridional shift of local PNJ axis can affect the downward wave-activity injection into the troposphere.

One possible mechanism that induces the interannual variability of westerly jet structures both in the stratosphere and troposphere is ensemble effect of eddy momentum and heat fluxes. To estimate the effect of eddy momentum flux on the interannual variations of westerlies by eddies associated with low-pass-filtered submonthly anomalies the feedback forcing on the geopotential height field is estimated through a formula analogous to (2.2.1). In this evaluation, primes in (2.2.1) should denote low-pass-filtered anomalies and the over bars indicate monthly mean. Then the wind acceleration within a month due to the eddy momentum flux is estimated as the corresponding geostrophic westerly tendency. The zonal-mean feedback forcing of high-pass-filtered eddies with cut off period of 8 days, which are equivalent to baroclinic, transient migratory eddies, are also diagnosed in the troposphere. In section 3.3.1, it was shown that the downward wave-activity injection to the south of Australia (Fig. 3.4) is associated with poleward shift of the PNJ axis over the southern Indian Ocean (Fig. 3.6). Figure 3.38 suggests that enhanced westerly wind acceleration due to the feedback forcing from submonthly anomalies contributes positively to the maintenance of the poleward shift of the PNJ in the lower-stratosphere and also around the tropopause and troposphere. In the South Atlantic case mentioned in section 3.3.2, the poleward shift of the stratospheric PNJ and the enhancement of the tropospheric SPJ (Fig. 3.10) are maintained in part by the westerly wind acceleration due to the feedback forcing from submonthly anomalies (Fig. 3.39). However, high-frequency eddies do not seem to contribute to the enhancement of the SPJ over the South Atlantic (Fig. 3.40). We must note that the eddy forcing often tends to sustain the westerlies jet anomalies by changing eddy amplitudes, latitudinal positions or eddy shapes, for example in the variability of NAM and SAM (Limpasuvan and Hartmann 1999; Lorenz and Hartmann 2001). Thus the above-mentioned results do not exclude other possible mechanisms on the variation of the westerly jet structures.

3.5 Conclusion

We have discussed the climatology and interannual variability of local vertical wave-activity propagation in SH late winter (August and September), particularly on the downward wave-activity injection into the troposphere, associated formation of local waveguide around the tropopause and enhancement of submonthly fluctuations both in the troposphere and the stratosphere. The climatology of upward and downward wave-activity propagation is active in the South Pacific and the South Atlantic. There, the axes of the PNJ and SPJ are overlapped each other, which contributes to suitable condition for vertical propagation.

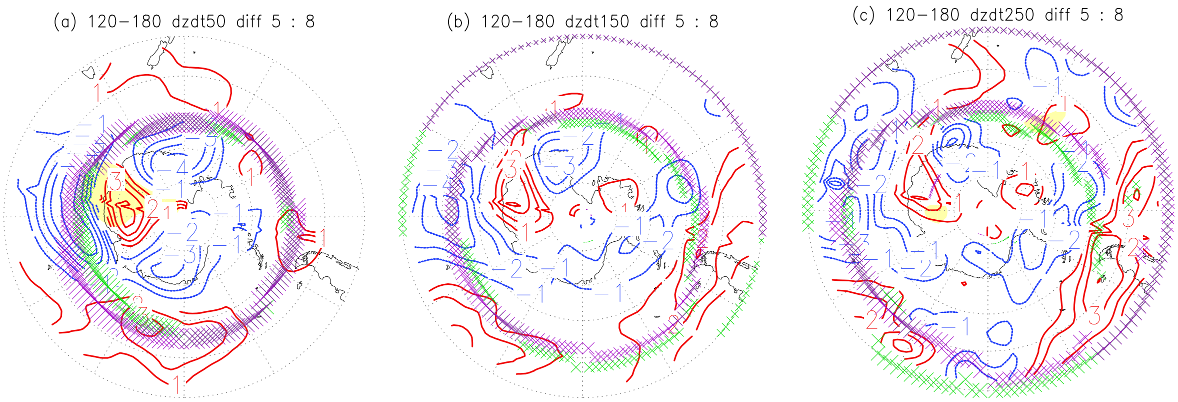

Figure 3.38: (a) Composite difference of monthly-mean westerly acceleration due to the momentum flux of low-pass-filtered submonthly eddies on 50-hPa level between "active" and "inactive" months to the south Australia. Contour interval is 1 [m/s/day] and zero contours are omitted. Yellow and purple shading denotes the difference is positively and negatively significant at 90% level. Red crosses and green dots are the same as in Fig. 3.6a. (b) The same as in (a) but for 150 h-hPa level. (c) The same as in (a) but for 250 h-hPa level.

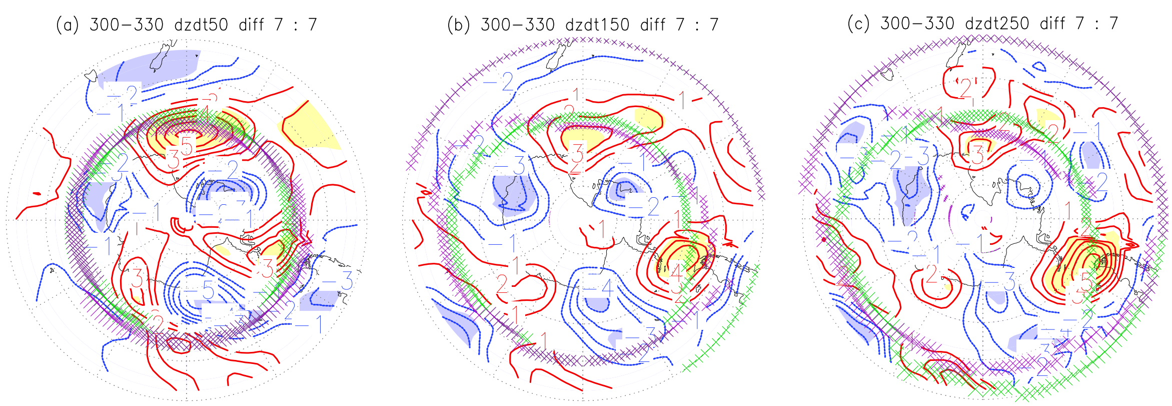

Figure 3.39: (a) The same as in Fig. 3.38a but for a difference composite map between "active" and "inactive" months over the South Atlantic. (b) The same as in (a) but for 150 h-hPa level. (c) The same as in (a) but for 250 h-hPa level.

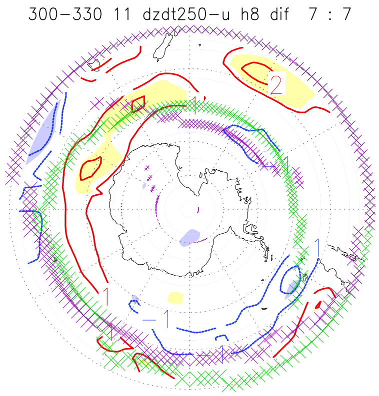

Figure 3.40: The same as in Fig. 3.39c but for feedback forcing from high-pass-filtered eddies.

Associated with this upward and downward propagation, submonthly fluctuations are active in the stratosphere and the troposphere.

As for the interannual variability, we show interannual variations of locally averaged downward wave-activity flux as it is, to the south of Australia, where prominent cases were observed in 1997, and the South Atlantic, where is maximum area of climatological-mean downward wave-activity injection. Associated with upstream of or around the enhanced downward wave-activity injection, the stratospheric PNJ shifts poleward and the tropospheric SPJ is enhanced.

Interannual variability in vertical submonthly wave-activity propagation under the influence of SAM and ENSO, which are the dominant modes of interannual variability in the SH troposphere, is also discussed. We have revealed that their influence is limited except for the La Niña case observed over the Southeastern Pacific. It is thus concluded that downward wave-activity injection tends to be more sensitive to local changes in the PNJ and SPJ rather than global changes associated with SAM and ENSO.

In association with changes of the SPJ and PNJ, especially when large downward wave-activity injection is observed, the waveguide structures around the tropopause become more preferred structures for the vertical wave-activity injection, which is linked to enlarged κ_s there. The contributors to increased κ_s depend on case by case, the meridional curvatures and/or the vertical curvatures of monthly-mean westerlies.

Since the reliable data period is restricted from 1979 when the observation of artificial satellites came to be available, the statistical significance of our analysis may be not enough to discuss the interannual variations owing to the little number of the sampled events. Thus for the further analysis, numerical model experiments would be required to confirm the above-mentioned results to obtain the larger number of samples.

Chapter 4

General Conclusion

Through a case study and statistical study, we have proposed a new aspect of the dynamical linkage between the stratosphere and troposphere in the wintertime extratropics. In most of the previous studies, planetary waves in the stratosphere are considered as deviations from the zonal mean state and their propagation characteristics in a meridional plane are discussed for each harmonic component. In this conventional framework, however, a localized wave source of the planetary wave, if exist, cannot be identified. In contrast, we take another framework in which the stratospheric wave disturbances propagate as "wave packets" defined as circulation anomalies from the time-mean field and observed as wave-train-like structure. The three-dimensional propagation of a wave packet depends on local waveguide structure associated with the zonally-asymmetric field that is slowly varying in time and space.

The essential features of the downward wave-activity propagation associated with wave packets observed in the SH are illustrated in a schematic diagram in Fig. 4.1. (i) Tropospheric circulation anomalies amplify at a particular location associated with an incoming quasi-stationary Rossby wave train and/or the local feedback forcing from synoptic-scale migratory eddies; (ii) wave activity emanating upward from the developed anomalies reaches the lower stratosphere, if exists, through a localized vertical waveguide or "chimney", lead-

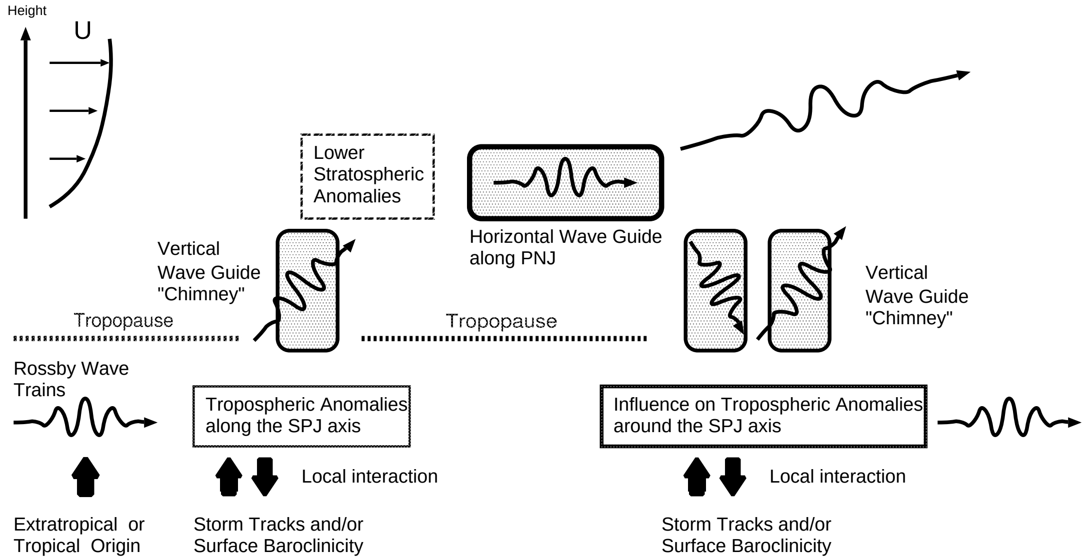

Figure 4.1: Schematic diagram of a quasi-stationary Rossby wave train with a tropospheric origin propagating in the lower stratosphere. Because of the "prism effect"of the vertically sheared PNJ, only the wave activity associated with the lowest zonal wavenumber(s) can keep propagating farther upward. The rest of the wave activity associated with higher wavenumbers can be refracted back downward to the troposphere if the wave train reaches the PNJ exit where a vertical waveguide (or "chimney") forms. The downward injected wave activity can trigger the development of tropospheric anomalies locally, which can further amplify in the presence of feedback forcing from a local storm track and/or through interaction with near-surface baroclinicity.

ing to the development of circulation anomalies with the opposite sign in the stratosphere; (iii) if a waveguide extends downstream along the PNJ, the wave activity propagates eastward along it, forming a zonally and meridionally-confined wave train in the lower stratosphere; (iv) anomalies developing at the leading edge of the lower-stratospheric wave train, if they reach the PNJ exit where another "chimney" forms, release part of the associated wave activity downward across the tropopause, contributing to the local development of tropospheric circulation anomalies with the opposite sign; and (v) downstream wave-activity emanation from the matured tropospheric anomalies occurs with the subsequent formation of another wave train in the troposphere, or in some occasions, wave activity re-emanates back into the stratosphere.

In Chapter 2, case studies of downward wave-activity flux observed in the late winter of 1997 are presented. There, submonthly fluctuations in the troposphere are amplified with the downward wave-activity injection from a locally-confined wave train in the lower-stratosphere. The wave trains formed with upward wave-activity injection from another tropospheric circulation anomalies farther upstream. Upward and downward propagation are consistent with waveguide structures suggested by maxima of the refractive index for stationary Rossby waves.

The climatology and interannual variability of vertical wave-activity propagation are discussed in Chapter 3. Upward and downward propagation is prominent over the South Pacific and South Atlantic, where the climatological mean axes of the lower-stratospheric polar-night jet (PNJ) and the tropospheric subpolar jet (SPJ) are overlapped one another. Associated with prominent vertical wave-activity propagation, submonthly fluctuations in the stratosphere and troposphere are active in these regions. In association with interannual variability, enhanced downward wave-activity injection across the tropopause in late winter (August and September) to the southeast of Australia and over the South Atlantic tends to be associated with the poleward shift of the SPJ axis and the strengthened SPJ. Downstream of the regions of enhanced downward wave-activity injection, tropospheric submonthly fluctuations also tend to be enhanced. Hemispheric variability associated with the Southern Hemispheric annular mode (SAM) or El Niño/Southern Oscillation (ENSO) tends to yield only limited influence on downward wave-activity injection, which implies the greater importance of local anomalies in the jet structures in the stratosphere and troposphere for interannual modulations in the downward wave-activity injection.

As mentioned in the introduction, the dynamical linkage between the stratosphere and troposphere has been discussed primarily in the context of SSW and/or the annular modes (e.g. Baldwin and Dunkerton 1999), in relation to the interaction between the entire polar vortex and planetary waves. Among those literature, one may think Perlwitz and Harnik (2003, hereafter referred to as PH03; 2004), in which downward wave propagation from the stratosphere to the troposphere is discussed, may be similar to our analysis. As already mentioned, however, the mechanisms discussed in PH03 differ fundamentally from those in our examples. PH03 discussed the reflection at a "reflecting surface", which is formated by negative vertical zonal wind shear, of the entire planetary waves embedded in the zonally uniform westerlies, which should be distinguished from the downward wave-activity injection in our examples due to the *refraction* of a zonally-confined Rossby wave packet in the positively vertically sheared westerlies through their "prism" effect (Fig. 1.17). Thus, downward influence on the tropospheric circulation tends to be more localized in our examples than the corresponding downward influence as the reflection of the entire planetary waves presented in PH03 or associated with the annular modes.

By using a model that is linearized around zonally-symmetric zonal mean wind, Chen and Robinson (1992) argued that the large vertical wind shear tends to suppress the upward planetary wave propagation from the troposphere into the stratosphere. Our study shows that for the formation of local waveguide structure around the tropopause through which wave activity propagates upward and downward, the meridional and vertical curvatures are also important, which are not considered in the work of Chen and Robinson (1992).

An implication of our study is that realistic representation of the localized three-dimensional waveguide structure associated with the lower-stratospheric PNJ, including those "chimneys", in an operational model is potentially an important factor for successful extended weather forecasts in the cold season. Another implication of our study is that in the study of quasi-stationary tropospheric circulation anomalies in the wintertime extratropics, wave-activity injection from lower-stratospheric wave trains must be considered as a possible contributor to their development.

Appendix A

A wave-packet behavior of stratospheric waves in a simple numerical model

In a strict definition of a wave packet, a zonal scale of a wave packet must be sufficiently smaller than that of the basic state. In this study and some previous studies mentioned in Chapter 1, however, a zonally-confined wave packet structure that consists mainly of the zonal wavenumber one to three (k=1-3) components has been discussed, whose zonal scale is not necessarily sufficiently smaller than the length of the latitude circle. In this Appendix, a wave-packet behavior of a stratospheric wave is discussed by using a simple numerical model.

The model equation is based on a time-dependent, quasi-geostrophic potential vorticity equation linearized about the zonally uniform westerlies (1.46; p.27) in a beta channel (Held 1983) along the 60° latitude circle. The lower-boundary condition is given with linearized thermodynamic equation as

$$\frac{\partial}{\partial t}\left(\frac{\partial\psi^*}{\partial z}-\frac{N^2}{g}\psi^*\right)+U\frac{\partial}{\partial x}\frac{\partial\psi^*}{\partial z}-\frac{\partial\psi^*}{\partial x}\frac{\partial U}{\partial z}=-\frac{N^2}{f_0}\left(U\frac{\partial h_T}{\partial x}+\alpha\nabla^2\psi^*\right), \qquad \text{(A.1)}$$

where α is the diffusion coefficient equivalent to 5-day damping, and the orography h_T [m]

is given as a Gaussian-type mountain with its peak at 0° longitude.

$$h_T(\lambda,t) = 100 \times (\exp(-4096\lambda^2) + \exp(-4096(\frac{2\pi-\lambda}{2\pi})^2)) \times \exp(-(\frac{t-4[day]}{2[day]})^2) \quad \text{(A.2)}$$

for $t < 4[day]$ and

$$h_T(\lambda,t) = 100 \times \exp(-4096\lambda^2) \quad \text{(A.3)}$$

for $t > 4[day]$. The amplitudes are the almost the same among the cosine components of h_T for k=1-3. The model domain is set from 0° to 720° in longitude to eliminate the upstream influence of the mountain under the cyclic boundary condition imposed. The top of the model domain is set at the level as high as 300 km in altitude and the integration was terminated before the streamfunction response would reach the top boundary. The mean westerly wind speed is 5 [m/s] at the surface and linearly increases with height by 8 [m/s] for every 10 km. The Brunt-Väisälä frequency is set to 0.016 [1/s] for all altitudes.

By the 10th day of the numerical integration (Fig. A.1a), a wave train propagates upward from the forcing region and then downward after reaching 100°E. Wave activity that propagated through the bottom of the stratosphere has already reached the troposphere in the far field between 120° and 240°. By the 16th day (Fig. A.1b), the stratospheric response has amplified further, and the tropospheric response around 200°E has further amplified along the ray for the k=2 component. The turning level for the response roughly corresponds to that predicted theoretically for the k=2 component.

Eddy streamfunctions on the 16th day associated with the individual zonal harmonic components of k=1-3[1] are shown in Fig.A.2. Phase lines of the $k = 1$ component are tilted westward with height, implying its upward propagation, but no signature can be seen that suggests its downward refraction. The other components are in equivalent barotropic structures without suggesting any obvious signature of their vertical propagation.

[1]Because the model domain is set from 0° to 720° in longitude, those components are equivalent to the k=2, 4 and 6 components in the model domain.

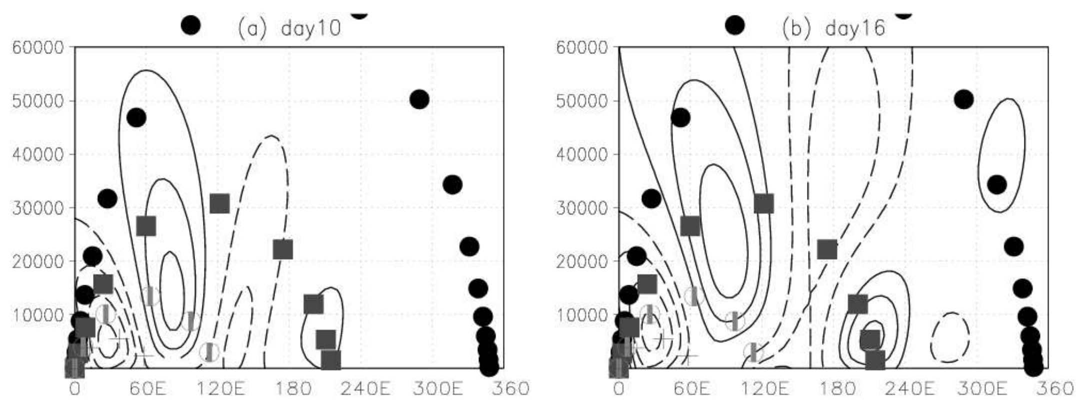

Figure A.1: (a) The same as in Fig. 1.9, but for the response on the 10th day in a numerical model where a localized orographic forcing is placed at 0° longitude under the zonally uniform westerlies with linear shear. Closed circles, closed squares, open circles with vertical lines and crosses denote the rays of the k=1, 2, 3 and 4 components, respectively. (b) The same as in (a) but on 16th day.

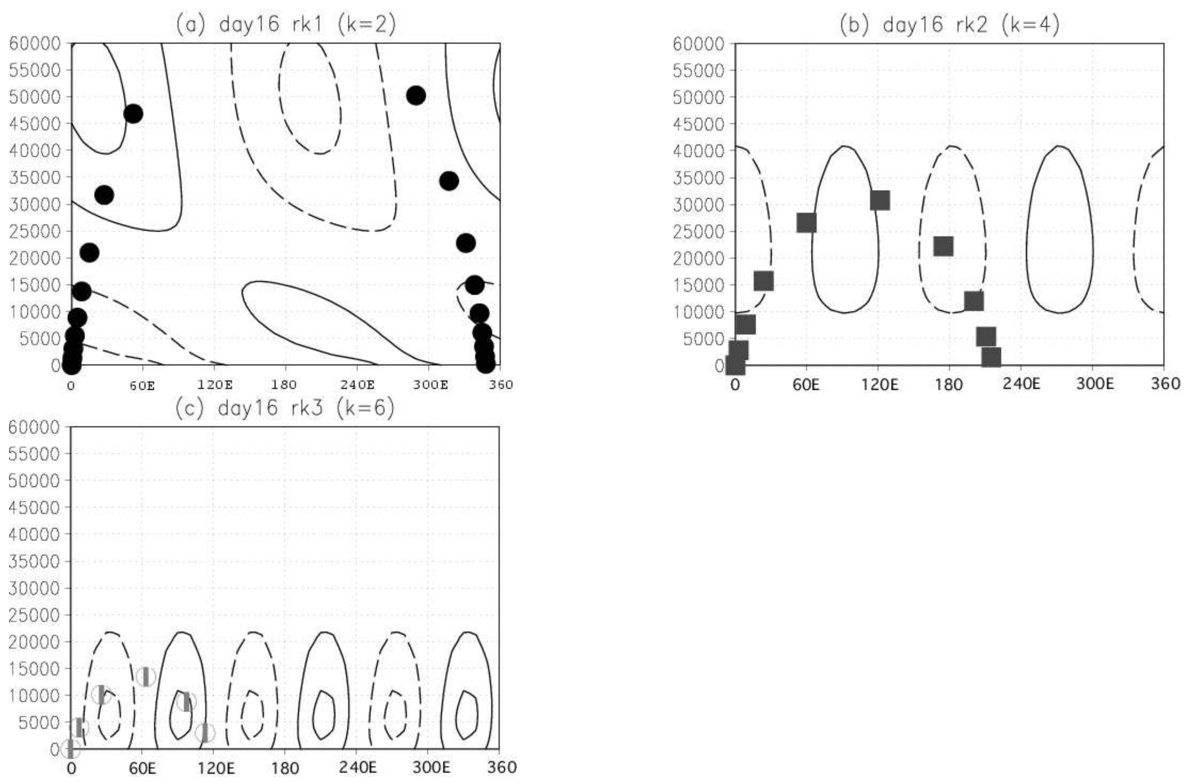

Figure A.2: (a) As in Fig. A.1b, but for eddy streamfunction only for the $k = 1$ component. The contour interval is half of that in Fig. A.1. (b) The same as in (a) but for the $k = 2$ component. (c) The same as in (a) but for the $k = 3$ component.

However, combinations of two of the three harmonic components hint wave-packet structures suggestive of vertical propagation. The combination of the k=1 and 2 components (Fig. A.3a) suggests eastward and upward propagation of a wave-packet structure as far as 200°E and the following downward propagation around 240°E with eastward tilted phase lines. The combination of the k=2 and 3 components (Fig. A.3b) also suggests an upward and downward wave-packet structure in the upstream half of the model domain with westward and eastward tilted phase lines around 40°E and 120°E, respectively, although the signal is confined mainly in the lower stratosphere and troposphere. The wave-packet structure depicted in Fig. A.1b can be well reproduced as the combination of the k=1, 2 and 3 components (Fig. A.3c)[2]. Those model results support the notion that stratospheric wavy disturbances composed mainly of the zonal harmonics of k=1, 2 and 3 can form wave packet structures. It is therefore more straightforward to interpret the amplification of localized tropospheric circulation anomalies as seen in Fig. A.1 as being associated with local downward wave packet propagation than as being associated with propagation of the decomposed indivisual harmonics.

[2]Note that k=0.5, 1.5 and 2.5 components, which come from the double length in longitude of the model domain, are not included in Fig. A.3c.

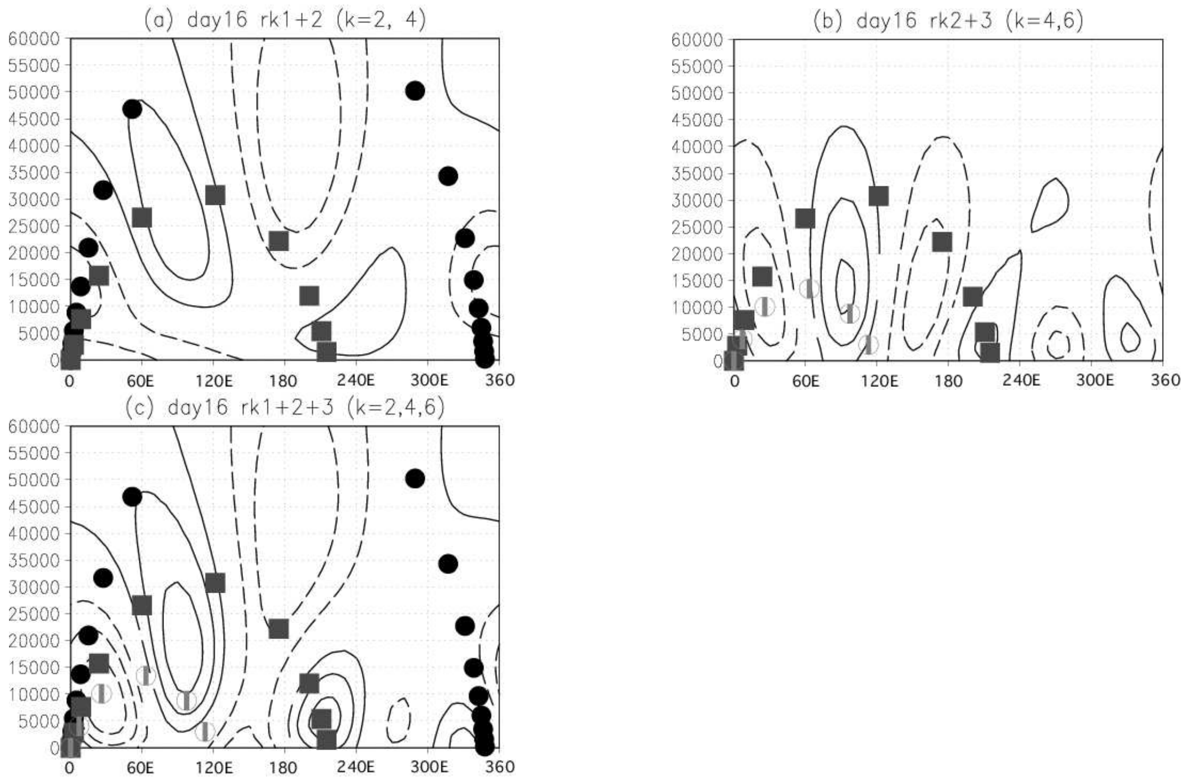

Figure A.3: Reproduction of the wave packet structure depicted in Fig. A.1b through (a) the combination of the k=1 and 2 components (Figs. A.2a and b), (b) the combination of the k=2 and 3 components (Figs. A.2b and c), and (c) the combination of k=1-3 components (Figs. A.2a, b and c).

Appendix B

On the use of time filtering

In this study, we analyze anomaly fields associated with submonthly fluctuations, which have been defined as local deviations of an 8-day low-pass filtered time series from the 31-day running-mean fields. Here, we show that the submonthly fluctuations thus defined are adequate to analyze the linkage between the stratosphere and troposphere in the form of wave-packet propagation.

Figure B.1a shows the same one-point correlation maps as in Fig. 1.12c (p. 23) but based on the unfiltered daily time series. Though the statistical significance is lowered slightly, upward-propagating wave-packet signature is noticeable as observed in Fig. 1.12c. Such an upward-propagating wave-packet signature as in Fig. B.1a is not obvious in the corresponding one-point correlation maps based on the 31-day moving averaged time series and the 8-day high-pass filtered time series (Figs. B.1b and c, respectively). These differences in reproducing the upward propagating wave-packet signature among the three kinds of time series justify our definition of anomalies based on the two kinds of time filtering.

As another confirmation, coherency of the tropospheric circulation at a base grid with the stratosphere is analyzed. Before showing the result, the power spectra for the unfiltered and anomaly time series of 400-hPa and 50-hPa level at (90°W, 60°S), the reference grid point for Fig. B.1, have been evaluated for the late-winter period from 1st August to 3rd

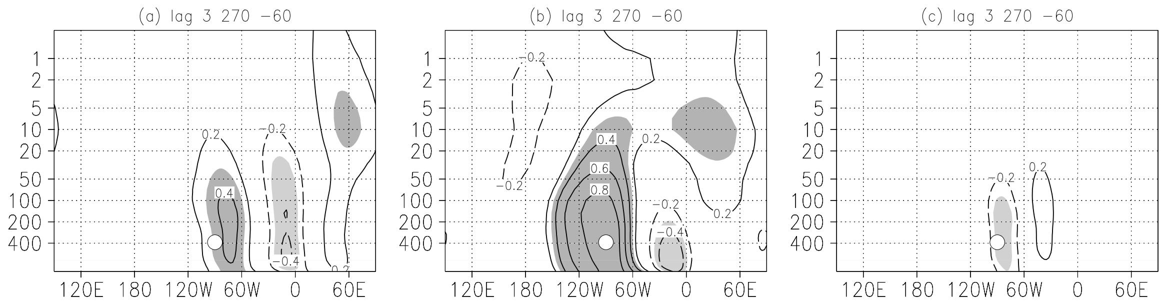

Figure B.1: The same as in Fig. 1.12c but based on (a) unfiltered time series, (b) 31-day running mean, and (c) 8-day high-pass-filtered time series.

October over the 20 year-period between 1980 to 1999 (Fig. B.2). The two kinds of filtering used for our definition of the anomaly retains the power for the periods from 8 to 32 days, while efficiently reducing the power on other time scales both in the troposphere and lower stratosphere.

Figure B.3 shows maps of the coherency squared between local height fluctuations and the 400-hPa height at (90°W, 60°S) as the reference time series for the three subseasonal time scales as indicated. In this "one-point coherency-squared map" for the periods from 8 to 32 days (Fig. B.3b), the coherency is high not only in the vicinity of the reference point but also in remote domains upstream and downstream of the reference point. The secondary maximum (∼0.3) is observed in the stratosphere about 60° downstream of the reference point. This downstream stratospheric signal weakens in the corresponding map for 64-day period (Fig. B.3a), since most of the upward-propagation signal is confined to the submonthly time scales (B.1b). The coherency squared in the far field is also weak for the subweekly periods (between 4.2 and 7.1 days) (Fig. B.3c). Figure B.3b suggests the linkage between the troposphere and lower stratosphere is strongest in submonthly periods. Thus it is conjectured that our definition of the anomalies as submonthly fluctuations is adequate in the study of the linkage between the stratosphere and troposphere in the form of wave-packet propagation.

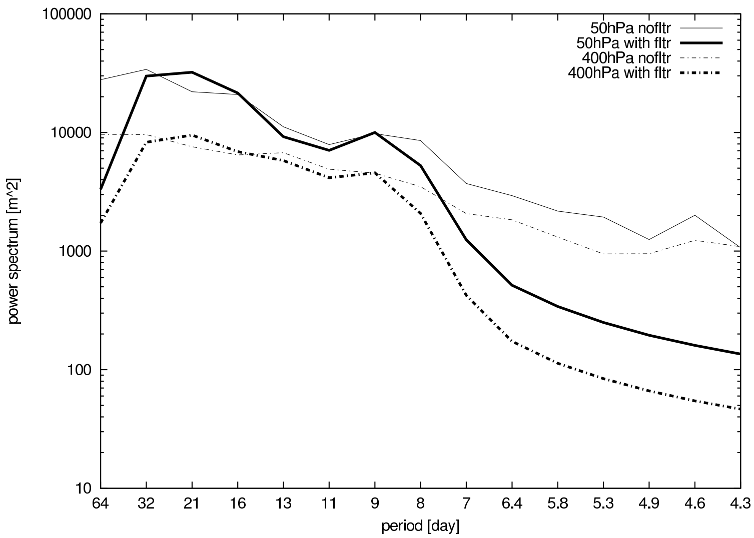

Figure B.2: Power spectra for geopotential height fluctuations at (90°W, 60°S) in the late winter period between 1st August and 3rd October for 20 years from 1980 to 1999. The spectra for unfiltered and low-pass-filtered anomaly time series of 50-hPa level are shown by thin and thick solid lines, respectively, and spectra for unfiltered and low-pass-filtered anomaly time series of 400-hPa level by thin and thick broken lines, respectively.

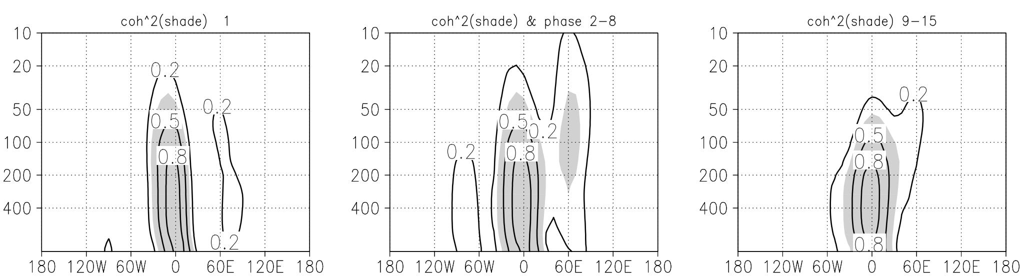

Figure B.3: Zonal-height sections for coherency squared between local geopotential height fluctuations and the 400-hPa height fluctuations at (90°W, 60°S) for the late-winter period between 1st August and 3rd October over 20 years from 1980 to 1999. For the periods of (a) 64 days, (b) 8-32 days, and (c) 4.2-7.1 days. The contours are for 0.2, 0.5 and 0.8. Shading denotes regions coherency squared exceeds 0.3.

References

Andrews, D. G. and McIntyre, M. E. 1976 Planetary waves in horizontal and vertical shear: The generalized Eliassen-Palm relation and the mean zonal acceleration. *J. Atmos. Sci.*, **33,** 2031–2048

Andrews, D. G., Holton, J. R. and Leovy, C. B. 1987 *Middle atmosphere dynamics,* Academic Press, 489 pp.

Baldwin, M. P. and O'Sullivan, D. 1995 Stratospheric effects of ENSO-related tropospheric circulation anomalies. *J. Climate,* **8,** 649–667

Baldwin, M. P. and Dunkerton, T. J. 1999 Propagation of the Arctic Oscillation from the stratosphere to the troposphere. *J. Geophys. Res.*, **104,** 30937–30946

Bates, J. R. 1977 Dynamics of stationary ultra-long waves in middle latitudes. *Q. J. R. Meteorol. Soc.*, **103,** 397–430

Boville, B. A. 1984 The influence of the polar night jet on the tropospheric circulation in a GCM. *J. Atmos. Sci.*, **41,** 1132–1142

Blackmon, M. L., Madden, R. A., Wallace, J. M. and Gutzler, D. S. 1979 Geographical variations in the vertical structure of geopotential height fluctuations. *J. Atmos. Sci.*, **36,** 2450–2466

Charney, J. G. and Drazin, P. G. 1961 Propagation of planetary-scale disturbances from the lower into the upper atmosphere. *J. Geophys. Res.*, **66,** 83–110

Chen, P., and Robinson, W. A. 1992 Propagation of planetary waves between the troposphere and stratosphere. *J. Atmos. Sci.*, **49,** 2533–2545

Christiansen, B. 2001 Downward propagation of zonal mean zonal wind anomalies from the stratosphere to the troposphere: Model and reanalysis. *J. Geophys. Res.*, **106,** 27307–27322

Dickinson, R. E. 1968 Planetary Rossby waves propagating vertically through weak westerly wind wave guides. *J. Atmos. Sci.*, **25**, 984–1002

Eliassen, A. and Palm, E. 1961 On the transfer of energy in stationary mountain waves. *Geofys. Publ.*,**22**, 1–23

Geller, M. A. and Alpert, L. C. 1980 Planetary wave coupling between the troposphere and the middle atmosphere as a possible sun-weather mechanism. *J. Atmos. Sci.*, **37,** 1197–1215

Harnik, N. 2002 The evolution of a stratospheric wave packet. *J. Atmos. Sci.*, **59,** 202–217

Hartley, D. E., Villarin, J. T., Black, R. X. and Davis, C. A. 1996 A new perspective on the dynamical link between the stratosphere and troposphere. *Nature*, **391,** 471–473

Held, I. M. 1983 Stationary and quasi-stationary eddies in the extratropical troposphere: Theory. *Large-Scale Dynamical Processes in the Atmosphere.* Hoskins, B. J. and Pearce, R. P., Eds., Academic Press, 127–168.

Held, I. M., Ting, M. and Wang, H. 2002 Northern Winter Stationary Waves: Theory and Modeling. *J. Climate*, **15,** 2125–2144

Hio, Y. and Hirota, I. 2002 Interannual variations of planetary waves in the Southern Hemisphere stratosphere. *J. Meteor. Soc. Japan.,* **80,** 1013–1027

Hio, Y. and Yoden, S. 2005 Interannual variations of the seasonal march in the Southern Hemisphere stratosphere for 1979-2002 and characterization of the unprecedented year 2002. *J. Atmos. Sci.*, **62,** 567–580

Hirota, I. and Sato, Y. 1969 Periodic variation of the winter stratospheric circulation and intermittent vertical propagation of planetary waves. *J. Met. Soc. Japan,* **47,** 390–402

Holton, J. R. 2004 *An introduction to dynamic meteorology*, Elsevier Academic Press, 535pp.

Hoskins, B. J. and Ambrizzi, T. 1993 Rossby wave propagation on a realistic longitudinally varying flow. *J. Atmos. Sci.*, **50,** 1661–1671

Hoskins, B. J. and Ambrizzi, T. 1993 Rossby wave propagation on a realistic longitudinally varying flow. *J. Atmos. Sci.*, **50,** 1661–1671

Hoskins, B. J. and Karoly, D. J 1981 The steady linear response of a spherical atmosphere to thermal and orographic forcing. *J. Atmos. Sci.*,**38,** 1179–1196

Itoh, H. and Harada, K. 2004 Coupling between troposphere and stratosphere leading modes. *J. Climate*, **17,** 320–336

Julian, P. R. and Labitzke. K. B. 1965 A study of atmospheric energetics during the January-February 1963. *J. Atmos. Sci.*, **22,** 597–610

Kalnary, M. E., Kanamitsu, M., Kistler, R., Collins, W., Deaven, D., Gandin, L., Iredell, M., Saha, S., White, G., Woollen, J., Zhu, Y., Leetmaa, A., Reynolds, R., Chelliah, M., Ebisuzaki, W., Higgins, W., Janowiak, J., Mo, K. C., Ropelewski, W., Wang, J., Jenne, R. and Joseph, D. 1996 The NCEP/NCAR 40-year reanalysis project. *Bull. Amer. Meteor. Soc.*, **77,** 437–471

Karoly, D. J. and Hoskins, B. J. 1982 Three dimensional propagation of planetary waves. *J. Meteorol. Soc. Jpn.*, **60,** 109–123

Karoly, D. J. 1983 Rossby wave propagation in a barotropic atmosphere. *Dyn. Atmos. Oceans*, **7,** 111–125

Kiladis, G. N. and Mo, K. C. 1999 Interannual and intraseasonal variability in the Southern Hemisphere. *Meteorology of the Southern Hemisphere*, Karoly, D. J. and Vincent, D. G., Eds., Amer. Meteor.Soc., 307–336.

Kodera, K., Yamazaki, K., Chiba, M. and Shibata, K. 1990 Downward propagation of upper stratospheric mean zonal wind perturbation to the troposphere. *Geophys. Res. Lett.*, **17,** 1263–1266

Kodera, K., Chiba, M. and Shibata, K. 1991 A possible influence of the polar night stratospheric jet on the subtropical tropospheric jet. *J. Meteorol. Soc. Jpn.*, **69,** 715–745

Kodera, K. and Chiba, M. 1995 Tropospheric circulation changes associated with stratospheric sudden warmings: A case study. *J. Geophys. Res.*, **100,** 11055–11068

Kodera, K., Kuroda Y. and Pawson, S. 2000 Stratospheric sudden warmings and slowly propagating zonal-mean zonal wind anomalies. *J. Geophys. Res.*, **105,** 12351–12359

Kodera, K. and Kuroda, Y. 2000a A mechanistic model study of slowly propagating coupled stratosphere-troposphere variability. *J. Geophys. Res.*, **105,** 12361–12370

Kodera, K. and Kuroda, Y. 2000b Tropospheric and stratospheric aspects of the Arctic Oscillation. *Geophys. Res. Lett.*, **27,** 3349–3352

Kuroda, Y. and Kodera, K. 1998 Interannual variability in the troposphere and stratosphere of the southern hemisphere winter. *Geophys. Res. Lett.*, **103,** 13787–13799

Kuroda, Y. and Kodera, K. 1999 Role of planetary waves in the stratosphere-troposphere coupled variability in the Northern Hemisphere winter. *Geophys. Res. Lett.*, **26,** 2375–2378

Kuroda, Y. and Kodera, K. 2001 Variability of the polar night jet in the Northern and Southern Hemispheres. *J. Geophys. Res.*, **106,** 20703–20713

Lau, N. C. and Nath, M. J. 1991 Variability of the baroclinic and barotropic transient eddy forcing associated with monthly changes in the mid-latitude storm tracks. *J. Atmos. Sci.*, **48,** 2589–2613

Limpasuvan, V. L. and Hartmann, D. L. 1999 Eddies and the annular modes of climate variability. *Geophys. Res. Lett.*, **26,** 3133–3136

Lorenz, D. J. and Hartmann, D. L. 2001 Eddy-zonal flow feedback in the Southern Hemisphere. *J. Atmos. Sci.*, **58,** 3312–3327

Matsuno, T. 1970 Vertical propagation of stationary planetary waves in the winter Northern Hemisphere. *J. Atmos. Sci.*, **27,** 871–883

Matsuno, T. 1971 A dynamical model of the stratospheric sudden warming. *J. Atmos. Sci.*, **28,** 1479–1494

Muench, H. S. 1965 On the dynamics of the wintertime stratosphere circulation. *J. Atmos. Sci.*, **22,** 349–360

Nakamura, H., Nakamura, M. and Anderson, J. L. 1997 The role of high- and low-frequency dynamics in blocking formation. *Mon. Wea. Rev.*, **125,** 2074–2093

Nakamura, H. and Honda, M. 2002 Interannual seesaw between the Aleutian and Icelandic lows. Part III: Its influence upon the stratospheric variability. *J. Meteor. Soc. Japan*, **80,** 1051-1067

Nakamura, H. and Fukamachi, T. 2004 Evolution and dynamics of summertime blocking over the Far East and the associated surface Okhotsk high. *Q. J. R. Meteorol. Soc.*, **130,** 1213–1233

Nakamura, H. and Shimpo, A. 2004 Seasonal variations in the Southern Hemisphere storm tracks and jet streams as revealed in a reanalysis data set. *J. Climate*, **17,** 1828–1844

Nishii, K. and Nakamura, H. 2004a Lower-stratospheric Rossby wave trains in the Southern Hemisphere: A case study for late winter of 1997. *Q. J. R. Meteorol. Soc.*, **130,** 325–346

Nishii, K. and Nakamura, H. 2004b Tropospheric influence on the diminished Antarctic ozone hole in September 2002. *Geophys. Res. Lett.*, **31,** –, doi:10.1029/GL019532

Nishii, K. and Nakamura, H. 2005 Upward and downward injection of Rossby wave activity across the tropopause: A new aspect of the troposphere-stratosphere dynamical linkage. *Q. J. R. Meteorol. Soc.*, **131,** 545–564

Perlwitz, J. and Harnik, N. 2003 Observational evidence of a stratospheric influence on the troposphere by planetary wave reflection. *J. Climate,* **16,** 3011–3026

Perlwitz, J. and Harnik, N. 2004 Downward coupling between the stratosphere and troposphere: The relative roles of wave and zonal mean processes *J. Climate*, **17,** 4902–4909

Plumb, R. A. 1985 On the three-dimensional propagation of stationary waves. *J. Atmos. Sci.*, **42,** 217–229

Polvani, L. M. and Kushner, P. J. 2002 Tropospheric response to stratospheric perturbations in a relatively simple general circulation model. *Geophys. Res. Lett.*, **29,** 1114–,doi:10.1029/2001GL014284

Quiroz, R. S. 1986 The association of stratospheric warmings with tropospheric blocking. *J. Geophys. Res.*, **91,** 5277–5285

Randel, W. J. 1987 A study of planetary waves in the Southern winter troposphere and stratosphere. Part I: Wave structure and vertical propagation. *J. Atmos. Sci.*, **44,** 917–935

Randel, W. J. 1988 The seasonal evolution of planetary waves in the Southern Hemisphere stratosphere and troposphere. *Q. J. R. Meteorol. Soc.*, **114,** 1385–1409

Randel, W. J. and Newman, P. A. 1999 The stratosphere in the Southern Hemisphere. *Meteorology of the Southern Hemisphere*, Karoly, D. J. and Vincent, D. G., Eds., Amer. Meteor. Soc., 307–336.

Sato, Y. 1974 Vertical structure of quasi-stationary planetary waves in several winters. *J. Meteor. Soc. Japan.*,**52,** 272–282

Scinocca, J. F. and Haynes, P. H. 1998 Dynamical forcing of stratospheric planetary waves by tropospheric baroclinic eddies. *J. Geophys. Res.*, **55,** 2361–2392

Shiotani, M. and Hirota, I. 1985 Planetary wave-mean flow interaction in the stratosphere: A comparison between Northern and Southern Hemispheres. *Q. J. R. Meteorol. Soc.*, **111,** 309–334

Shiotani, M., Shimoda, N. and Hirota, I. 1993 Interannual variability of the stratospheric circulation in the Southern Hemisphere. *Q. J. R. Meteorol. Soc.*, **119,** 531–546

Taguchi, M. and Hartmann, D. L. 2004 Interference of extratropical surface climate anomalies induced by El Niño and stratospheric sudden warmings. *Geophys. Res. Lett.*, **32,** L04709, doi:10.1029/2004GL022004

Takaya, K. and Nakamura, H. 2001 A formulation of a phase-independent wave-activity flux for stationary and migratory quasi-geostrophic eddies on a zonally-basic flow. *J. Atmos. Sci.*, **58,** 608–627

Thompson, D. W. J. and Wallace, J. M. 2000 Annular mode in the extratropical circulation. Part I: Month-to-month variability. *J. Climate*, **13,** 1000–1016

Thompson, D. W. J. and Wallace, J. M. 2001 Regional climate impacts of the Northern Hemisphere annular mode. *Science,* **293,** 85–89

Thompson, D. W. J., Baldwin, M. P. and Solomon, S. 2005 Stratosphere-troposphere coupling in the Southern Hemisphere. *J. Atmos. Sci.*, **62,** 708–715

Uryu, M. 1974 Mean zonal flows induced by vertically propagating Rossby wave packet. *J. Meteor. Soc. Japan*, **52,** 481–489

Vera, C., Silverstri, G., Barros, V. and Carril, A. 2004 Differences in El Nino Response over the Southern Hemisphere. *J. Climate*, **17,** 1741–1753

Yoden, S., Yamaga, T., Pawson, S. and Langematz, U. 1999 A composite analysis of the stratospheric sudden warmings simulated in a perpetual January integration of the Berlin TSM GCM. *J. Meteorol. Soc. Jpn.*, **77,** 431–445

Zhou, S. T, Miller, A. J., Wang, J. and Angell, J. K. 2002 Downward-propagating temperature anomalies in the preconditioned polar stratosphere. *J. Climate*, **15,** 781–792

Acknowledgments

I would like to thank Prof. H. Nakamura for courteous direction throughout the course of this study. I am grateful to Profs. M. Takahashi, H. Niino, T. Hibiya, M. Sato and K. Sato for their valuable comments and suggestions. I would also like to thank Profs. I. Hirota and D. J. Karoly and Dr. Y. Tomikawa for their comments and encouragement. Advice of Dr. K. Takaya on a wave-activity flux has been helpful. Discussions with Drs. T. Miyasaka and T. Sampe have been precious and enjoyable. Finally, I wish to express my deep appreciation to my family for their hearty encouragement and support.